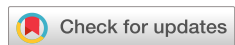


REVIEW ARTICLE | OCTOBER 27 2021

Orbital angular momentum of light for communications [F](#)

Alan E. Willner ; Kai Pang ; Hao Song ; Kaiheng Zou; Huibin Zhou



Appl. Phys. Rev. 8, 041312 (2021)

<https://doi.org/10.1063/5.0054885>

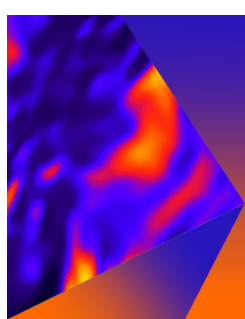
 CHORUS



View
Online



Export
Citation



Applied Physics Letters

Special Topic: Mid and Long Wavelength Infrared Photonics, Materials, and Devices

Submit Today

 AIP
Publishing

Orbital angular momentum of light for communications

Cite as: Appl. Phys. Rev. **8**, 041312 (2021); doi:10.1063/5.0054885

Submitted: 22 April 2021 · Accepted: 28 September 2021 ·

Published Online: 27 October 2021



View Online



Export Citation



CrossMark

Alan E. Willner,^{a)} Kai Pang,^{a)} Hao Song, Kaiheng Zou, and Huibin Zhou

AFFILIATIONS

Department of Electrical and Computer Engineering, University of Southern California, Los Angeles, California 90089, USA

^{a)}Authors to whom correspondence should be addressed: willner@usc.edu and kaipang@usc.edu

ABSTRACT

Structured light, especially beams carrying orbital angular momentum (OAM), has gained much interest due to its unique amplitude and phase structures. In terms of communication systems, multiple orthogonal OAM beams can be potentially utilized for increasing link capacity in different scenarios. This review describes challenges, advances, and perspectives on different aspects of the OAM-based optical communications, including (a) OAM generation/detection and (de)multiplexing, (b) classical free-space optical communication links, (c) fiber-based communication links, (d) quantum communication links, (e) OAM-based communications in different frequency ranges, (f) OAM-based communications using integrated devices, and (g) novel structured beams for communications.

© 2021 Author(s). All article content, except where otherwise noted, is licensed under a Creative Commons Attribution (CC BY) license (<http://creativecommons.org/licenses/by/4.0/>). <https://doi.org/10.1063/5.0054885>

TABLE OF CONTENTS

I. INTRODUCTION	2	1. Divergence	14
II. OAM AND ITS APPLICATIONS IN COMMUNICATIONS	2	2. Misalignment	15
A. Background of OAM	2	3. Turbulence	15
1. OAM of light beams	2	C. Potential mitigation methods for different challenges	17
2. Laguerre-Gaussian (LG) modal basis set and complex modal spectrum	3	1. Mitigation methods for the beam divergence	17
B. Application of OAM in communications	4	2. Mitigation methods for misalignment	21
1. OAM multiplexing and encoding	5	3. Mitigation methods for atmospheric turbulence	22
2. Various potential challenges	5	D. OAM-based optical communications for airborne platforms	26
3. Different frequency ranges	6	1. Challenges for airborne optical communication links	26
C. Digital modulation formats	7	2. OAM-multiplexed FSO links involving UAV platforms	26
III. OAM GENERATION, DETECTION, AND (DE)MULTIPLEXING	8	E. OAM-based optical communications in underwater environments	28
A. OAM generation and detection	8	1. Propagation effects in underwater environments	28
B. OAM multiplexing and demultiplexing	9	2. OAM-multiplexed underwater communication links	28
C. Summary	10	F. OAM-based diversity system	30
IV. OAM-BASED FREE-SPACE OPTICAL COMMUNICATION SYSTEMS	12	G. Summary	31
A. OAM-multiplexed and -encoded free-space links	12	V. OAM-BASED FIBER COMMUNICATION SYSTEMS	31
1. OAM-multiplexed free-space links	12	A. OAM modes in fibers	31
2. OAM-encoded free-space links	13	B. Random mode coupling in the fiber	31
3. LG-based free-space links by varying both modal indices	13		
B. Challenges in an OAM-based FSO link	14		

C. Potential techniques for mitigating OAM mode coupling	34
1. MIMO equalization	34
2. Adaptive optics	34
3. Novel fibers	35
D. OAM fiber amplifiers.....	37
E. Summary.....	38
VI. OAM IN QUANTUM COMMUNICATIONS.....	38
A. OAM-based quantum encoding.....	38
B. Free-space OAM-based quantum key distribution (QKD).....	38
1. Basic concept of OAM-based QKD.....	39
2. OAM-based QKD systems beyond laboratory distances.....	39
3. Adaptive optics for OAM-based quantum links	40
C. OAM-based QKD in underwater environments	40
D. Fiber-based OAM QKD links.....	42
E. OAM-based quantum secret sharing among multiple parties	42
F. Summary.....	42
VII. OAM-BASED COMMUNICATION SYSTEMS IN DIFFERENT FREQUENCY RANGES.....	43
A. OAM-multiplexed links in the millimeter-wave range	43
B. THz links using OAM multiplexing	44
C. Challenges for millimeter-wave/THz OAM-multiplexed systems	44
1. Turbulence-induced system degradation for THz-OAM links	45
2. Multi-path and receiver aperture effects.....	46
D. Summary	46
VIII. INTEGRATED DEVICES FOR OAM COMMUNICATIONS.....	47
A. Ring-resonator-based OAM emitter/receiver	47
B. Circular phase array OAM emitter/receiver	49
C. Subwavelength optical OAM antenna	49
D. Summary	51
IX. NOVEL STRUCTURED BEAMS FOR MDM COMMUNICATIONS.....	51
A. Bessel-type beams	52
B. Other types of structured beams	53
C. Summary	55
X. SUMMARY AND PERSPECTIVE	61

I. INTRODUCTION

“Structured light”—especially orbital angular momentum (OAM)—is a topic of growing interest in the optics community, not only for its inherent properties but also for its possible applications. Will it impact sensing, imaging, or micromanipulation?^{1–3} This review will explore the possibilities of OAM for data communications.

Structured light generally refers to an optical beam with a tailored spatial amplitude/phase distribution and corresponding unique properties.⁴ One type of structured light involves OAM beams that are also known as vortex beams because of their donut-shaped intensity profiles with a null at the center.^{5–7} In addition, such OAM beams have twisting helical phase fronts while propagating, which is often

characterized by the OAM order (i.e., ℓ). The value of ℓ indicates the number of 2π phase shifts around the center of the beam’s phase profile. Interestingly, OAM can be carried even by a single photon in the quantum domain.⁸

It is well known that Laguerre–Gaussian (LG) modes are a complete two-dimensional orthogonal modal basis set. As a subset of the LG modal basis set, different OAM modes (with different ℓ values) are orthogonal with each other.^{9,10} Importantly, based on such orthogonality, OAM beams could be utilized for a communication system in the following two different ways:

- (1). Multiplexing: The total data capacity could be potentially increased by multiplexing multiple OAM beams, each carrying an independent data channel at the transmitter side. After coaxially propagating in the free space or fiber, these OAM beams on different channels could be efficiently demultiplexed at the receiver side. Importantly, there would be little inherent channel crosstalk due to the orthogonality between different OAM beams. Consequently, the total system capacity could be increased by a factor of N , where N represents the number of multiplexed OAM beams.^{11–13}
- (2). Encoding: Photon efficiency can be increased if a beam or single photon is encoded into one of many possible OAM values, thus making a large alphabet for possible data symbols within a discrete time window. The achievable data bits per photon increases as $\log_2 N$, where N represents the number of orthogonal encoding states.^{14–17}

The field of OAM-based optical communications (i) is considered young and rich with scientific and technical challenges, (ii) holds promise for technological advances and applications, and (iii) has produced much research worldwide. In this review, a general introduction of OAM and its applications in communications will be first presented in Sec. II. Subsequently, we will describe challenges, advances, and perspectives on different aspects of the OAM-based optical communications in the following sections, including (a) OAM generation/detection and (de)multiplexing (Sec. III), (b) classical free-space optical (FSO) communication links (Sec. IV), (c) fiber-based communication links (Sec. V), (d) quantum communication links (Sec. VI), (e) OAM-based communications in different frequency ranges (Sec. VI), (f) OAM-based communications using integrated devices (Sec. VIII), and (g) novel structured beams for communications (Sec. IX).

II. OAM AND ITS APPLICATIONS IN COMMUNICATIONS

A. Background of OAM

1. OAM of light beams

It is well known that a light wave can carry spin angular momentum (SAM) that is associated with the polarization of the electric field.¹⁸ When the polarization of a light wave is linear, it means no SAM is carried. However, when its polarization vector rotates along the beam axis (i.e., left or right circularly polarized light), the light has an SAM of $\pm \hbar$ (\hbar is reduced Planck’s constant).⁶

As another type of angular momentum, a light wave can also carry OAM. In general, OAM can be utilized to characterize the “twisted” helical phase front of a light beam when its wavevector spirals around the beam axis. Moreover, such a helical phase front of an

OAM-carrying beam is usually represented by $\exp(i\ell\theta)$, where θ is the azimuthal coordinate and ℓ is the number of 2π phase shifts in the phase profile of the beam.⁵ In addition, the sign of ℓ (positive or negative) corresponds to the direction of the phase helices (clockwise or counterclockwise) in the phase profile. Due to the phase singularity in such a helical phase profile, an OAM beam with a nonzero ℓ (i.e., OAM order) usually has a donut-shaped intensity profile, as shown in Fig. 1.

In contrast to SAM with only two different states, OAM can be theoretically quantified as an infinite number of states, which means ℓ can be any integer. It should be noted that OAM beams with different ℓ values are orthogonal with each other while propagating coaxially. For example, considering two OAM beams with ℓ_1 and ℓ_2 , respectively,⁷

$$u_1(r, \theta, z) = A_1(r, z) \exp(i\ell_1\theta), \quad (1)$$

$$u_2(r, \theta, z) = A_2(r, z) \exp(i\ell_2\theta), \quad (2)$$

where (r, θ, z) is the cylindrical coordinate and refers to the radial, azimuthal position, and propagation position. Such an orthogonality between different OAM beams can be represented by⁷

$$\int_0^{2\pi} u_1(r, \theta, z) u_2^*(r, \theta, z) d\theta = \begin{cases} 0 & \text{if } \ell_1 \neq \ell_2 \\ A_1 A_2^* & \text{if } \ell_1 = \ell_2 \end{cases}. \quad (3)$$

This is significantly important when they are utilized in communications, which will be further discussed in Sec. II B.

2. Laguerre-Gaussian (LG) modal basis set and complex modal spectrum

In general, an OAM beam could refer to any helically phased light beam, irrespective of its radial distribution. However, a complete two-dimensional (2D) modal basis can generally be characterized by two modal indices. For example, LG modes have ℓ and p indices, corresponding to azimuthal and radial distribution, respectively.^{9,10} The electric field of LG modes can be represented by^{5,6}

$$LG(r, \theta, z; \ell, p) = \sqrt{\frac{2p!}{\pi(p+|\ell|)!}} \frac{1}{w(z)} \left(\frac{r\sqrt{2}}{w(z)} \right)^{|\ell|} \exp\left(\frac{-r^2}{w^2(z)}\right) L_p^{|\ell|} \left(\frac{2r^2}{w^2(z)} \right) \exp(i\ell\theta) \exp\left(\frac{ik_0 r^2 z}{2(z^2 + z_R^2)}\right) \exp\left[-i(2p+|\ell|+1)\tan^{-1}\left(\frac{z}{z_R}\right)\right], \quad (4)$$

where the $1/e$ radius of the Gaussian term is given by $w(z) = w(0)[(z^2 + z_R^2)/z_R^2]^{1/2}$ [$w(0)$ is the beam waist], z_R is the Rayleigh range, and $(2p+|\ell|+1)\tan^{-1}(z/z_R)$ is the Gouy phase. $L_p^{|\ell|}$ are the generalized Laguerre polynomials and (r, θ, z) is the cylindrical coordinate.⁶ Figure 2(a) shows the intensity and phase profiles of some LG beams. For the LG beam with a non-zero ℓ value, $p+1$ represents the number of rings in the intensity profile, while ℓ represents the number of 2π phase shifts along the azimuthal direction in the phase profile. Theoretically, LG beams with different ℓ and/or p values are

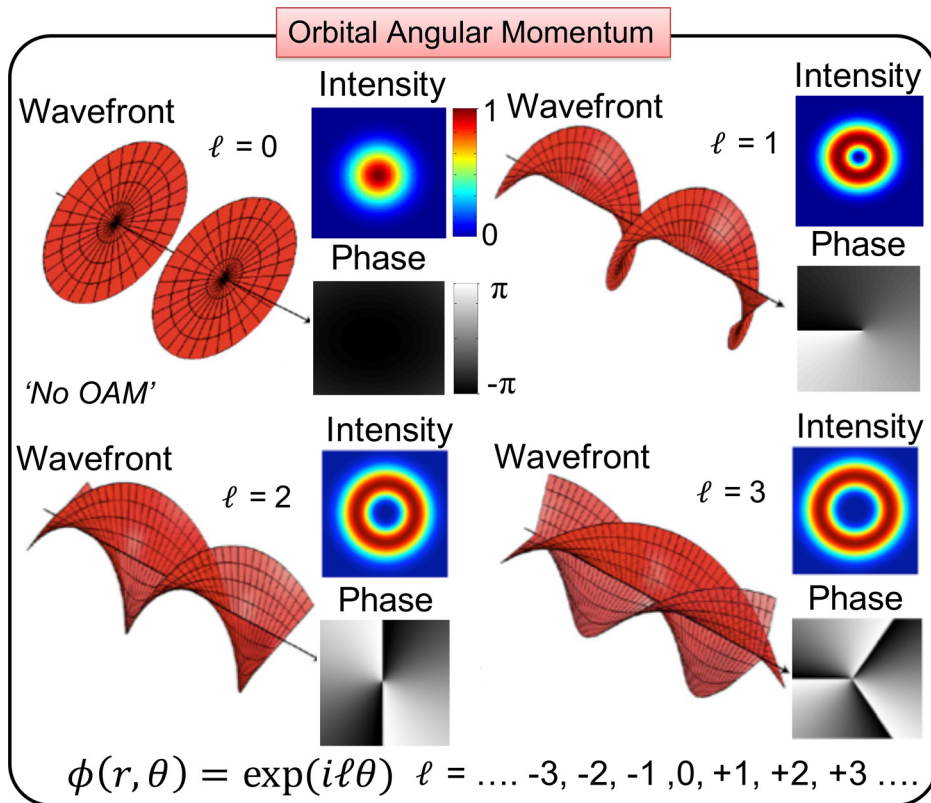


FIG. 1. The wavefronts, intensity profiles, and phase profiles of OAM beams with different ℓ values. Reproduced with permission from A. M. Yao and M. J. Padgett, Adv. Opt. Photonics 3, 161 (2011).⁶ Copyright 2011 Optical Society of America.

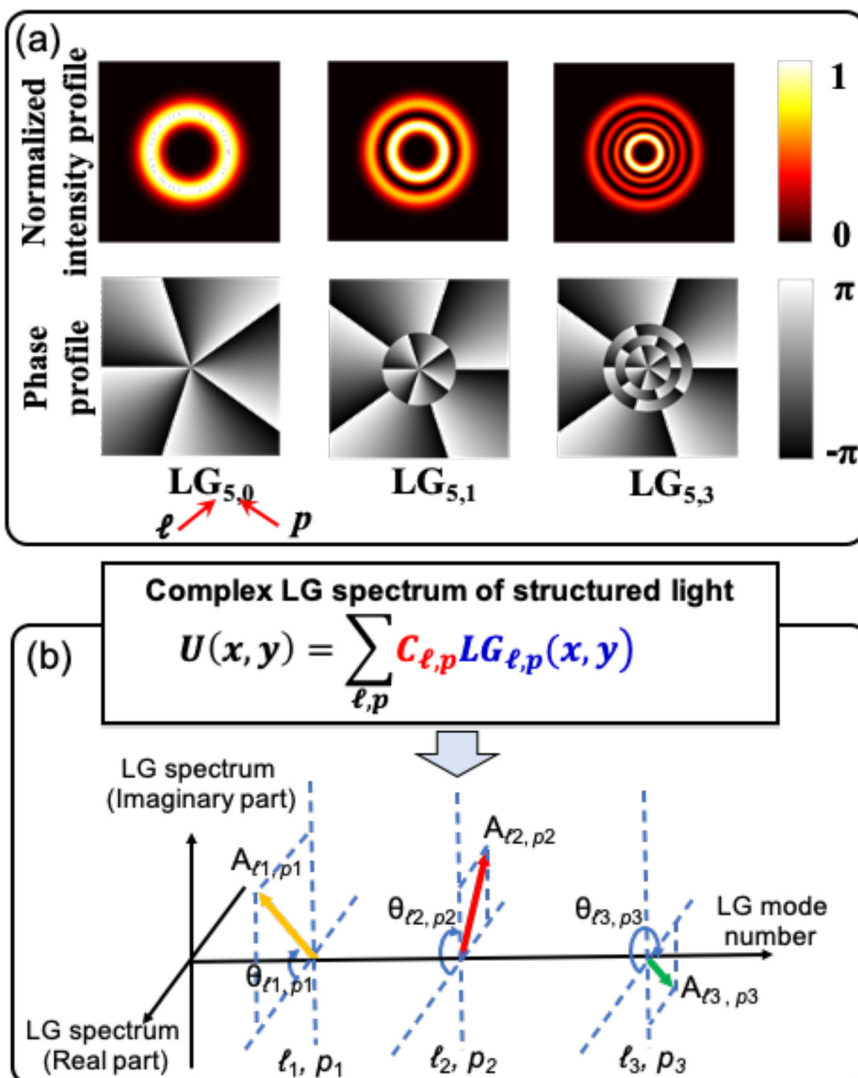


FIG. 2. (a) Intensity and phase profiles of LG beams with different pairs of indices (ℓ, p). (b) A structured beam can be decomposed into a set of LG modes with different ℓ and p values. The coefficients of LG components can be represented by a complex modal spectrum. Reproduced with permission from Li *et al.*, J. Opt. Soc. Am. B 34, 1 (2017).¹⁹ Copyright 2017 Optical Society of America.

orthogonal with each other for a given beam waist and propagation distance, which can be represented by^{9,10,20}

$$\int_0^\infty \int_0^{2\pi} LG(r, \theta, z; \ell_1, p_1) LG^*(r, \theta, z; \ell_2, p_2) r d\theta dr \\ = \begin{cases} 0 & \text{if } \ell_1 \neq \ell_2 \text{ or } p_1 \neq p_2 \\ 1 & \text{if } \ell_1 = \ell_2 \text{ and } p_1 = p_2 \end{cases}. \quad (5)$$

Such orthogonality of different LG modes also ensures the potential utilization of 2D LG modal basis in communication systems, which will be further discussed in Secs. II B and IV A.

Since LG modes are a complete 2D modal basis set, a structured beam can generally be decomposed into LG modes with different ℓ and p values. In general, the coefficients of LG components can be represented by a complex modal spectrum, as shown in Fig. 2(b). Moreover, it should be noted that each complex coefficient contains

both amplitude and phase information, which can be tuned such that a specific structured beam would be generated by a coherent superposition of these LG components for a desired function.²¹

Aside from LG beams, there has recently been much interest in other novel types of spatially structured beams, such as Bessel-type beams, Airy-type beams, and pin-like beams,^{4,22–29} and some of these beams have been reported and explored in various applications. Details will be further discussed in Sec. IX.

B. Application of OAM in communications

In the optical communications community, there is a growing interest in achieving high-capacity communication links. Previously, different physical properties of a light wave (e.g., wavelength, polarization, amplitude, and phase) have been explored to increase the data capacity. For example, the technique of multilevel amplitude/phase

modulation formats has facilitated dramatic increases in capacity and spectral efficiency.^{31–35} In addition, another typical method of increasing the data capacity is transmitting multiple independent data channels on light waves at different wavelengths or polarizations, which are wavelength-division multiplexing (WDM)^{31–33} or polarization-division multiplexing (PDM),^{31–35} respectively.

Recently, spatial modes have been under intense investigation in various areas.⁶ As one of the spatial orthogonal modal basis sets, OAM modes could potentially provide an infinite number of orthogonal OAM states. Therefore, OAM might be potentially utilized in communication systems, which would further increase the transmission capacity.

1. OAM multiplexing and encoding

There are generally two ways of utilizing OAM in communications. The first approach is so-called mode-division multiplexing (MDM), which is a subset of space-division multiplexing (SDM).^{12,36,37} In such a scheme, different OAM beams are utilized to carry different independent data channels. As shown in Fig. 3(a), since N independent data-carrying beams can be spatially multiplexed and simultaneously propagated over the same spatial medium (free space or fiber), the system's total data capacity would be increased by a factor of N . At the receiver side, due to the orthogonality between different OAM modes, different data-carrying beams can be efficiently demultiplexed with little inherent crosstalk. Moreover, MDM is generally compatible with the aforementioned WDM or PDM techniques. This means that in a WDM or PDM system, multiple orthogonal OAM beams that carry independent data channels could be located at each wavelength or polarization, thus further increasing the system's spectral efficiency (i.e., bit/s/Hz) and the total data capacity.^{11,12,38}

In addition, OAM modes can also be utilized in a data-encoding system. In this approach, N different OAM states can be encoded as N different data symbols, which represent “0,” “1,” ..., “ $N - 1$.” At the transmitter side, a sequence of OAM states are generated and sent in such a system at different times. Therefore, within each symbol period,

the light beam occupies one of N possible OAM states, and the number of information bits encoded equals $\log_2 N$, as shown in Fig. 4. At the receiver, the data can be efficiently separated and decoded by checking the received OAM state with little inherent crosstalk due to the orthogonality of different OAM states. It should be noted that this approach could also be utilized in quantum communications systems in which every single photon exists in one of the N possible OAM states. As a result, this would provide a photon efficiency of up to $\log_2 N$ bits per photon and, thus, could potentially achieve higher photon efficiency.^{15,17}

Recently, these two approaches have been demonstrated and employed mostly on large optical tables using bulky and expensive devices. Some examples of experimental demonstrations will be presented in Secs. IV–VII in different scenarios. However, for future OAM-based communication systems, integrated devices would seem to be significant due to their cost-effective, power-efficient, and compact features,³⁹ which will be further discussed in Sec. VIII.

On a fundamental level, these two techniques require that different modes can be efficiently combined and separated with little cross-talk, so almost any complete orthogonal modal basis set could be utilized. It should be noted that there have been some experimental demonstrations of communication links in free space or fiber based on other modal basis sets, such as LG, Hermite–Gaussian (HG), and linearly polarized (LP) modes.^{11–13,20,36,41,42} In general, an orthogonal modal basis set could be represented by two modal indices both of which can be employed in a communication link to further increase the transmission capacity.^{13,43} For example, such a 2D approach was experimentally demonstrated in an FSO MDM system based on LG or HG beams,^{13,20} which will be shown in detail in Sec. IV A.

2. Various potential challenges

In general, OAM modes could be potentially utilized in various communication systems. For example, the OAM-based MDM systems could be deployed either in free space or fiber. For different scenarios,

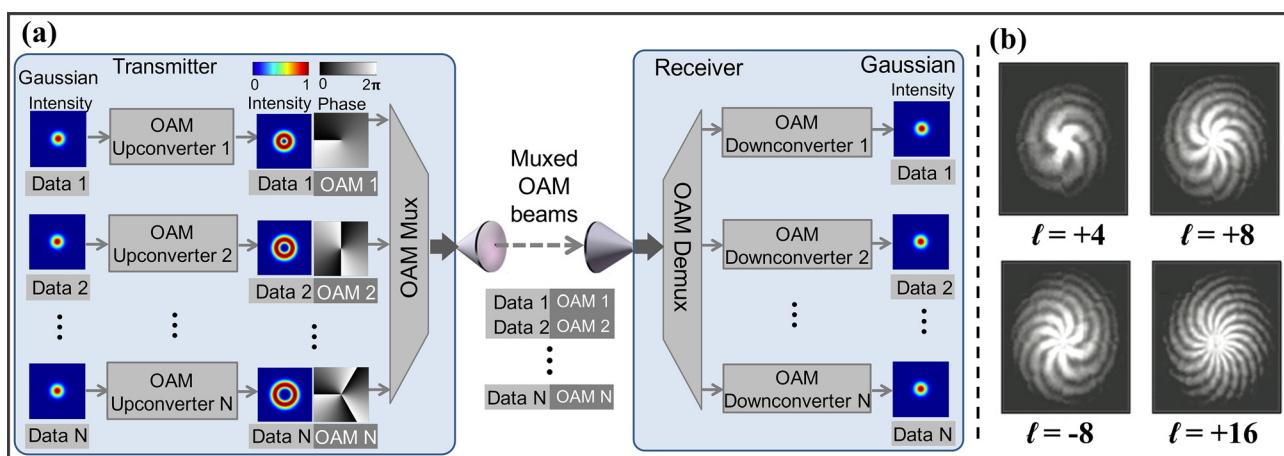


FIG. 3. (a) Concept of OAM-multiplexed free-space optical (FSO) links. Multiple independent data-carrying OAM beams can be multiplexed, spatially copropagate, and be demultiplexed with little crosstalk, thereby multiplying the system's data capacity. Reproduced with permission from A. E. Willner, Opt. Photonics News **32**, 34 (2021). Copyright 2021 Optical Society of America. (b) Different interferograms corresponding to OAM $+4$, OAM $+8$, OAM -8 , and OAM $+16$ beams. The interferograms can be obtained by the interference between each OAM beam and a Gaussian beam. In these interferograms, the number of twists indicates the magnitude of ℓ , with the sign implied by the twist direction. Reproduced with permission from Wang *et al.*, Nat. Photonics **6**, 488 (2012). Copyright 2012 Macmillan Publishers.

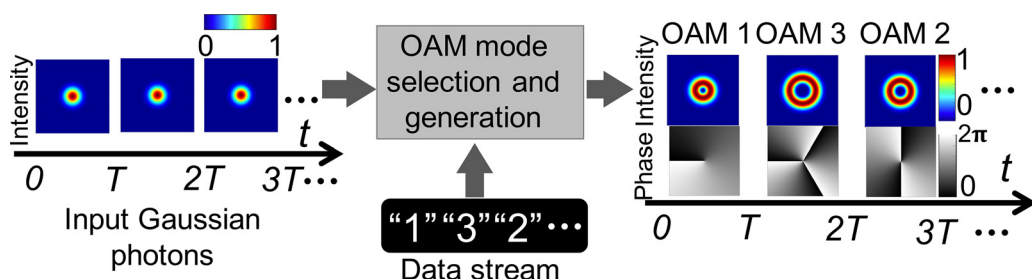


FIG. 4. (a) Concept of data encoding using OAM modes. Within each symbol period (T), the light photon/beam occupies one of N possible modes and the number of information bits encoded equals $\log_2 N$. Reproduced with permission from A. E. Willner, Opt. Photonics News **32**, 34 (2021).³⁰ Copyright 2021 Optical Society of America.

there are different key challenges, which might induce power loss and intermodal power coupling in communication systems, as shown in Fig. 5.

For free-space links, atmospheric turbulence is one of the key issues that can cause a random phase distortion to the transverse beam profile. Such random distortion is time-variant, and thus, it could induce dynamic intermodal power coupling.⁴⁴ As a result, this issue would induce modal coupling and crosstalk in both classical and quantum communication links.^{44–47} Moreover, in an OAM-based communication link, the receiver should be able to “distinguish” the transmitted spatial modes. When the receiver aperture size is limited and there is misalignment between the transmitter and the receiver, there could be relatively large power leakage in other undesired modes, and thus, the receiver could potentially fail to “distinguish” the actual transmitted modes.⁴⁸ Furthermore, the divergence of free-space higher-order beams tends to be more significant than that of lower-order OAM beams. For a receiver with a limited-size aperture, it would be harder to capture the whole higher-order OAM beams and, thus, induce power loss. Moreover, the beam truncation of a circular aperture could further induce modal power coupling to some LG modes with different p modes, leading to inter-channel crosstalk in LG-mode-based communication links.^{48–50} Some details and potential mitigation methods will be discussed in Secs. IV B and IV C.

For fiber-based links, the MDM and quantum encoding systems can also be achieved based on OAM modes. However, the fiber channel is distinct from the free space mainly in the following aspects.

(i) As the beam is guided in the fiber, it does not diverge.

(ii) The fiber will often cause cross-modal power coupling within the same mode group or between mode groups due to temperature gradients, different kinds of inhomogeneities, bends, and other non-idealities. In general, the intra-modal-group power coupling is relatively stronger. Some potential methods for mitigating mode coupling will be discussed in Sec. V C.

3. Different frequency ranges

As an orthogonal modal set, OAM modes can be manifested in many types of electromagnetic (EM) and mechanical waves and have been recently explored in acoustic, radio, millimeter, and THz waves for wireless communication links.^{51–64}

For OAM-based communication links operated in different frequency ranges, there tends to be a trade-off between the effects of beam divergence and wave-matter interaction, as shown in Fig. 6.

- (i) Divergence: OAM beams at lower frequencies have larger beam divergence. When the receiver's aperture size is limited, it becomes more difficult to capture enough of the beam for data channel recovery. Such a problem might be more serious when a higher-order OAM mode is used.
- (ii) Interaction with matter: there tends to be much more wave-matter interaction at higher frequencies. For example, optical waves suffer more atmospheric-turbulence-induced distortion and modal power coupling than radio waves in OAM-based links.

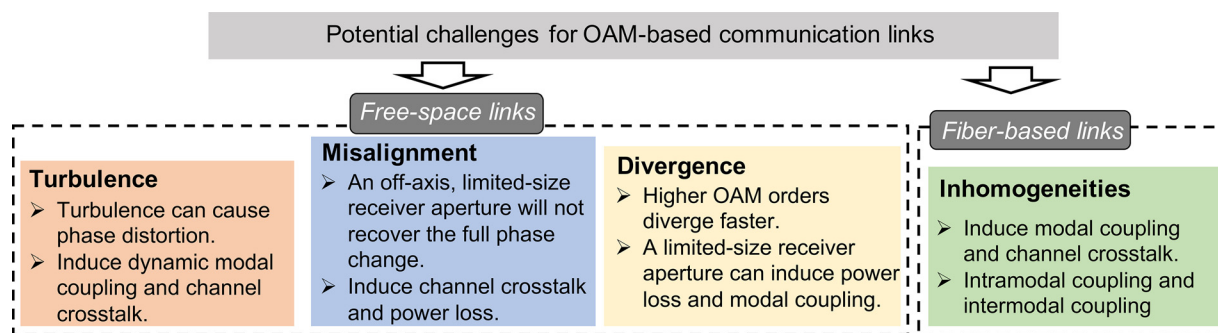


FIG. 5. Potential challenges for OAM-based communications systems. Reproduced with the permission from Willner *et al.*, APL Photonics **6**, 030901 (2021).⁴⁰ Copyright 2021 AIP Publishing.

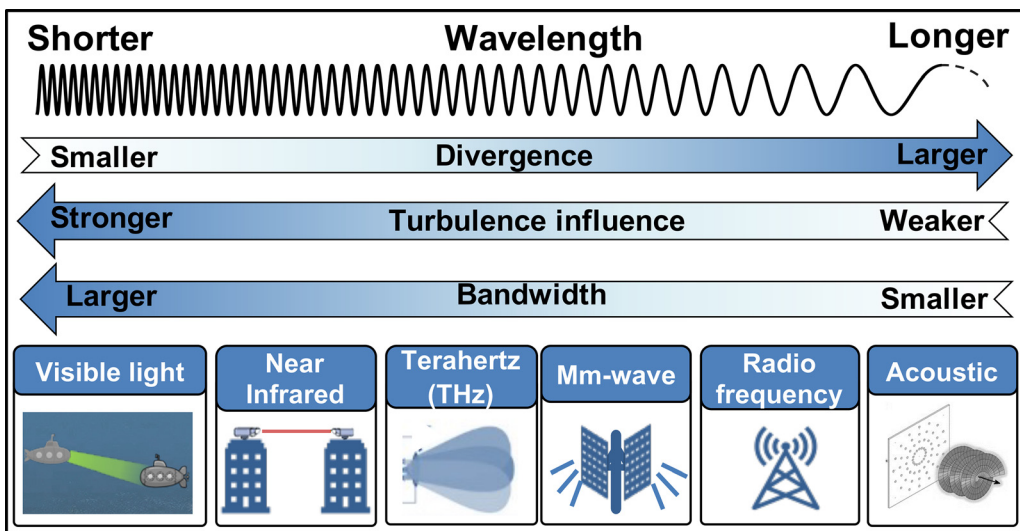


FIG. 6. OAM can be manifest in many types of electromagnetic and mechanical waves, such that it might be potentially used in different frequencies for communications. Reproduced with permission from A. E. Willner, Opt. Photonics News 32, 34 (2021).³⁰ Copyright 2021 Optical Society of America.

C. Digital modulation formats

In OAM-multiplexed communication links, digital data signals can be modulated on the amplitude and phase of the optical wave temporally, as shown in Fig. 7(a). In the amplitude modulation, the bits in the data streams are mapped to multiple amplitude levels of the optical wave. For example, an on-off keying (OOK) signal has two possible amplitude levels representing the bit “0” and “1.” Since only a single photodiode is required at the receiver to recover the amplitude

information, such modulation is usually considered to have a low cost and simple implementation.⁶⁵

In contrast, in the phase modulation, the bits are mapped to the temporal phase, and the amplitude remains constant. As an example, the quadrature phase shift keying (QPSK) has four possible phase levels, and one QPSK symbol can carry two bits. In addition, the amplitude and phase modulation can be simultaneously utilized to increase the number of bits carried by one symbol. As an example,

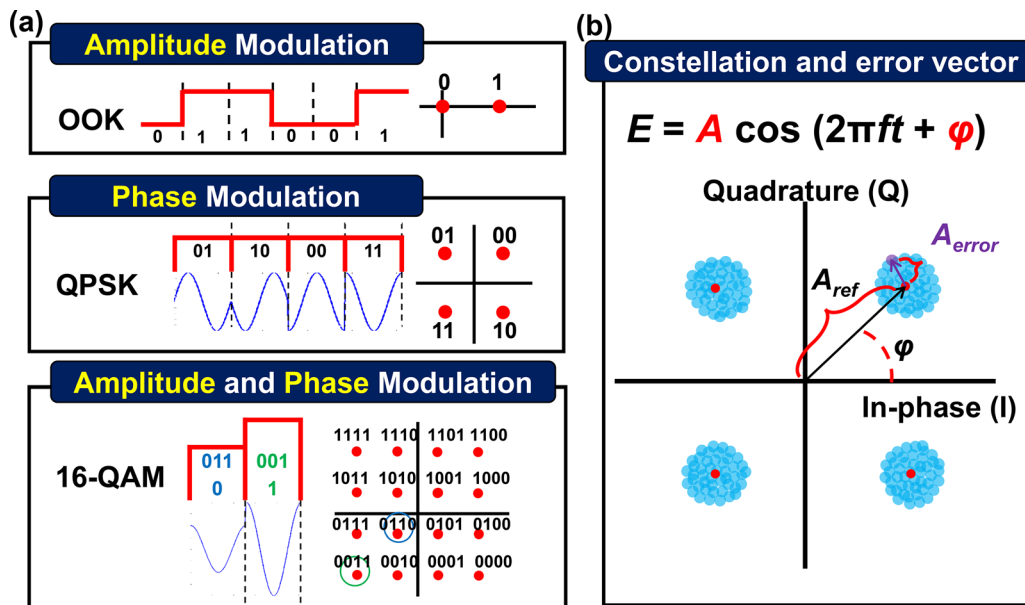


FIG. 7. (a) The data signal can be modulated on the amplitude and/or phase of an optical wave [e.g., on-off keying (OOK), quadrature phase shift keying (QPSK), and 16-quadrature amplitude modulation (16-QAM)]. (b) The constellation and the error vector of a QPSK signal.

16-quadrature-amplitude-modulation (16-QAM) has 16 possibilities mapped on the in-phase and quadrature amplitude axes encoding four bits of information. Unlike the amplitude modulated signals, coherent detection is often used at the receiver to extract the phase information when the temporal phase is also encoded with data.⁶⁶ In a coherent receiver, the received signal is sent to a 90° hybrid along with the continuous-wave (CW) local oscillator (LO) laser and detected by balanced photodiodes.⁶⁶

The quality of the received signal can be characterized by the bit error rate (BER), which is defined as the ratio between the number of bit errors and the total number of the received bits.⁶⁷ Alternatively, error vector magnitude (EVM) can be used to determine the quality of the received signal.⁶⁷ As shown in Fig. 7(b), the received symbols are represented by the points on the constellation according to their amplitudes and temporal phases. Due to the noise and distortions during transmission, the received symbol may deviate from the transmitted symbol, resulting in an error vector A_{error} . The EVM is calculated by the ratio between the root mean square of the error vectors A_{error} and the reference vector A_{ref} ,⁶⁷

$$\text{EVM}(\%) = \frac{\sqrt{\frac{1}{N} \sum_{i=0}^N |A_{\text{error},i}|^2}}{|A_{\text{ref}}|} \times 100\% \quad (6)$$

III. OAM GENERATION, DETECTION, AND (DE)MULTIPLEXING

For an OAM-based communication system, fundamental functions include OAM generation, detection, and (de)multiplexing. Generally, it is desirable to generate OAM beams with high mode purity and detect OAM beams efficiently. Moreover, in an OAM-multiplexed system, developing efficient and scalable techniques for (de)multiplexing the coaxial OAM beams is challenging. These methods could be either bulky or integrated. In this section, we will focus on the bulky methods. The integrated methods will be discussed in Sec. VIII.

A. OAM generation and detection

Generally, there are multiple types of approaches for OAM generation and detection. The first method is the spatial phase control, which can spatially (de)modulate a single beam in the azimuthal direction θ with a factor of $\exp(-i\ell\theta)$. One straightforward way to implement this method is to use a spiral phase plate (SPP) that has a helical dielectric surface,^{68,69} as shown in Fig. 8(a-1). The height gradient of the surface along the azimuthal direction is given as⁶⁸

$$\frac{\partial h}{\partial \theta} = \frac{\ell\lambda}{2\pi(n-1)}, \quad (7)$$

where λ and n are the wavelength and refractive index of the SPP, respectively. The simplicity of the structure makes it feasible to be applied in different frequency domains.^{51,70,71}

However, the OAM order of the generated beam by the SPP-based approach is generally fixed. One reconfigurable approach is to use a computer-generated hologram (CGH), as shown in Fig. 8(a-2). Such a hologram could be implemented by a spatial light modulator (SLM) or a digital micromirror device. Importantly, the generated OAM beam can be modified by simply updating the hologram. However, the mode purity could be affected by the unmodulated light, which could be due to the direct reflection from the surface glass or “dead area” between the pixels.⁷² Hence, a “fork” hologram, which combines the spiral phase pattern and linear phase ramp (grating), is applied to separate the first-order modulated light and the zeroth-order unmodulated light, as shown in Fig. 8(a-3). The “fork” hologram can be characterized by⁷³

$$\Psi = \exp(-i\Phi) = \exp\left[-i\left(\ell\theta + \frac{2\pi x}{T}\right)\right], \quad (8)$$

where Φ and T are the phase distribution and the period of the linear phase ramp, respectively. It should be noted that, in most cases, the resulting beam generated by a spiral phase pattern is not a pure LG mode (e.g., $LG_{\ell,p=0}$), but rather a superposition of modes with different radial indices ($\sum_p LG_{\ell,p}$). To generate a pure $LG_{\ell,p}$ mode with high mode purity, one should jointly control both the phase and amplitude of the input beam.^{74–77} This could be achieved by a phase-

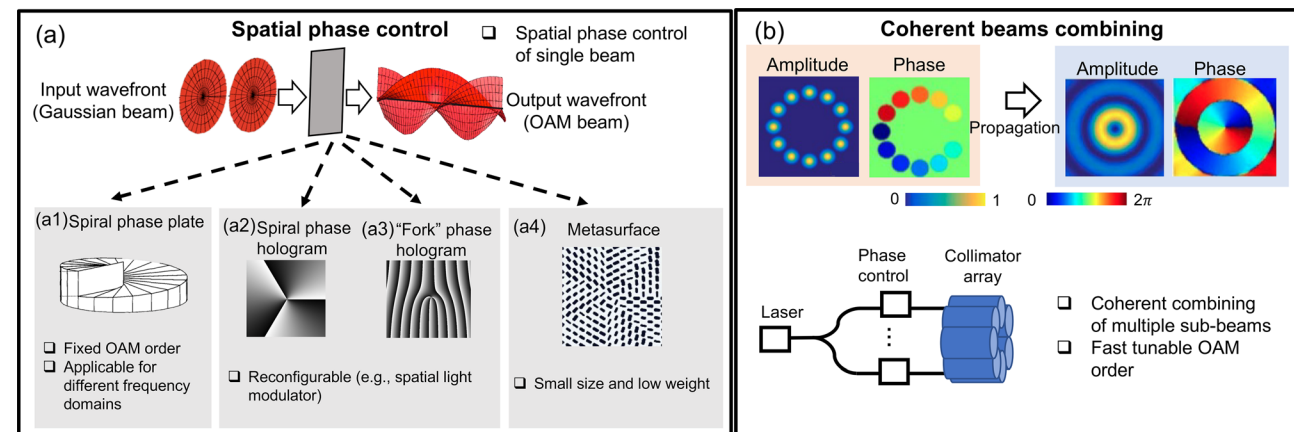


FIG. 8. OAM generation by (a) utilizing the spatial phase control of a single beam or (b) combining multiple coherent beams. Different ways to implement the spatial phase control of a Gaussian beam include (a-1) a spiral phase plate, (a-2) a spiral phase hologram, (a-3) a “fork” phase hologram, and (a-4) a metasurface.

only SLM. Specifically, the phase of the beam is spatially modulated by loading a phase pattern on the SLM. In addition, the amplitude of the beam can be spatially controlled by adding a grating pattern whose diffraction efficiency is carefully designed at different positions.^{74–77}

Compared with the CGH approach, which could be limited in some applications requiring a small footprint,⁷⁸ recent development of novel materials enables OAM generation using an ultrathin metasurface, which assembles a 2D array of diffractive optical elements with variant subwavelength structures along the azimuthal direction,^{79–83} as shown in Fig. 8(a–4). By engineering metasurfaces, OAM beams could be generated with a high conversion efficiency over a broad bandwidth.⁸³ Moreover, different OAM orders can be achieved independently for different polarizations.^{81,82}

Furthermore, OAM generation could be achieved not only by manipulating a single beam but also coherently combining multiple sub-beams. The theoretical expression of OAM generation by coherently combining sub-beams with each carrying a specific phase is as follows:⁸⁴

$$u_{out} = \sum_{k=1}^N u_k = \sum_{k=1}^N u_0(x - R \cos \theta_k, y - R \sin \theta_k) \exp(-i\ell\theta_k), \quad (9)$$

where N is the number of sub-beams, u_k and $\theta_k = \frac{2\pi k}{N}$ are the electric field and azimuthal location of the k -th beam, respectively, and R is the center-to-center distance between the individual beam and synthesized beam, as shown in Fig. 8(b). By tuning the relative phase between different sub-beams, a desired OAM beam could be generated. Moreover, based on high-speed phase modulation, the approach could potentially generate an OAM beam with a fast-tunable order.⁸⁵ Furthermore, similar ideas of coherent beam combinations in a circular phase array could also be applied to other frequency domains (Sec. VII) and in integrated device (Sec. VIII).

Some of the aforementioned OAM generation methods are not limited in free-space applications but could be applied to OAM generation in fiber as well. OAM generation in fiber could be achieved using various methods, including the free-space coupling of OAM beams (e.g., SPP⁷⁰ and phase hologram¹¹) or utilizing fiber-based mode converters (e.g., photonic lanterns⁸⁶ and long-period gratings⁸⁷).

In addition, most approaches of the OAM generation methods above could also be used for OAM detection.⁷ Specifically, the OAM beam could be converted back to a Gaussian-like beam by propagating through a conjugate SPP, phase hologram, or metasurface.⁷

B. OAM multiplexing and demultiplexing

Multiple approaches have been demonstrated to multiplex OAM beams with different orders. One straightforward way is to use beam splitters. Each beam splitter could coaxially multiplex two beams with a proper alignment, and N independent OAM beams could be multiplexed by $N - 1$ cascaded beam splitters, as shown in Fig. 9(a). Even though there is $1/N$ intrinsic loss theoretically, the simplicity of the beam splitter approach makes it appropriate for lab demonstrations.

A more efficient (de)multiplexing method is to use cascade interferometers, as shown in Fig. 9(b). First, the OAM beam is split into two branches of the Mach-Zehnder interferometer (MZI). For one of the branch, a pair of Dove prisms is used to perform an OAM-dependent phase shift as follows:⁸⁸

$$\Delta\Phi = \ell\alpha, \quad (10)$$

where $\alpha/2$ is the relative angle between the two Dove prisms. Subsequently, the beams from the two branches with an OAM-dependent phase difference are coherently combined with constructive and destructive interference at two output ports, respectively. Hence, two different OAM modes could be efficiently separated into different output ports based on different induced phase differences between the two branches, as shown in Fig. 9(b-1). By cascading MZIs and carefully designing the phase delays of the MZI branches, multiple OAM beams with different OAM orders would be demultiplexed to different output ports of the MZIs, as shown in Fig. 9(b-2). In order to demultiplex N OAM modes, $N - 1$ interferometers are generally required. Furthermore, similar idea could be applied for radial modes by replacing the Dove prisms with a lens.⁸⁹

The functions of mode generation and multiplexing (or mode demultiplexing and detection) can be further achieved in one device simultaneously. One straightforward way is to combine multiple fork phase patterns together to form a single phase plate, that is, Dammann optical vortex grating (DOVG), as shown in Fig. 10(a). The theoretical expression of the DOVG is as follows:⁹⁰

$$\Psi = \exp(-i\Phi) = \sum_{n=-N/2}^{N/2} E_n \exp\left[-in \times \left(\Delta\ell\theta + \frac{2\pi x}{T}\right)\right], \quad (11)$$

where N is the total number of diffraction orders, T is the period of the grating, n is the diffraction order from $-N/2$ to $N/2$, and $\Delta\ell$ is the interval of the OAM order. $|E_n|^2 = 1/N$ is the power of the n -th order normalized with respect to the total power. From the input side, a Gaussian beam is incident from the n -th-order diffractive direction to the DOVG. At the output, the diffraction component in the same zeroth-order diffractive direction will be generated with the OAM order of $n \times \Delta\ell$. Therefore, multiple incident beams from different order diffractive directions could be used to generate and multiplex different OAM beams. Theoretically, DOVG induces $1/N$ insertion loss caused by non-zeroth-order diffraction at the output.

Compared with the DOVG approach, a more efficient and scalable method is to utilize two phase plates to achieve log-polar transformation between the spiral spatial phase of OAM beams and tilted spatial phase,⁹¹ as shown in Fig. 10(b). In this scheme, the first phase plate performs a log-polar transformation that geometrically maps “concentric circles” to “parallel straight lines.” As a result, the point at the input plane (x, y) is transformed to the new point (u, v) in the output Fourier plane where $u = -a \ln\left(\frac{\sqrt{x^2+y^2}}{b}\right)$ and $v = \arctan\left(\frac{y}{x}\right)$. Here, a and b are the scaling factors. Then, the second phase plate is placed at the Fourier plane to correct the phase error and collimate the transformed beams. Therefore, using two phase plates could achieve the efficient sorting of different OAM beams with no inherent loss. As the transformation is reciprocal, such a log-polar-based mode sorter could also be used for OAM generation and multiplexing.

Even though the log-polar transformation is scalable to a large number of modes, it could only be applied on a 1D mode basis.⁹² One way to generate and multiplex LG modes with 2-D modal indices is to use a multi-plane light convertor (MPLC) to shape the wavefront of the input light at multiple propagating distances. A unitary transform from multiple Gaussian beams at different locations to multiple LG beams with different (ℓ, p) pairs could be accomplished as shown

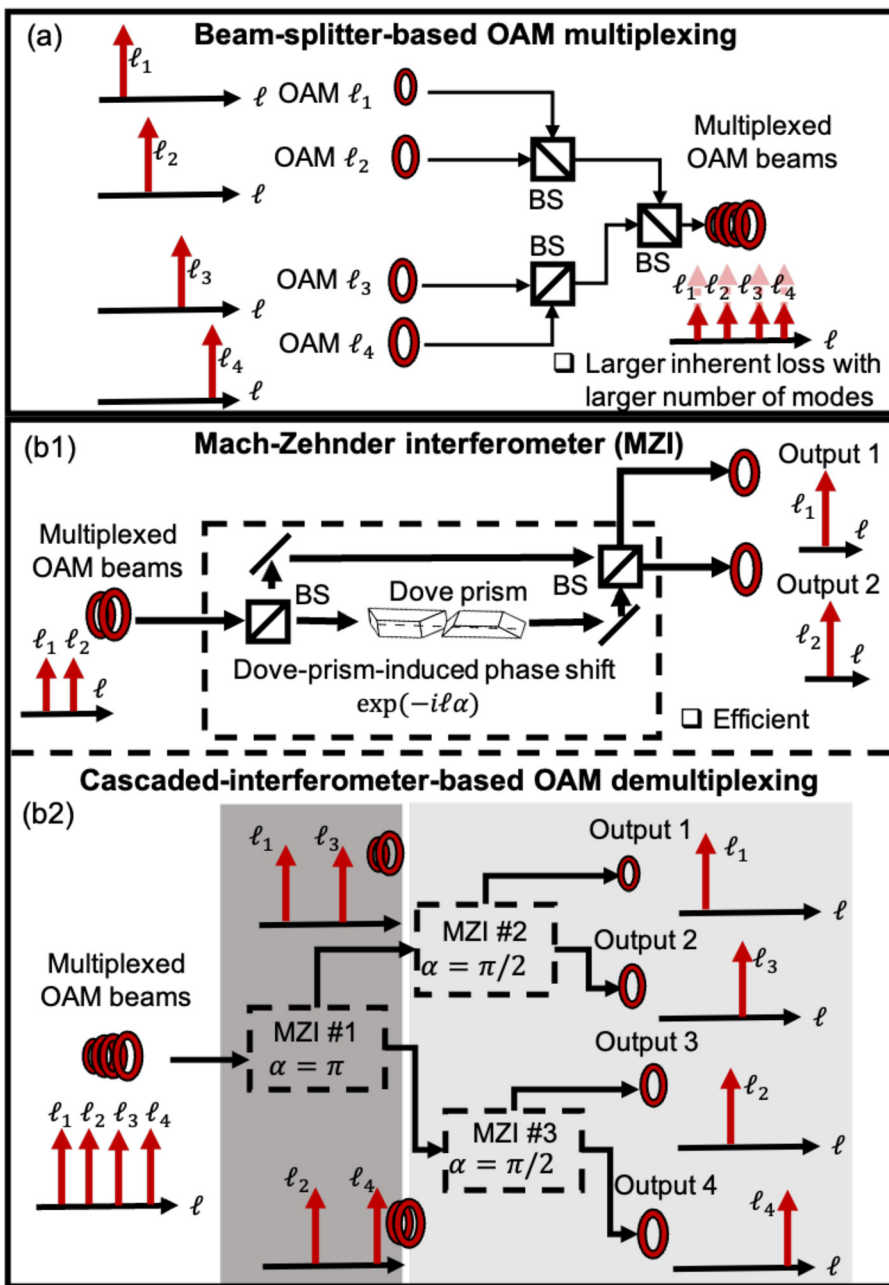


FIG. 9. (a) Concept of OAM multiplexing using beam splitters. BS: beam splitter. (b-1) Concept of OAM demultiplexing using a Mach-Zehnder interferometer (MZI) with a Dove-prism-induced phase shift. The Dove prism could induce an OAM-dependent phase shift in one branch. With the constructive and destructive interference, two different OAM modes could be efficiently separated into different output ports based on different induced phase difference between the two branches. (b-2) One example of demultiplexing OAM beams with neighboring mode orders using cascaded MZIs.

in Fig. 10(c).⁹² Generally, the phase patterns of MPLC could be determined by the wavefront matching method. The theoretical expression of the phase pattern at each propagation distance is as follows:⁹²

$$\Phi(z = z_k) = \arg \left\{ \sum_{i=1}^N u_{\text{input},i}(z = z_k) u_{\text{output},i}^*(z = z_k) \right\}, \quad (12)$$

where $u_{\text{input},i}$ and $u_{\text{output},i}^*$ are the i -th input field forward propagating and conjugate output field backward propagating at $z = z_k$, respectively. N is the number of the input and output fields. It has been

experimentally demonstrated to generate 210 LG modes using a 7-plane MPLC device with an insertion loss of <-12 dB.⁹² However, this approach might require an accurate alignment of these phase plates in order to achieve a high mode purity.^{92,93}

C. Summary

In this section, various OAM generation/detection approaches are first discussed. Subsequently, different methods for (de)multiplexing multiple coaxial OAM beams are presented. In order to further

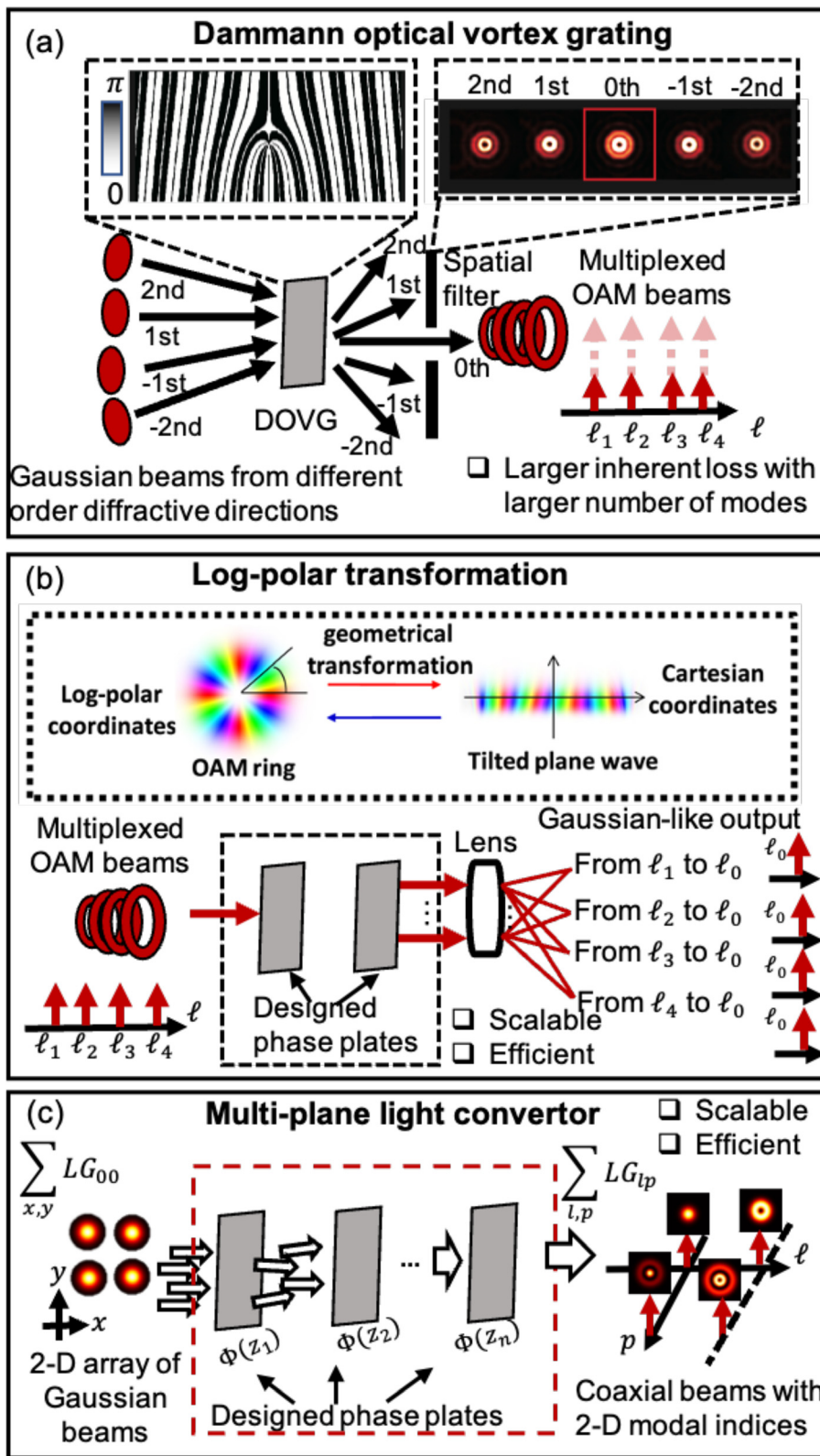


FIG. 10. (a) Concept of Dammann optical vortex grating for generating and multiplexing OAM beams. (b) Concept of log-polar transform for efficiently generating and multiplexing OAM beams. (c) Concept of multi-plane light convertor for efficiently generating and multiplexing LG beams with different 2D modal indices. Reproduced with permission from Willner *et al.*, *Adv. Opt. Photonics* 7, 66 (2015).⁷ Copyright 2015 Optical Society of America.

improve and deploy OAM generation/detection/(de)multiplexing techniques for OAM-based communication systems, some desirable features could include (i) efficient OAM mode generation with a high mode purity and (ii) fast tunability covering a range of OAM modes.

IV. OAM-BASED FREE-SPACE OPTICAL COMMUNICATION SYSTEMS

As compared to RF links, optical links can generally provide more bandwidth and higher data capacity due to the higher carrier wave frequency. Moreover, OAM modes can be potentially used in a free-space optical communication system (MDM or encoding systems) for high data capacity. However, in free-space links, there are some critical issues that induce power loss and channel crosstalk, including divergence, misalignment, and atmospheric turbulence. In this section, we will review (i) typical experimental demonstrations of OAM-multiplexed or -encoded free-space optical communications, (ii) potential challenges in an OAM-based free-space link, (iii) reported approaches for mitigating power loss and channel crosstalk, and (iv) OAM-based communication systems for airborne platforms or underwater environments.

A. OAM-multiplexed and -encoded free-space links

In general, the flexibility of the OAM-based communication enables its compatibility with (i) either direct detection or coherent detection techniques, (ii) different modulation formats, and (iii) other multiplexing techniques (e.g., WDM and PDM). In this subsection, two different ways (i.e., OAM multiplexing and OAM encoding) of utilizing OAM for communication will be discussed. Furthermore,

both short-distance laboratory and long-distance field demonstrations will be shown.

1. OAM-multiplexed free-space links

Initial demonstrations of OAM-multiplexed optical communications include a free-space OOK link that multiplexed an OAM beam and a Gaussian beam.⁹⁴ Subsequently, an OAM-multiplexed link⁹⁵ with a spectral efficiency of 12.8-bit/s/Hz has been achieved using four OAM modes, each carrying a 10.7-Gbaud 16-QAM signal. Later on, the spectral efficiency is doubled by combining PDM into the OAM-multiplexed link.¹² Eight OAM channels, each carrying an independent 42.8-Gbaud 16-QAM signal, could be used to achieve a communication link with a total capacity of 1.4 Tbit/s ($4 \times 4 \times 2 \times 42.8$ Gbit/s), as shown in Fig. 11(a).

The following experiment further increases the link capacity to 100 Tbit/s by combining OAM multiplexing with PDM and WDM.³⁸ Figures 11(b-1)–11(b-3) show the steps used in the proof-of-concept demonstration. First, two groups of OAM beams ($\ell = \{+4, +10, +16\}$ and $\{+7, +13, +19\}$), are generated and multiplexed using a beam splitter. Each beam carries 42 WDM channels with the channel spacing of 100 GHz. Second, the six multiplexed beams are split into two copies. One copy is decorrelated in free space and reflected to create another six OAM beams with inverse charges. Then, these two copies are combined to prepare 12 multiplexed OAM beams. Third, the 12 multiplexed OAM beams are again split into two copies. One copy is decorrelated in free space and polarization-rotated by 90°, and then two copies are combined to generate 24 OAM beams. The observed WDM signal spectrum on one of the demultiplexed OAM

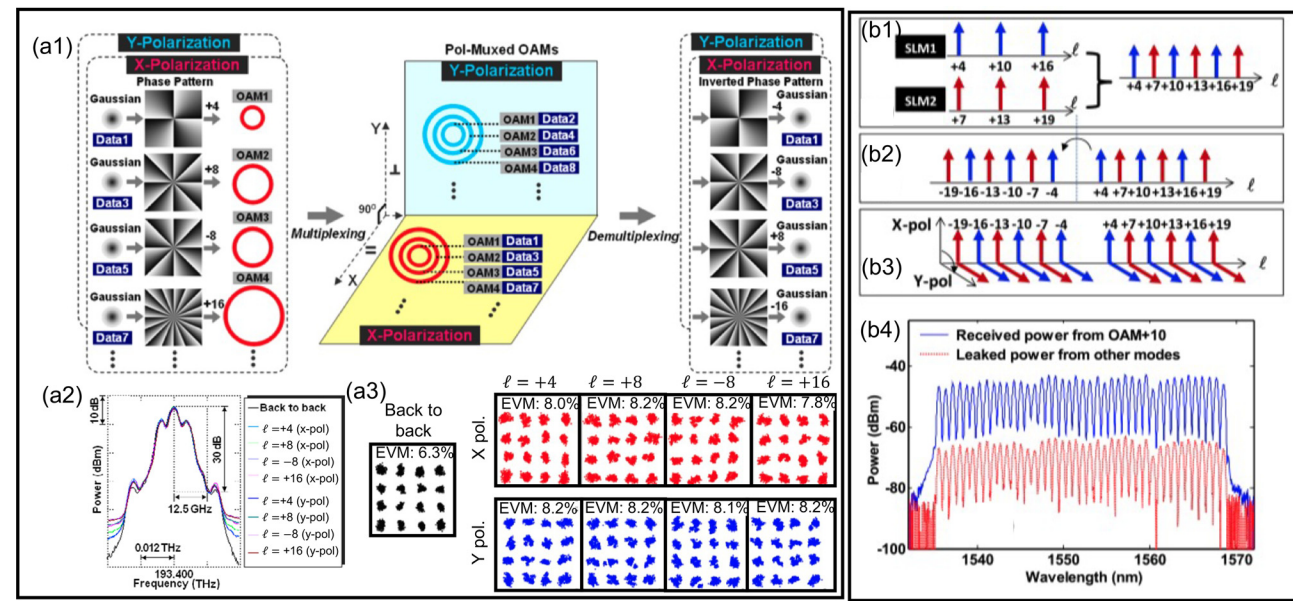


FIG. 11. (a-1)–(a-3) Concept and experimental results of a free-space OAM-multiplexed link combining PDM. (a-1) Concept of an OAM-multiplexed link combined with PDM. Pol-muxed: polarization-multiplexed. (a-2) Measured spectrum and (a-3) constellations of 16-QAM signals for four pol-muxed OAM beams. Reproduced with permission from Wang *et al.*, Nat. Photonics **6**, 488 (2012).¹² Copyright 2012 Macmillan Publishers. (b-1)–(b-4) Concept and experimental results of a free-space OAM-multiplexed link combining PDM and WDM. (b-1)–(b-3) Concept of generating 24 multiplexed OAM beams with two polarizations. (b-4) The optical spectrum of the received power of the WDM channels carried by the OAM beam of $\ell = +10$. Reproduced with permission from Huang *et al.*, Opt. Lett. **39**, 197 (2014).³⁸ Copyright 2014 Optical Society of America.

beams ($\ell = +10$) is shown in Fig. 11(b). Moreover, by utilizing 54.139-Gbit/s 8-QAM signals carried on 368 wavelengths, 2 polarizations, and 26 OAM beams, a free-space data link with a total data rate of 1.036 Pbit/s and a spectral efficiency of 112.6 bit/s/Hz has been demonstrated.⁹⁶ Both demonstrations indicate that OAM is compatible with existing degrees of freedom (e.g., amplitude/phase/wavelength/polarization).

For the aforementioned OAM-based communication links, the experimental demonstrations are generally conducted in the laboratory over short distances of ~ 1 m. There have been several experimental demonstrations that utilize OAM multiplexing for a long-distance free-space links in the field environment.^{97,98} For example, a 120-m free-space OAM-multiplexed link with the total capacity of 400 Gbit/s has been demonstrated,⁹⁷ as shown in Figs. 12(a-1)–12(a-3). The transmitted OAM beams ($\ell = \pm 1, \pm 3$), each carrying a 100-Gbit/s QPSK data channels, are transmitted. The transmitted OAM beams at site #1 are reflected twice by two mirrors placed 30 m away at site #2 to achieve an aggregated 120-m propagation path. The BERs of the four data channels carried by the OAM beams are achieved below the 3.8×10^{-3} forward error correction (FEC) limit as shown in Fig. 12(a-3). In addition, a 260-m two-OAM-multiplexed communication link between two buildings has also been demonstrated. Each OAM beam carries 16-QAM signals to achieve an 80-Gbit/s aggregated data rate.⁹⁸ Potential challenges in a long-distance OAM-based free-space link will be discussed in Sec. IV B.

2. OAM-encoded free-space links

The OAM-encoded scheme is realized by encoding each data symbol with a unique OAM mode, i.e., representing the data stream as a sequence of different OAM beams. Based on this scheme, a classical free-space OAM-encoded link has been demonstrated.¹⁴ By utilizing

the programmable SLM, one of the eight OAM states ($\ell = \pm 16, \pm 12, \pm 8, \pm 4$) is transmitted at a time. To achieve a high data rate, fast switching might be required between different OAM modes. Using high-speed lithium-niobate switches, a 20-Gbit/s OAM-encoded link using four OAM modes ($\ell = \pm 1, \pm 3$) has been demonstrated.¹⁵ The application of the OAM encoding scheme in the quantum communication link will be discussed in Sec. VI.

Aside from the efforts of achieving long-distance OAM-multiplexed links, an OAM-based encoding system over a link distance of 143 km has been achieved.¹⁶ Figure 12(b-1) shows the concept and the experimental setup for the 143-km OAM-encoded link between two islands. The transmitted beam is modulated by an SLM with specific phase patterns to generate different superpositions of OAM modes. After being magnified by a telescope, the expanded beam propagates through the free space over 143 km. At the receiver, a camera records the received mode structures. The lobed modal structure is visible for different superpositions of OAM modes $\ell = \pm 1, \ell = \pm 2$, and $\ell = \pm 3$, as shown in Fig. 12(b-2). By introducing a relative phase of π , rotation of the mode structure of the $\ell = \pm 3$ is clearly recorded. By distinguishing images of different OAM mode superpositions, the OAM-based encoded data are recovered with an error rate of 8.33%. Due to the effects of atmospheric turbulence, a pattern recognition algorithm based on an artificial neural network is applied. The results indicate that it is feasible to achieve the free-space OAM-based link over a kilometer-scale distance.

3. LG-based free-space links by varying both modal indices

The aforementioned MDM-based FSO communication systems are achieved by utilizing one-dimensional modal basis. Specifically, each OAM beam carries the same p value (i.e., LG mode with $p = 0$

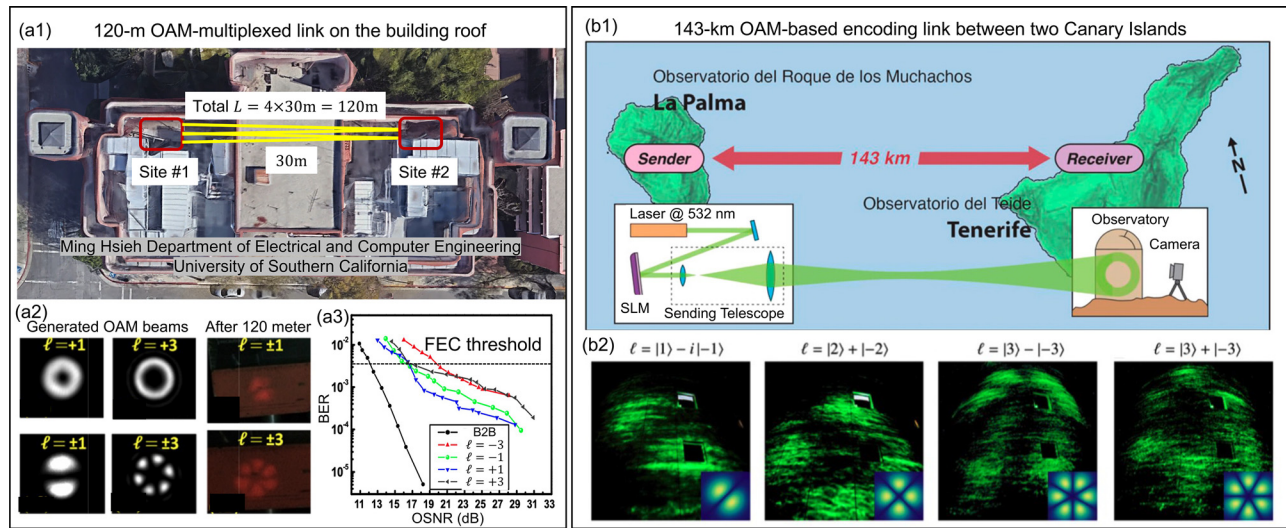


FIG. 12. (a-1)–(a-3) The 120-m OAM-multiplexed link. (a-1) Link layout of the 120-m OAM-multiplexed link on a building roof. (a-2) Measured intensity profiles and superpositions of OAM beams. (a-3) Measured BERs for all four OAM-multiplexed channels as a function of OSNR. B2B: back to back. Reproduced with permission from Ren *et al.*, Opt. Lett. **41**, 622 (2016).⁹⁷ Copyright 2016 Optical Society of America. (b-1) and (b-2) The 143-km OAM-based encoding link. (b-1) Link layout and experimental setup of the OAM-based encoding link. (b-2) Beam profiles of superpositions of OAM beams. Reproduced with permission from Krenn *et al.*, Proc. Natl. Acad. Sci. U. S. A. **113**, 13648 (2016).¹⁶ Copyright 2016 United States National Academy of Sciences.

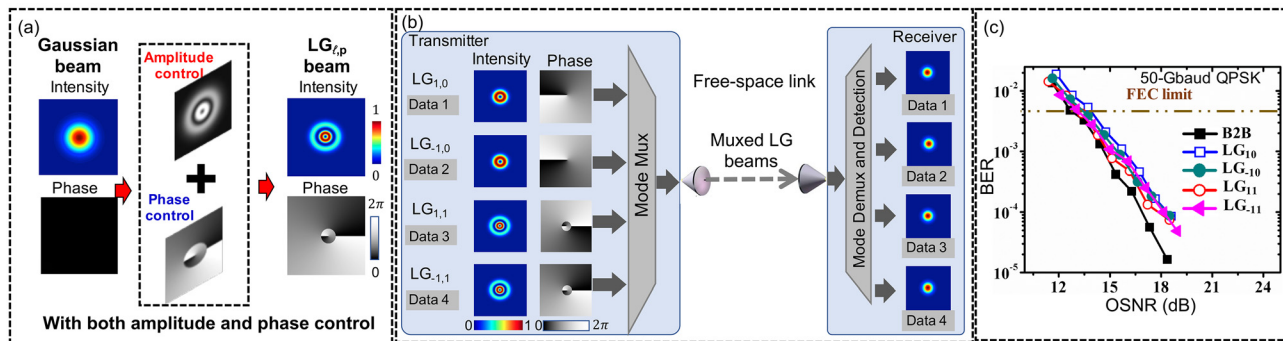


FIG. 13. (a) LG beam generation based on both the amplitude and phase control of the input Gaussian beam. (b) Concept of the four-LG-multiplexed link. (c) Measured BER performance of four data channels carried by different LG beams. B2B: back to back. Reproduced with permission from Pang *et al.*, Opt. Lett. **43**, 3889 (2018).¹³ Copyright 2018 Optical Society of America.

and different ℓ values). In addition, LG beams with different p values and same ℓ have been experimentally utilized in 200-Gbit/s MDM FSO links.²⁰ While various spatially orthogonal beams could be employed in these one-dimensional systems (varying ℓ values or varying p values), one could also utilize the two-dimensional modal basis (varying both ℓ and p values) to potentially support a larger set of mode-carrying channels.

As a proof of concept, a four-LG-multiplexing (LG_{10} , LG_{-10} , LG_{11} , LG_{-11}) link has been demonstrated,¹³ as shown in Fig. 13(b). Utilizing a designed hologram of SLM,⁹⁹ the amplitude and phase profiles of the input data-carrying Gaussian beam could be controlled, as shown in Fig. 13(a). As a result, a desired $\text{LG}_{\ell,p}$ beam with specific radial and azimuthal indices could be generated. In such a link, each LG beam carries a 100-Gbit/s QPSK channel to achieve a total data rate of 400 Gbit/s with the BERs lower than the FEC limit, as shown in Fig. 13(c). In addition, an LG-encoded system has been demonstrated by encoding information using four LG modes.⁴³ The information of a 2-bit gray-scale image representing four possible pixel values of “00,” “01,” “10,” and “11” has been successfully encoded and decoded utilizing four $\text{LG}_{\ell,p}$ modes (LG_{50} , LG_{-50} , LG_{21} , LG_{-21}). In order to maintain orthogonality among different LG modes, the receiver aperture would be required to fully capture the data-carrying beam. This might induce some potential challenges in LG-based free-space links, especially when the receiver has a limited-size aperture, which will be discussed in Sec. IV B.

B. Challenges in an OAM-based FSO link

There are some critical issues in an OAM-based FSO system, including channel power loss, inter-modal power coupling, and inter-channel crosstalk. As shown in Fig. 14, there are many causes of these issues for OAM-based FSO links:

- (a) Divergence: The divergence of free-space higher-order OAM beams tends to be more significant than that of OAM beams with lower mode orders. When the receiver aperture size is limited, it is harder to capture the whole OAM beam with a higher mode order and, thus, induces power loss. Moreover, the beam truncation in the radial direction could further induce modal power coupling to some LG modes with different p values.^{9,48–50}

- (b) Misalignment: In an OAM link, the receiver should be able to “distinguish” the transmitted modes. When the transmitter and receiver are misaligned (i.e., not coaxial), the limited-size receiver could potentially fail to fully capture the phase change in the azimuthal direction. At the receiver side, there could be relatively higher power leakage in other undesired modes, making it difficult for the receiver to “distinguish” the actual transmitted modes..^{48,100}
- (c) Turbulence: When an optical beam propagates through a turbulent medium, a random phase distortion is induced on the transverse beam profile. Such phase distortion breaks the orthogonality between different modes. Thus, the time-variant random phase distribution could induce dynamic intermodal power coupling. This might be in the order of milliseconds.^{44–47}

1. Divergence

In an FSO link, the system is sometimes limited by the size of optical components (e.g., limited-size receiver aperture), and thus the beam divergence could increase the difficulty of fully capturing the beam profile. This could induce signal power loss, which lowers the signal-to-noise ratio (SNR) and, thus, affects the BER performance of the recovered signal in a communication system. In general, various system parameters are related to beam divergence, including wavelength, propagation distance, and transmitted beam size.⁴⁸ Specifically, the beam divergence of an MDM system is also dependent on the

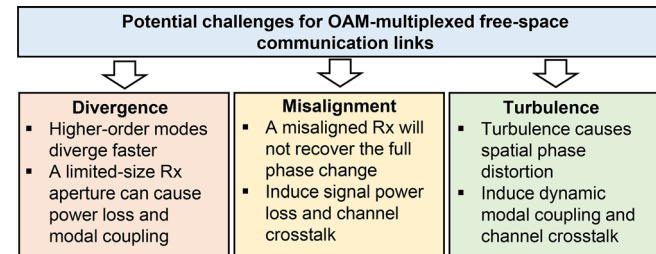


FIG. 14. Potential challenges for OAM-based free-space communication links.

mode indices. The beam width is a function of propagation distance z and is defined as:^{9,101}

$$W_{\ell,p}(z) = 2\sigma_{\ell,p}(z), \quad (13)$$

where $\sigma_{\ell,p}(z)$ is the square root of the second moment of the beam intensity profile.^{9,101} It was investigated that, for a given $LG_{\ell,p}$ beam, the beam width $W_{\ell,p}(z)$ is related to the beam waist $w(z)$, as shown in Eq. (14),^{9,101}

$$W_{\ell,p}(z) = w(z)M, \quad (14)$$

where $\sqrt{M} = 2p + |\ell| + 1$,^{9,101,102} and ℓ and p are the LG mode indices for azimuthal and radial directions, respectively. Equation (14) indicates that the divergence effects become more significant with increasing mode order,^{9,49,102,103} and, thus, make it harder to fully capture higher-order beams with a limited-size receiver aperture. This would result in power loss of the transmitted channel, as shown in Fig. 15. Moreover, for a communication link using LG modes with various p values, the divergence effects could potentially induce both power loss and inter-channel crosstalk. This is due to the fact that the truncation effect of a circular limited-size aperture at the receiver side can also lead to a modal leakage from the desired mode to other LG modes with various p values.^{48,49,104} Therefore, the divergence-related parameters should be carefully chosen to mitigate channel power loss and inter-channel crosstalk in an LG-based communication link.⁴⁸

2. Misalignment

In an ideal FSO link, the receiver and the optical axes would be aligned perfectly. However, the jitter and vibration of the transmitter/receiver platform could lead to transmitter–receiver misalignment, including relative lateral displacement and receiver angular error.

In a communication link using Gaussian beams, the transmitter–receiver misalignment could lead to power loss, as the limited-size

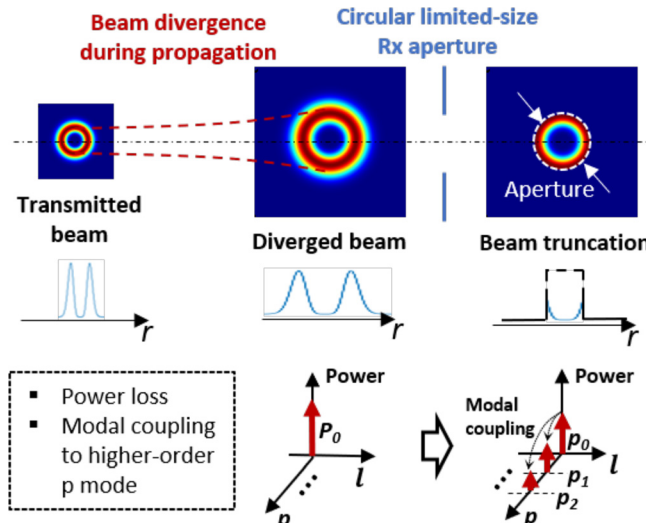


FIG. 15. The divergence-induced beam truncation by the circular limited-size receiver aperture. Power loss of the desired mode and power coupling between different p modes are induced.

receiver aperture might fail to fully capture the beam profile. However, in an OAM-based communication link, such misalignment could induce not only power loss but also inter-channel crosstalk. This is due to the fact that the receiver with a limited-size aperture might fail to fully recover azimuthal phase change and, thus, induces inter-modal power coupling. Figures 16(a-1)–16(a-3) show the scheme of system alignment and the received phase profiles when the transmitter and receiver are perfectly aligned, aligned with lateral displacement, and aligned with receiver angular error, respectively.

The lateral displacement and angular error induced modal coupling have been theoretically investigated.¹⁰⁰ It has been shown that both types of misalignment would cause spreading of the OAM spectrum and induce power coupling to other modes. The normalized power distribution of different modes when the transmitter and receiver are aligned with lateral displacement or receiver angular error is shown in Figs. 16(b) and 16(c), respectively.⁴⁸ As the lateral displacement increases, the normalized power on the other modes increases, while the normalized power on the transmitted mode decreases. This is due to a larger mismatch between the received beams and the receiver aperture. Such modal coupling could potentially induce inter-channel crosstalk in an OAM-based link. Furthermore, power coupling from OAM +3 to OAM +1 and OAM +5 is lower than that of neighboring OAM modes (i.e., OAM +2, +4). Therefore, an OAM-based link with larger spacing of OAM order tends to be more tolerant to lateral displacement. Moreover, the simulation results indicate that there is a similar trend regarding receiver angular error. When the receiver angular error increases, the normalized power on the undesired mode increases, and the power on the transmitted mode decreases. Therefore, various misalignment issues, including lateral displacement and receiver angular error, should be considered in an OAM-based communication link.

3. Turbulence

Turbulence effects may be manifest in atmospheric and underwater environments. In this subsection, we discuss atmospheric turbulence effects. Specifically, temperature fluctuations and air currents in a turbulent atmosphere cause the appearance of eddies. These eddies lead to fluctuations of the local index of refraction at any position in the atmosphere.⁴⁴ Typically, the average size of the turbulent eddies could be characterized by two parameters. One is the inner scale l_0 , and the other is outer scale L_0 , typically on the order of millimeters and meters, respectively.⁴⁴ When a light beam passes through a turbulent atmosphere, dynamic phase shifts at different cross-sectional locations will be induced. Such differential phase shifts can cause a phase front distortion to the transmitted beam.¹⁰⁵ Under typical conditions, the dynamic phase front distortion could vary on a millisecond timescale.^{44,106}

The turbulence strength and turbulence fluctuation⁴⁴ could be quantified by the refractive index structure constant C_n^2 and the Rytov variance σ_R^2 , respectively. C_n^2 is also known as atmospheric refractive index inhomogeneities. The values of C_n^2 in the atmosphere are typically in the range from $10^{-17} \text{ m}^{-2/3}$ (relatively weaker turbulence strength) to $10^{-13} \text{ m}^{-2/3}$ (relatively stronger turbulence strength).⁴⁴ σ_R^2 represents the intensity fluctuation of the optical beam after propagating through a turbulent medium. The value of σ_R^2 is typically related to the refractive index inhomogeneities C_n^2 , optical wavelength λ , and

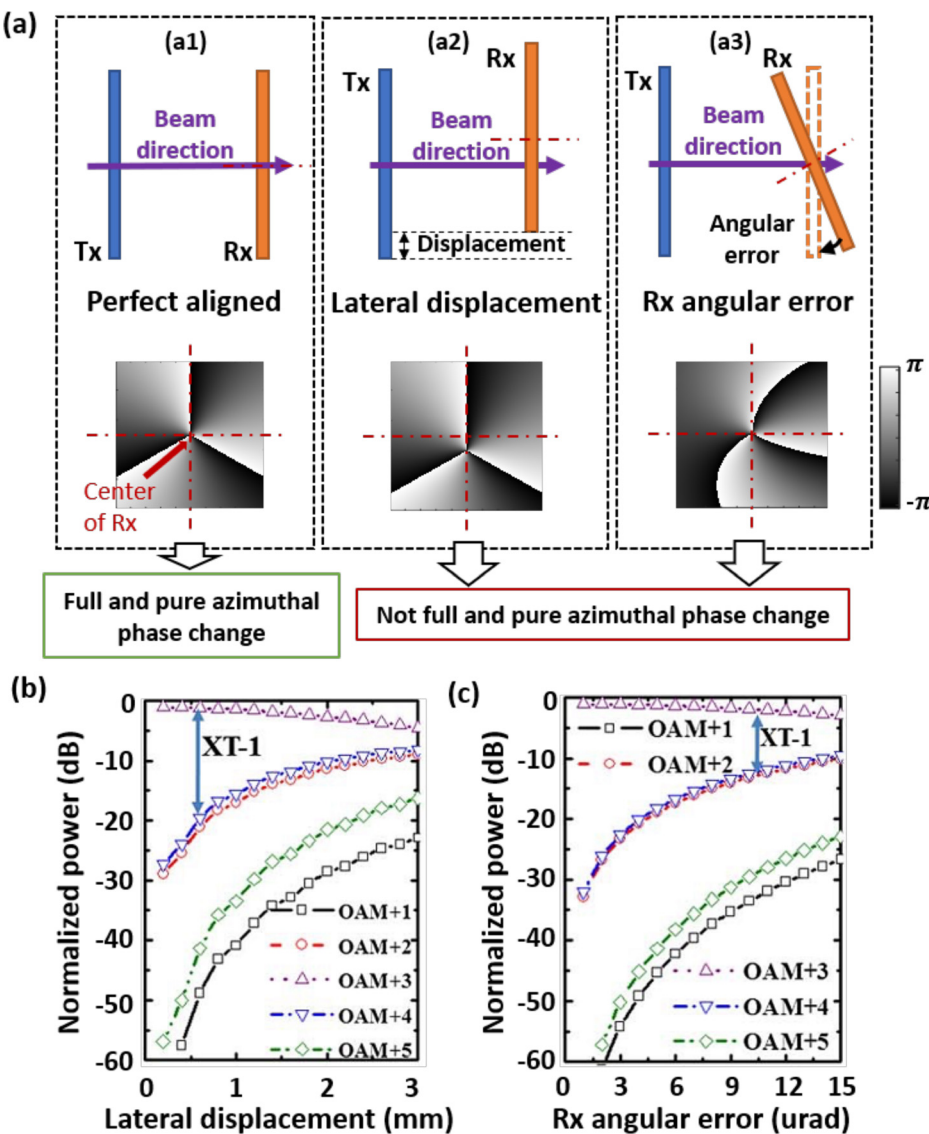


FIG. 16. Schemes of the system alignment and the received phase profiles when the Tx and Rx are (a-1) perfectly aligned, (a-2) aligned with lateral displacement, and (a-3) aligned with receiver angular error. (b) and (c) Simulated power distribution among different OAM modes with different lateral displacement and receiver angular error. Link distance: 100 m; transmitted OAM order: +3; the beam size at transmitter (Tx): 3 cm; receiver (Rx) aperture size: 4.5 cm; XT-1: crosstalk between the nearest-neighboring OAM modes. Reproduced with permission from Xie et al., Optica 2, 357 (2015). Copyright 2015 Optical Society of America.⁴⁸

the propagating distance L .⁴⁴ Generally, a higher value of σ_R^2 represents stronger turbulence fluctuation.

Various models have been reported to simulate beam propagation through a turbulent atmosphere.^{44,107,108} One of the simplified turbulence models is the Kolmogorov turbulence model.^{44,108} The power spectral density of the refractive index fluctuations given by the Kolmogorov model is⁴⁴

$$\Phi_n^K(\kappa) = 0.033 C_n^2 \kappa^{-11/3} \quad \text{for } 1/L_0 \ll \kappa \ll 1/l_0, \quad (15)$$

where κ is the angular spatial frequency vector. According to the Kolmogorov spectrum model, the relationship between C_n^2 and σ_R^2 can be represented as⁴⁴

$$\sigma_R^2 = 1.23 C_n^2 k^{7/6} L^{11/6}, \quad (16)$$

where $k = 2\pi/\lambda$ is the wavenumber and L is the propagation distance. As an alternative to C_n^2 , the Fried parameter, r_0 , is the radius representing atmospheric coherence length.^{109,110} r_0 defines an circular area outside of which atmospheric turbulence becomes uncorrelated.¹⁰⁹ In the Kolmogorov turbulence model, r_0 of a plane wave is given by^{109,110}

$$r_0 = 1.68(C_n^2 L k^2)^{-3/5}. \quad (17)$$

There have been several methods to investigate the atmospheric turbulence effect on an OAM-based link.^{45–47,110} Figure 17(a) shows a rotating phase plate used as one of the turbulence effect emulation methods. The modal power leakage is characterized by measuring the modal power ratio of the distorted beam, as shown in Fig. 17(b). Under the relatively weaker turbulence ($C_n^2 = 2.5 \times 10^{-16} \text{ m}^{-2/3}$), most power of the desired OAM mode (i.e., OAM +3) could be

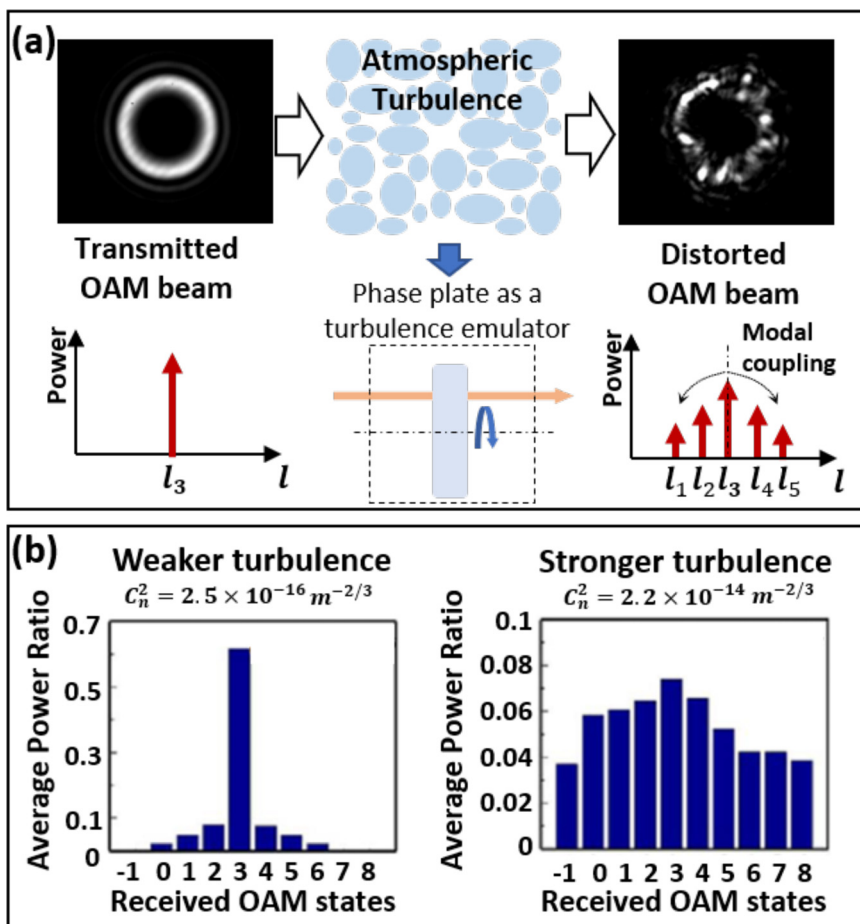


FIG. 17. (a) Concept of the atmospheric turbulence effect on the OAM beam. Such turbulence effect could be emulated by a rotating phase plate with the pseudorandom phase distribution based on Kolmogorov spectrum statistics. Inset shows the measured distorted OAM beam profile. (b) Measured power ratio of each received OAM state under the turbulence effect with $C_n^2 = 2.5 \times 10^{-16} m^{-2/3}$ (relatively weaker) or $C_n^2 = 2.2 \times 10^{-14} m^{-2/3}$ (relatively stronger). Transmitted OAM order: $+3$; C_n^2 : the effective atmospheric structure constant. Reproduced with permission from Ren *et al.*, Opt. Lett. **38**, 4062 (2013).⁴⁶ Copyright 2013 Optical Society of America.

received. However, under relatively stronger turbulence ($C_n^2 = 2.2 \times 10^{-14} m^{-2/3}$), the power ratio of the undesired modes increases, which leads to relatively large signal power loss and inter-modal crosstalk.

C. Potential mitigation methods for different challenges

The challenges in an OAM-based free-space communication system discussed in Sec. IV B may cause power loss and modal crosstalk among the data channels. In order to achieve a good performance, some

mitigation methods have been reported to potentially alleviate the deleterious effects caused by these challenges, as shown but not limited to the approaches in Fig. 18. In this section, we will discuss the mitigation methods for the three main challenges of the OAM-based free-space communication systems in terms of the benefits and limitations.

1. Mitigation methods for the beam divergence

a. Using transmitter lenses for beam focusing. Due to the divergence of the OAM beam, the receiver aperture size may be required to

Challenges:

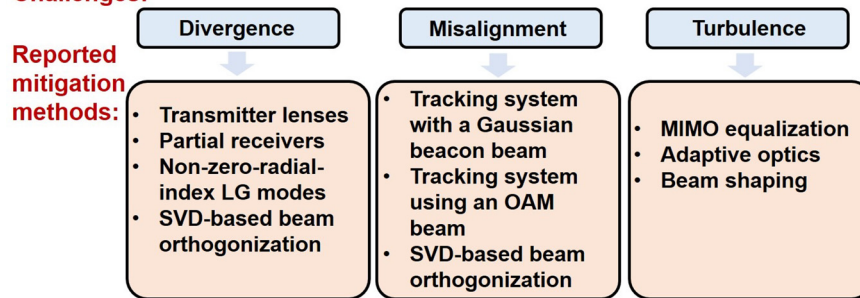


FIG. 18. Overview of the reported mitigation methods for different challenges in free-space OAM-based communication systems. SVD: singular value decomposition. MIMO: multi-input-multi-output.

be larger to capture a sufficient portion of the beam when the transmission distance becomes longer. However, the requirement of a larger aperture size might increase the cost of the receiver. Therefore, it might be desirable to reduce the OAM beam size at the receiver aperture. This can be achieved by placing lenses at the transmitter to focus the transmitted OAM beams.¹¹¹ The concept of using the transmitter lenses is shown in Figs. 19(a) and 19(b). A pair of lenses with focus lengths of f_1 and f_2 is placed at the transmitter. The multiplexed OAM beams pass through the lenses before transmitting out of the transmitter aperture. The lens pair has an equivalent focus length of f_0 , satisfying¹¹¹

$$\frac{1}{f_0} = \frac{1}{f_1} + \frac{1}{f_2} - \frac{d}{f_1 f_2}, \quad (18)$$

where d is the spacing between the two lenses. By tuning the spacing d , the beam size of the focused OAM beams at receiver can be changed.

Figure 19(c) shows the simulated power loss as functions of transmission distances with both a transmitter and receiver diameter of 10 cm. The simulation results show that power loss reduction using a lens pair with f_0 of 1 km could be achieved within a distance up to 2 km. However, a transmitter lens pair with a given f_0 could be a potential solution up to a specific propagation distance. For a longer distance, more accurate adjustment of d might be required.¹¹¹ In addition, it is shown that the transmitter lenses could help one to enhance the system robustness under angular errors. However, this method

would have a higher power penalty under lateral displacement compared to the link without transmitter lenses.¹¹¹

b. Partial receiver apertures for receiving OAM beams. Due to the divergence of OAM beams, the size of the receiver aperture is sometimes limited with the consideration of cost, such that it can only partially receive the transmitted beam. Such a receiver is referred to as “partial receiver.”^{113,114} As the OAM beam has a ring-like intensity profile, a partial receiver at the center of the beam may cause a relatively higher power loss. If the partial receiver is placed on the intensity maxima of the ring (off the beam center), the received power can be increased, as shown in Fig. 20(c). However, such displacement of the receiver might cause modal coupling, as shown in Fig. 20(d).

Moreover, placing two partial apertures symmetrically at the beam annulus might help one to further reduce the power loss and modal coupling,¹¹² the concept of which is shown in Fig. 20(a). As an example, to receive the OAM +2 beam, the captured portion of the intensity and phase profiles of the two apertures are shown in Fig. 20(b). Figures 20(c) and 20(d) show the improvement of the received power and crosstalk using double partial receiver apertures. Compared to the case of placing a single aperture on the ring, the received power of double apertures has an increment of ~ 6 dB. As shown in Fig. 20(d), with double apertures, power coupling from OAM +2 to the modes that have an odd number of charge difference to OAM +2 (e.g., OAM -1, OAM +1, OAM +3) is reduced by ~ 10 dB

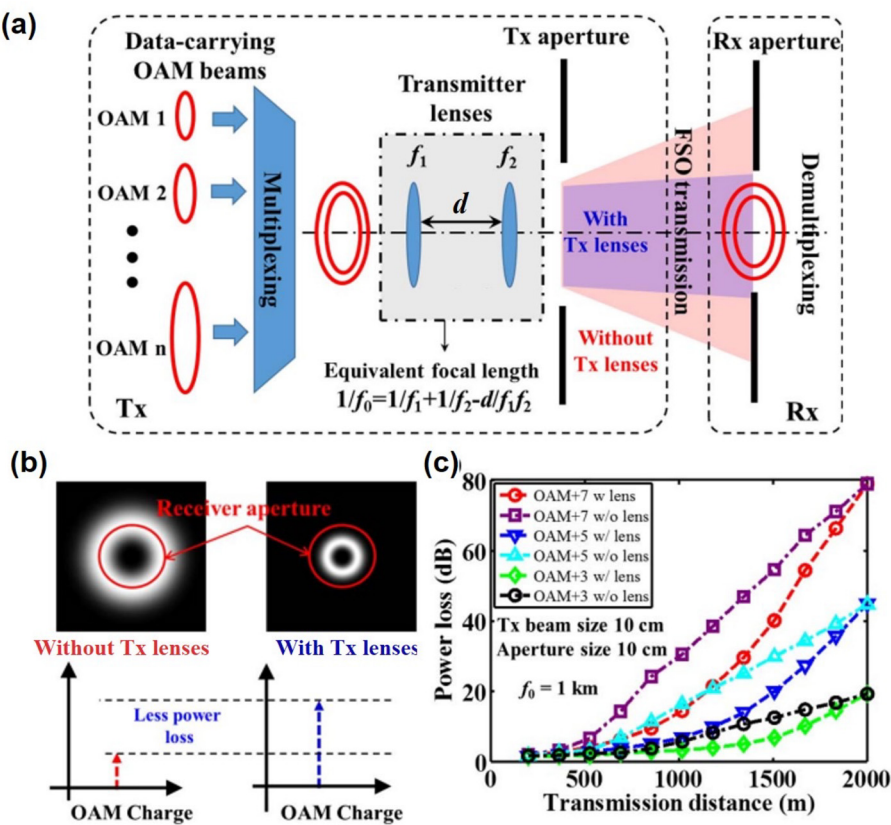


FIG. 19. (a) Concept of using a pair of lenses at the transmitter in OAM-based communication systems for mitigating the effects of beam divergence and limited-size apertures. (b) Intensity profiles of the received OAM beam with and without transmitter lenses. The received power of the OAM beam increases when transmitter lenses are used. (c) Simulated power loss as with various transmission distance for different OAM beams using transmitter lenses with an equivalent focal length of 1 km. Reproduced with permission from Li et al., Appl. Opt. 55, 2098 (2016).¹¹¹ Copyright 2016 Optical Society of America.

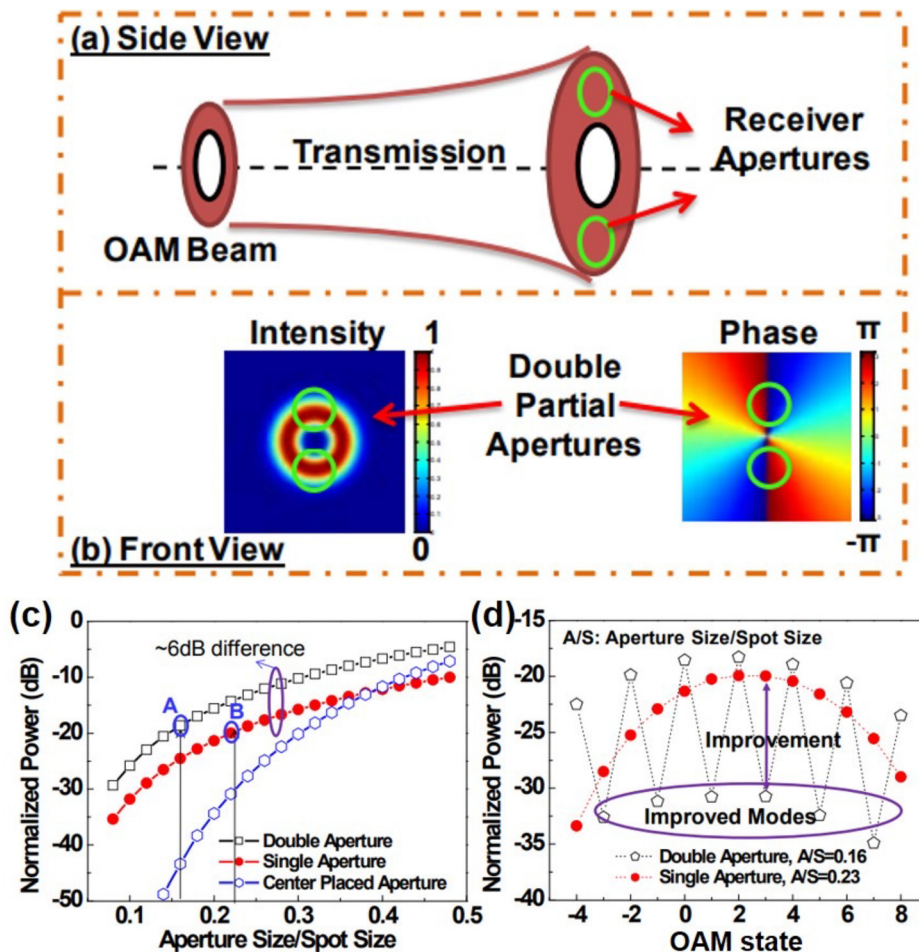


FIG. 20. (a) Concept of using double partial receivers in OAM-based communication systems for mitigating the effects of beam divergence and limited-size apertures. (b) Received intensity and phase of the OAM beam. (c) Experimentally measured normalized received power of the OAM +2 beam with different receiver apertures as functions of the aperture sizes. Case A: A/S = 0.16; case B: A/S = 0.23. (d) Experimentally measured power leakage from OAM +2 beam to other OAM modes with single (case A) and double (case B) partial receivers. In these two cases, the aperture size of case A is $\sqrt{2}$ as large as case B, resulting in the same total area.¹¹²

compared to the case of a single aperture. Therefore, a specific set of OAM modes might be selected in order to achieve a low crosstalk. Furthermore, using a partial receiver with more apertures might potentially further reduce the power loss and modal coupling effects. However, such a partial receiver cannot fully capture the azimuthal phase change, which induces modal coupling to other undesired modes. As a result, the number of OAM modes that could be used in a partial-receiver-based system might be limited. It should be noted that the similar concept could also be applied in millimeter-wave OAM communications.

c. Utilizing non-zero-radial-index LG beams. As mentioned above, an OAM beam has an intensity null at the beam center, which induces power loss when a limited-size receiver aperture is placed at the center. For an LG beam with a non-zero-radial-index (i.e., $p > 0$ LG beam), the size of the inner-most ring can be smaller than that of the ring of the zero-radial-index (i.e., $p = 0$ LG beam) LG beam with the same ℓ for a limited transmission distance, as shown in Fig. 21(a). Thus, utilizing LG beams with a $p > 0$ radial index might increase the received power with a limited receiver aperture size.¹⁹

Figures 21(b-1) and 21(b-2) show the simulated power loss of the LG beams with various receiver aperture diameters when the

transmitted beam diameter is 8 cm. As shown in Fig. 21(b1), when the transmission distance is 500 m, LG beams with $p > 0$ radial indices have less power loss than LG beams with $p = 0$ radial indices and the same ℓ value for relatively small receiver aperture sizes. As the receiver aperture size increases, the power loss of the $p > 0$ LG beams would become higher than that of the $p = 0$ LG beams. This might be due to the fact that the outer ring of the $p > 0$ LG beam is larger than the ring of the $p = 0$ LG beam. It can also be seen that when the transmission distance increases from 500 m to 1 km, the power loss reduction tends to decrease, as shown in Fig. 21(b2). This might be because that the $p > 0$ LG beam diverges faster than the $p = 0$ LG beam when both the ℓ value and the transmitted beam waist are the same. Furthermore, this method may also induce additional channel crosstalk in an MDM system based on the multiplexing of LG modes with different radial indices. This is due to the fact that the limited-size aperture may affect the orthogonality among these modes, which has been discussed in Sec. IVB.

d. Singular-value-decomposition-based beam orthogonalization using LG modes. In general, each independent data channel is transmitted on an optical beam using a single LG mode in an LG-based MDM system. However, the performance of such an MDM FSO

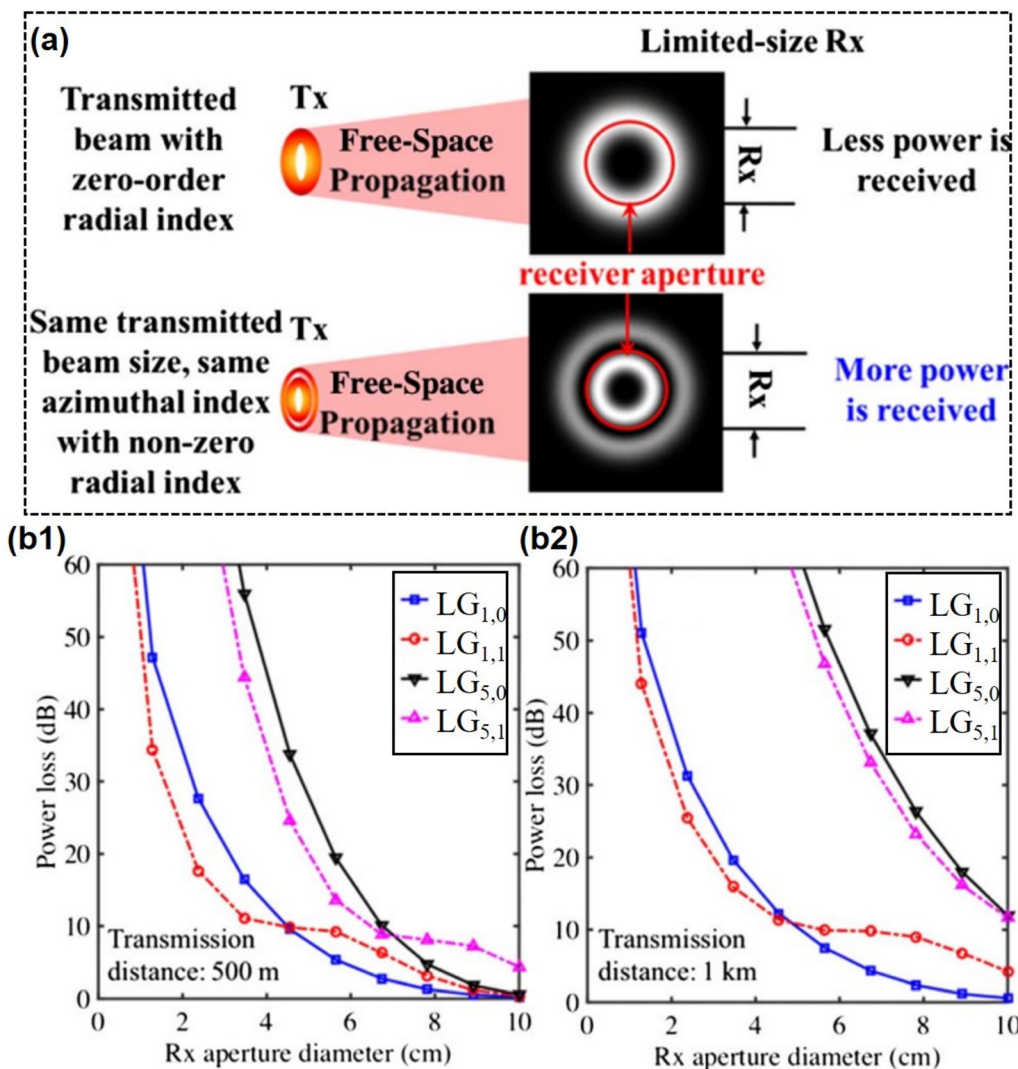


FIG. 21. (a) Concept of using non-zero-radial-index LG beams to reduce the power loss caused by the limited-size receiver aperture. (b-1) and (b-2) Simulated power loss of LG beams with radial indices of $p = 0$ and $p > 0$ with a transmitted beam diameter of 8 cm as a function of receiver aperture diameter with transmission distances of (b-1) 500 m and (b-2) 1 km. Reproduced with permission from Li *et al.*, J. Opt. Soc. Am. B **34**, 1 (2017).¹⁹ Copyright 2017 Optical Society of America.

system could be affected by a limited-size receiver. This impairment would result in deleterious signal power loss for the transmitted LG mode and power coupling from the transmitted LG mode to other LG modes with different p values, that is, modal crosstalk. One potential approach is to transmit each data channel on a single beam composed of multiple LG modes with complex coefficients to achieve smaller data-carrying beams at the Rx to mitigate the effects of the limited-size receiver, as shown in Fig. 22. By carefully designing the coefficients of each LG component, these data-carrying multi-mode beams could be spatially tailored and remain orthogonal to each other at the receiver.

The modal coupling caused by the limited aperture between the LG modal set can be described by a transmission matrix \mathbf{H} . This

approach is based on the singular value decomposition (SVD) of \mathbf{H} , as follows:¹¹⁵

$$\mathbf{H} = \mathbf{U} \cdot \Sigma \cdot \mathbf{V}^*. \quad (19)$$

For each channel, the transmitted beam is specifically designed and generated such that it comprises a set of LG modes. The complex coefficients of these LG components are obtained by column vectors of the \mathbf{V} . Due to the orthogonality between the column vectors of the \mathbf{V} , the transmitted beams on different channels are orthogonal with each other. After propagating over a certain distance and experiencing a limited-size receiver aperture, the independent beams still comprise such a set of LG modes. It should be noted that the complex weights of LG components for these resulting beams are the row vectors in the

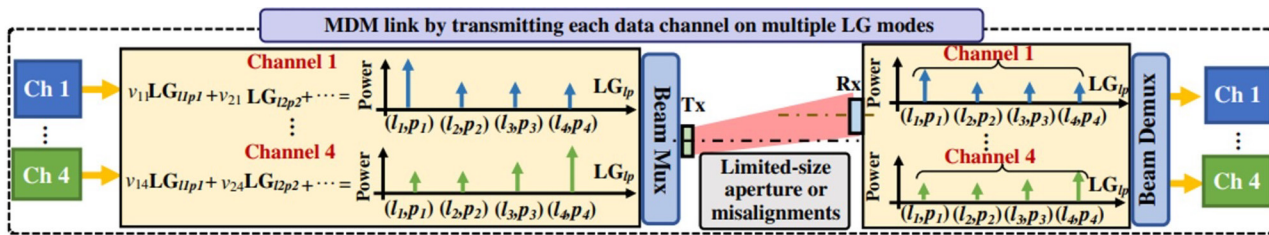


FIG. 22. Concept of transmitting each data channel on a designed single beam composed of a set of LG modes to reduce the power loss and crosstalk induced by the limited-size aperture or misalignments in an MDM link. Reproduced with permission from Pang *et al.*, Opt. Lett. **45**, 6310 (2020).¹¹⁵ Copyright 2020 Optical Society of America.

U matrix multiplied by the singular values in the Σ matrix. Consequently, these beams are still orthogonal with each other, which enables efficient demultiplexing at the receiver with little interchannel crosstalk.

Figure 23(a) presents measured power loss and crosstalk with different receiver aperture sizes for beams composed of single mode or multiple modes. When using single beam composed of one LG mode for each channel, the power loss and crosstalk increase as the aperture radius decreases. However, when using a single beam comprising multiple LG modes, the power loss is relatively low when the aperture radius is $1.0 - 1.6$ mm. In addition, the crosstalk for both channels also remains at a low level in this range due to the orthogonality preservation between the two beams after experiencing the limited-size aperture. It should be noted that this method can also be used to mitigate the power loss and modal crosstalk caused by the receiver aperture misalignment, which will be discussed later. To use this method, the transmission matrix H need to be measured. Since dynamic link impairments might cause a dynamic change in H , the measurement needs to be updated. Therefore, a feedback from the receiver to the transmitter might be required.

2. Mitigation methods for misalignment

a. Tracking system with a Gaussian beacon beam. A beam tracking system is important for the free-space OAM-based communication systems, especially when the link is dynamic that there may be

residual misalignment between the transmitter and receiver. The beam tracking with a beacon beam at a different wavelength than the signal beam is shown in Fig. 24(a). A beacon beam at the wavelength λ_2 with the fundamental Gaussian mode is transmitted co-axially with the OAM signal beams at the wavelength λ_1 . At the receiver, a tracking system is implemented to detect and compensate for the displacement between the transmitter and the receiver. In this system, a position-sensitive detector (PSD) is first utilized to detect the position information of the beacon Gaussian beam. Such a PSD has four cell quadrants (Q1 to Q4), which can detect the beam position by measuring the received optical power on them, as shown in Fig. 24(b). The outputs of the PSD are voltages V_x and V_y , which can be evaluated by¹¹⁹

$$V_x = \frac{(Q_2 + Q_4) - (Q_1 + Q_3)}{Q_1 + Q_2 + Q_3 + Q_4}, \quad (20)$$

$$V_y = \frac{(Q_1 + Q_2) - (Q_3 + Q_4)}{Q_1 + Q_2 + Q_3 + Q_4}.$$

Subsequently, V_x and V_y are sent to the controller as a feedback signal such that the angle of the FSM can be dynamically tuned to keep the transmitted OAM beams close to the PSD center. As an example, Figs. 24(c) and 24(d) show the result of the tracking for the displacement in one direction of the transmitted OAM beam. The beam centroids without tracking and with tracking using the beacon Gaussian beam are shown. The results indicate that the misalignment in the ± 5 -mm displacement range can be compensated for using the tracking system.

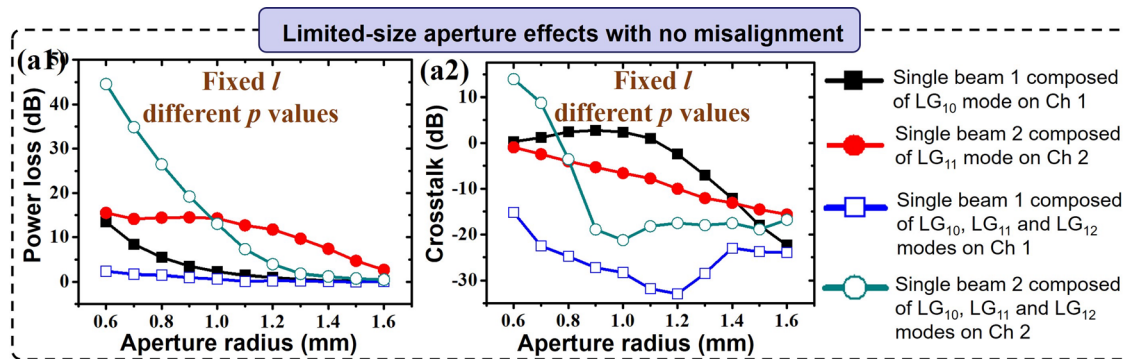


FIG. 23. The power loss and crosstalk mitigation of the limited-size-aperture effect using the SVD-based methods. Measured (a-1) power loss and (a-2) crosstalk induced by the limited-size aperture when transmitting data channels on beams composed of one LG mode or beams composed of multiple LG modes. Reproduced with permission from Pang *et al.*, Opt. Lett. **45**, 6310 (2020).¹¹⁵ Copyright 2020 Optical Society of America.

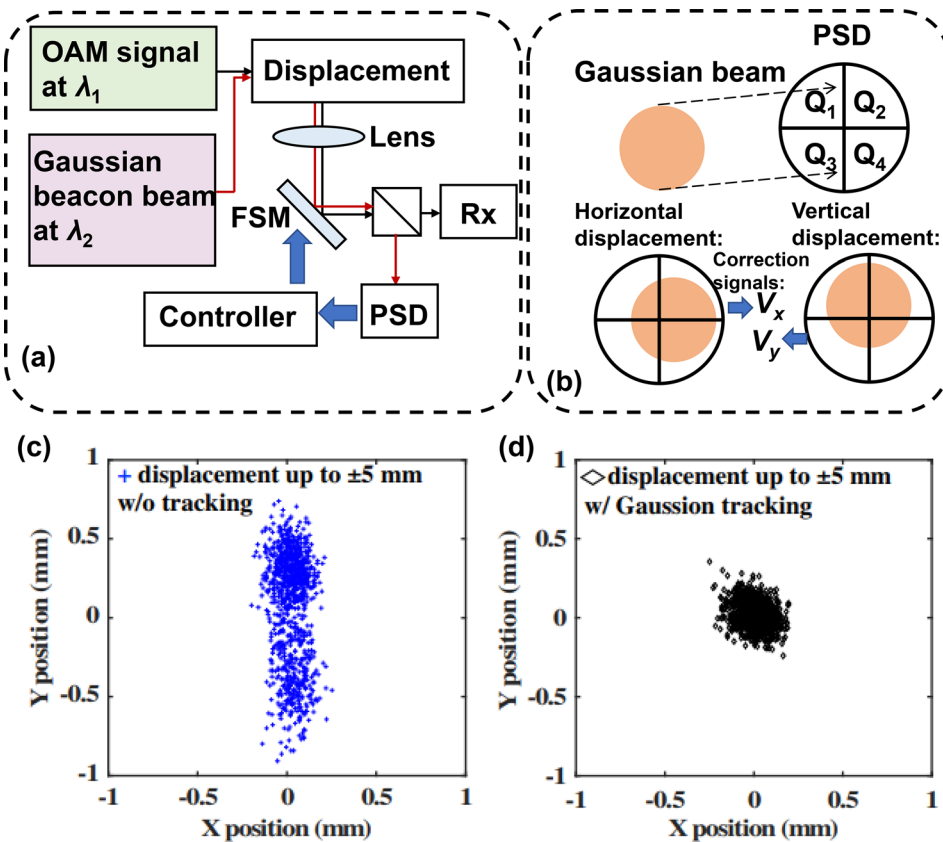


FIG. 24. (a) Basic setup of a displacement tracking system using a fast-steering mirror and a beacon beam at another wavelength. FSM: fast-steering mirror; PSD: position-sensitive detector; Rx: receiver. (b) The error signal from the PSD under different displacements. The center of the received OAM beam with respect to the aperture center (c) without tracking and (d) with tracking using the beacon Gaussian beam. Reproduced with permission from Li *et al.*, Opt. Lett. **43**, 2392 (2018).¹¹⁶ Copyright 2018 Optical Society of America.

However, such a tracking system requires an additional Gaussian beam as a beacon beam and an accurate alignment between the beacon beam and the transmitted OAM beam.

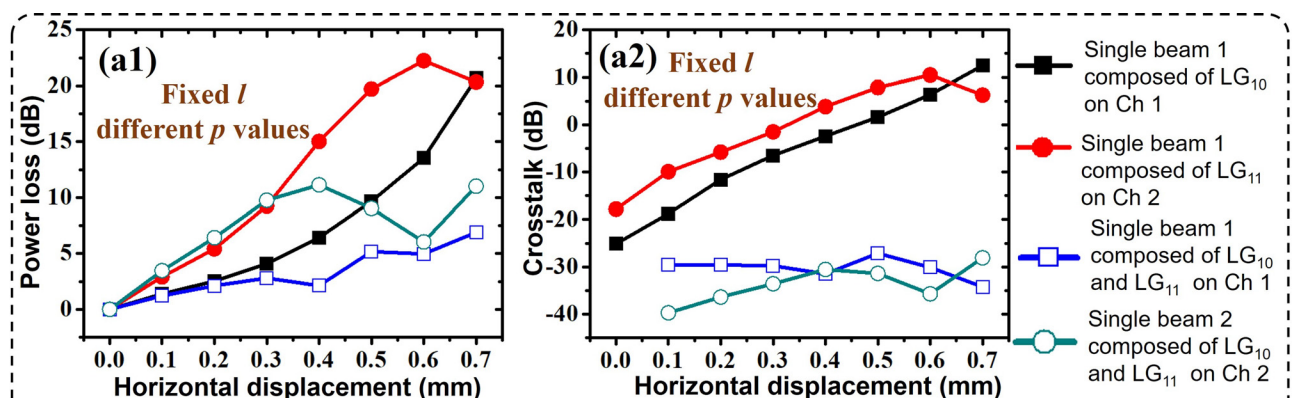
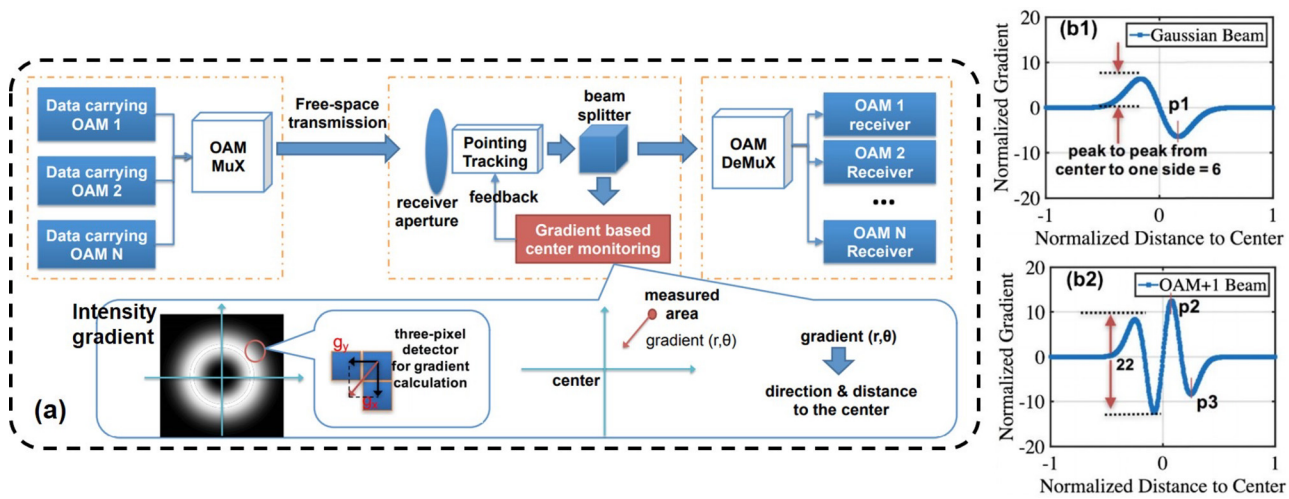
b. Tracking system using an OAM beam. In an OAM-based communication link, the transmitted OAM beam itself can be used for the tracking without using an additional Gaussian beacon beam. In general, the gradient of the OAM beam's intensity profile has (1) a direction pointing to the beam center along the radial direction and (2) varying strengths at different distances to the beam center. Due to the unique characteristics, the intensity gradient of the OAM beam can be potentially used to determine the position of the transmitted OAM beam. As shown in Fig. 25(a), the received OAM beam can be first split into two branches by a beam splitter. One of the two branches can be sent to a three-pixel detector to measure the gradient information by vector summation of two orthogonal components in horizontal and vertical directions. Subsequently, the measured intensity gradient can be used to determine the position of the beam and used as the correction signal to a tracking system. As shown by the intensity distributions in Figs. 25(b-1) and 25(b-2), the OAM beam may have a higher intensity gradient than the Gaussian beam. However, it should be noted that a higher order OAM beam could provide higher tracking accuracy but may operate over a smaller range of misalignment.¹¹⁸

c. Singular-value-decomposition-based beam orthogonalization using LG modes. Without a tracking system, the aforementioned SVD-

based beam orthogonalization using LG modes for divergence mitigation can also help one to reduce the power loss and crosstalk induced by the misalignment, as shown in Fig. 22. Figures 26(a) and 26(b) show the experimental results for the power loss and crosstalk mitigation of the misalignment effects using the SVD-based methods. Figure 26(a) shows that for the case of beams comprising one LG mode with different p values (LG_{10} , LG_{11}), as the horizontal displacement increases, both the power loss and crosstalk increases. However, for the case of beams comprising multiple LG modes, the power loss for both channels becomes lower when the displacement varies from 0.4 to 0.7 mm. In addition, the crosstalk for the beams comprising multiple LG modes on both channels remains at a relatively low level (< -27 dB). The case for the beams comprising multiple LG modes with different ℓ values (LG_{10} , LG_{-10}) is also investigated, as shown in Fig. 26(b). It is observed that using such an approach, the power loss can be reduced when the displacement varies from 0.8 to 1.1 mm. Moreover, the crosstalk for both channels also remains at a relatively low level (< -17 dB).

3. Mitigation methods for atmospheric turbulence

a. Turbulence mitigation using electrical multi-input-multi-output compensation. In common radio systems, multiple-input–multiple-output (MIMO) electronic channel-equalization digital-signal-processing (DSP) algorithms are widely used to “unwind” channel crosstalk when multiple independent transmitting antennas are communicating with multiple receiving antennas.¹²¹ In an OAM-based



communication link, multiple OAM beams can be considered as originating from multiple transmitting antennas. Therefore, similar approaches can be adopted to free-space OAM-based communication links to mitigate the crosstalk induced by the atmospheric turbulence. Figure 27(a) shows the concept of using a 4×4 MIMO equalization to recover four OAM channels after propagating through atmospheric turbulence. Four coherent receivers are used to detect the signals x_i , ($i = 1, 2, 3, 4$) carried by the four OAM beams as the input of the MIMO equalization. The output of the MIMO equalization can be expressed as¹²²

$$y_j = \sum_i w_{ij} * x_i, \quad (21)$$

where w_{ij} ($i, j = 1, 2, 3, 4$) is the coefficient vector. The coefficient vectors could be adaptively estimated to mitigate the channel crosstalk induced by the turbulence. Figure 27(b) shows the measured signal constellations of a four OAM-multiplexed link with turbulence effect with and without the MIMO equalization.¹²⁰ Four OAM beams each carrying a 20-Gbit/s QPSK signal are multiplexed and propagated co-axially through the emulated turbulence. Without the MIMO equalization, the received signals suffer from turbulence-induced crosstalk, resulting in EVMs of 24%, 46%, 33%, and 46%. With the MIMO equalization, the EVMs are reduced to 14%, 14%, 15%, and 21% for the four channels, respectively. The results indicate that the MIMO equalization method could mitigate the channel crosstalk among the transmitted OAM channels. However, the performance of this method could be degraded if most of the OAM beam power is coupled to the modes that are not detected and compared by the algorithm.¹²³ In addition, the MIMO equalization requires the reception of multiple data channels and may increase the electrical DSP complexity when increasing the number of OAM-carrying data channels.

b. Adaptive optics for turbulence mitigation. Without increasing the electrical DSP complexity, one optical method to compensate the turbulence effect is adaptive optics (AO). The concept of AO for mitigating turbulence effect in an OAM-based communication link is shown in Fig. 28. A Gaussian probe beam is transmitted co-axially with the OAM beams at different polarizations. An AO compensation system is built at the receiver, in which the turbulence-distorted Gaussian beam is separated from the distorted OAM beams to serve

as the probe for wavefront distortion estimations and required correction-pattern retrieval with a wavefront sensor (WFS). A feed-back controller is used to update the two wavefront correctors (e.g., DMD or SLM) to compensate the phase front of the Gaussian probe and the distorted OAM beams.¹²⁴ The far-field intensity profiles of the Gaussian beam and OAM beams, as shown in Figs. 28(b) and 28(c), indicate that the turbulence-induced distortion can be compensated by the AO system. It is noted that the probe beam could also be prepared at a separate wavelength instead of a different polarization.¹²⁵ In addition, the wavefront correction pattern can also be used for the pre-compensation of the OAM beams transmitted in the other direction for a bi-directional free-space OAM-based communication link.¹²⁶ However, the probe beam and the feedback loop used in the AO system could increase the complexity of the optical system. In addition, in order to accurately probe the distorted wavefront of beams, accurate alignment between the probe beam and OAM beams might be required especially for a long-distance link.

Furthermore, the AO-based method has also been demonstrated to simultaneously mitigate turbulence effects and demultiplex OAM channels using a wavefront-shaping-and-diffusing (WSD) approach^{128,129} or a single MPLC device.^{92,130} However, these approaches might require additional optical devices (e.g., an optical diffuser) or more complicated mitigation algorithms, which would increase the system complexity.

c. Turbulence mitigation by beam shaping at the transmitter. In general, using beam forming at the transmitter to mitigate channel cross-talk is a well-understood approach in radio.¹³² Similarly, free-space optical beam forming (or beam shaping) can be accomplished to mitigate turbulence effects.^{127,131} For example, this method could be achieved by transmitting each channel on a single beam comprised of multiple modes, such that each composite mode can have a complex coefficient in amplitude and phase, as shown in Fig. 29(a).¹²⁷ In order to obtain the complex coefficient of each composite mode, the complex transmission matrix is first retrieved using simple in-fiber power measurements without using WFS.¹²⁷ Subsequently, the complex coefficients are calculated based on the inverse of the measured transmission matrix. By transmitting each channel on a single beam composed of two OAM modes with the designed complex coefficients, the turbulence-induced channel crosstalk could be mitigated. This is because that, for each channel, the turbulence-induced modal coupling to the other undesired mode would

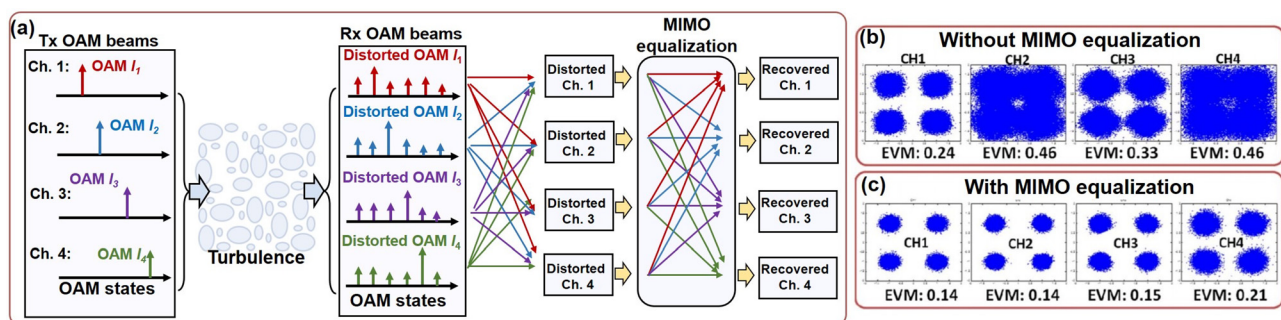


FIG. 27. (a) Concept of using MIMO equalization to mitigate the atmospheric turbulence of the OAM-based communication link. Measured constellations of the received signals (b) without and (c) with the 4×4 MIMO of multiplexed four OAM beams, each carrying a 20-Gbit/s QPSK data channel. EVM: error vector magnitude. Reproduced with permission from Huang et al., Opt. Lett. **39**, 4360 (2014).¹²⁰ Copyright 2014 Optical Society of America.

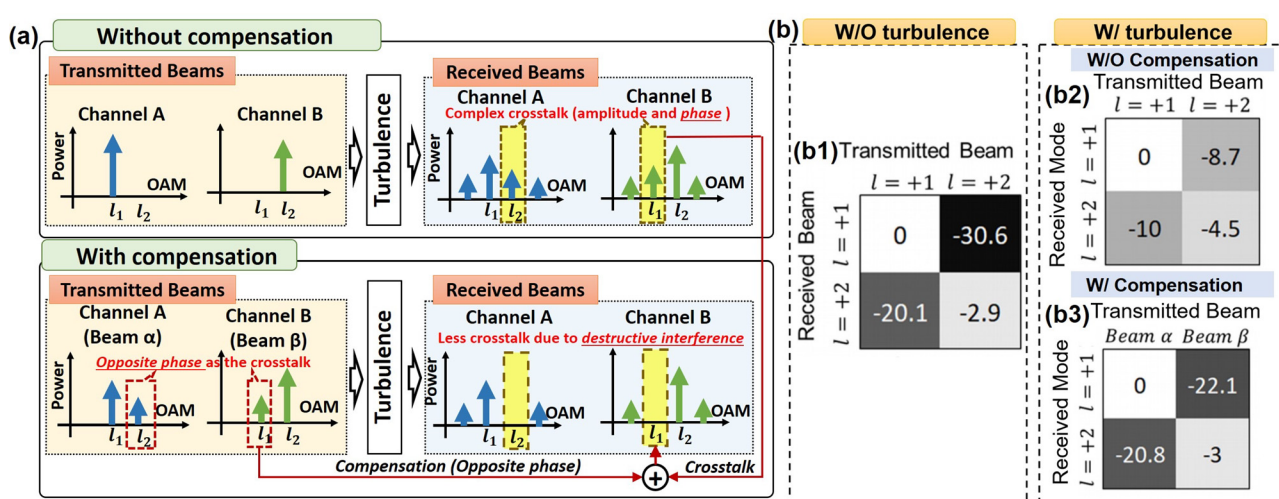
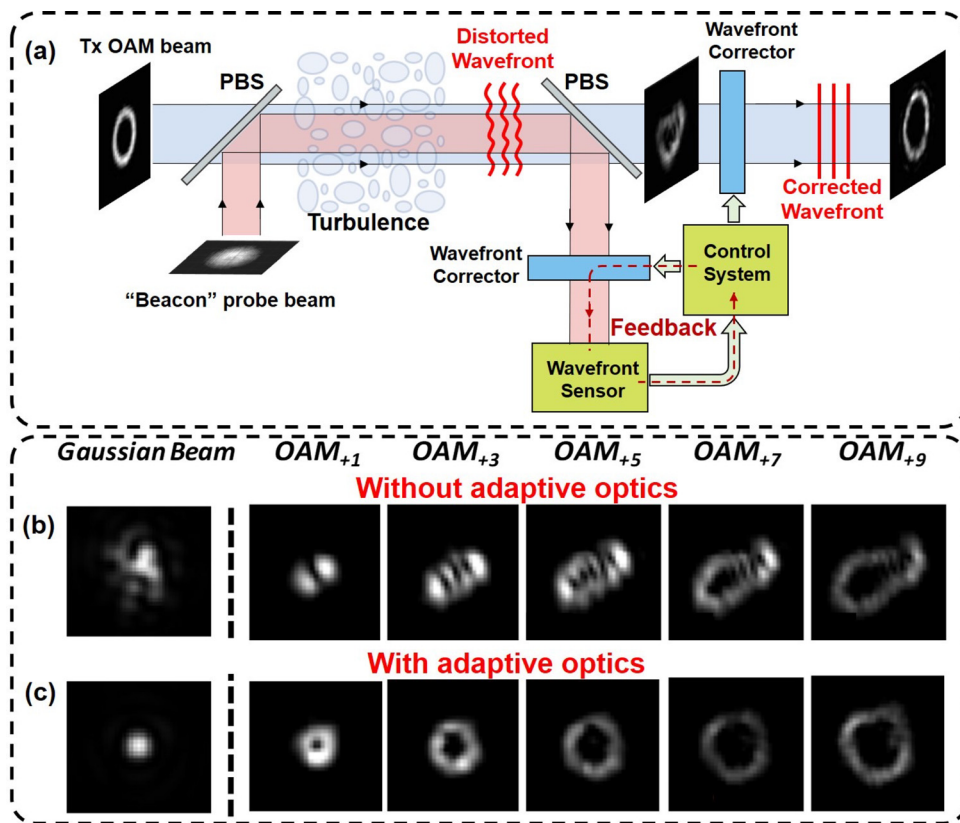


FIG. 29. (a) The concept of turbulence mitigation by transmitting each channel on a single beam comprised of multiple modes in a free-space OAM-based communication system. (b) The measured normalized transmission intensity matrices (b-1) without turbulence effects, as well as (b-2) without and (b-3) with turbulence compensation. Reproduced with permission from Song *et al.*, J. Lightwave Technol. 38, 82 (2020).¹²⁷ Copyright 2020 IEEE.

experience a destructive interference with the corresponding modal component of the transmitted beam.

As an example, the measured normalized transmission intensity matrices without turbulence effects, without and with turbulence compensation, are shown in Figs. 29(b-1)–29(b-3), respectively. With the turbulence effects, the crosstalk of the two channels increases to -8.7 and -5.5 dB in the absence of turbulence compensation. With turbulence compensation, the crosstalk decreases to -22.1 and -17.8 dB for the two channels. However, the number of required measurements could increase with the increasing size of the transmission matrix, thus resulting in a higher requirement of the measurement and feedback speed. In addition, this method might induce some power loss, as only a limited number of OAM modes are utilized.

In order to manipulate a larger number of modes, one phase conjugation approach to individually shape the amplitude and phase of each transmitted beam has been implemented in a 340-m outdoor free-space link,¹³¹ as shown in Fig. 30(a). In such an approach, the amplitude and phase profiles of each turbulence-distorted OAM mode could be first retrieved from a back-propagating probe beam with the same OAM order using off-axis digital holography analysis.¹³¹ Subsequently, each data-carrying beam is shaped based on the phase conjugation of the back-propagating probe beam. After the transmitted phase-conjugated beam propagates through the turbulence, an OAM beam with a relatively high mode purity and a relatively low modal coupling could be retrieved at the receiver, as shown in Fig. 30(b). However, in order to obtain the turbulence distortion information at the transmitter, back-propagating probe beams and other relatively complicated devices^{133,134} might be needed, which would increase the system complexity.

D. OAM-based optical communications for airborne platforms

With the developing demand for the data communications of airborne platforms over recent years, there has been an increasing need

for high-capacity FSO links between these airborne platforms and the corresponding ground stations.^{135–138}

1. Challenges for airborne optical communication links

Figure 31 illustrates various types of airborne and satellite FSO links. Each of these links has particular characteristics and corresponding challenges.

(1) Satellite-to-satellite links could have an ultra-long-distance transmission distance of >1000 km. The beam divergence is a challenge due to the long propagation distance.¹³⁹ (2) Satellite-to-ground-station links require a long transmission distance through the atmosphere. In such a link, a laser beam generally propagates through the Earth's atmosphere. Therefore, both the beam divergence and the accumulated turbulence are the main challenges.¹³⁹ (3) Airplane-to-ground-station links have a length of ~ 1 –100 km. As the airplane is usually moving fast, the misalignment could degrade the performance. In addition, the atmospheric turbulence is also an important issue in such links. (4) Unmanned-aerial-vehicles (UAV)-to-ground-station communications generally have relatively slow-moving UAVs hovering around the ground station. The link between the UAV and the ground station has a relatively shorter transmission distance of < 1 km. Such links may also be affected by atmospheric turbulence.^{140–143}

2. OAM-multiplexed FSO links involving UAV platforms

UAVs such as flying drones have gained interest recently because of their potential applications.^{140–143} In order to achieve high-speed communications, the OAM multiplexing technique might be potentially utilized in such a UAV platform. As shown in Fig. 32(a), an example of the OAM-multiplexed UAV communication link has been demonstrated.¹⁴⁰ Two OAM beams, each carrying 40-Gbit/s QPSK signals, are multiplexed at the ground station. The beams are

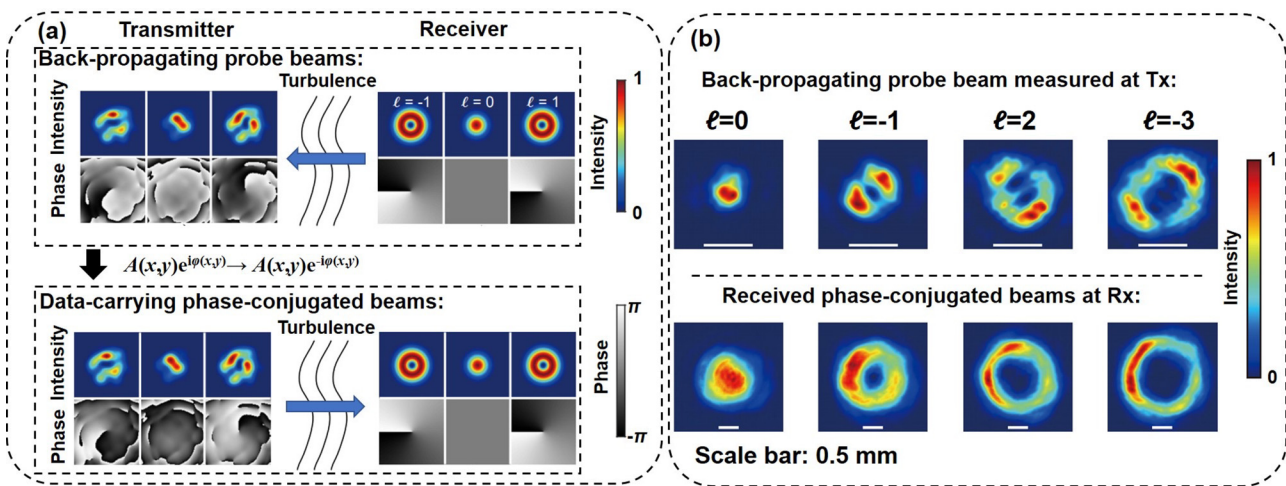
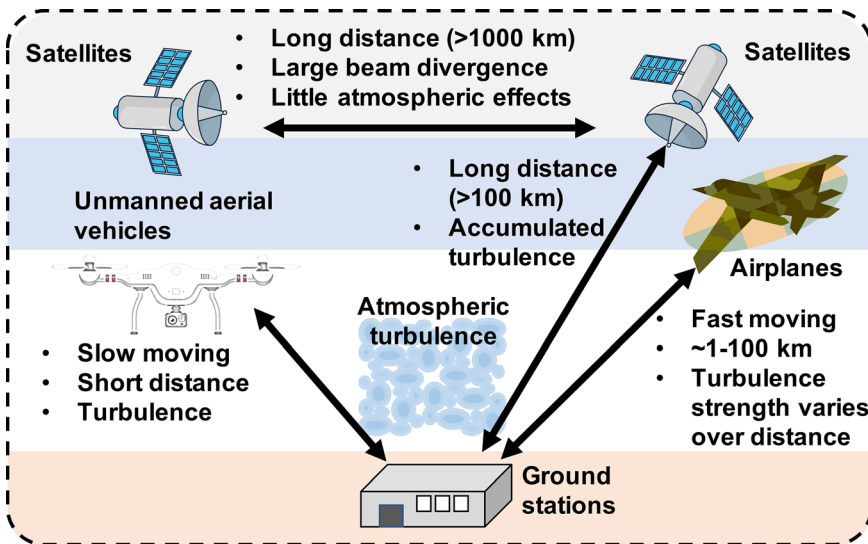


FIG. 30. (a) Concept of beam shaping by transmitting phase-conjugated beams from the transmitter (Tx) to the receiver (Rx). First, the amplitude and phase profiles of each turbulence-distorted OAM mode could be retrieved from a back-propagating probe beam with the same OAM order. Subsequently, the Tx generates and transmits the phase-conjugated beams to the Rx. The Rx receives the phase conjugate of the originally transmitted OAM modes with a relatively high mode quality and low modal coupling. (b) Measured intensity profiles of the back-propagating probe beams (at Tx) and the received phase-conjugated beams (at Rx). Reproduced with permission from Zhou *et al.*, Phys. Rev. Appl. 15, 034011 (2021). Copyright 2021 American Physical Society.



transmitted to the UAV, which is flown up to ~ 50 m away from the transmitter. Subsequently, the beams are reflected by a retro-reflector on the UAV to the receiver, which is located at the same place as the transmitter. A tracking system using a probe Gaussian beam is also employed to mitigate misalignment issues.

In such platforms, atmospheric turbulence might be one challenge, which could potentially affect the system performance. As discussed before, the transmitted OAM beam can be distorted by the turbulence. As a result, part of the transmitted power on one OAM mode can be coupled into other OAM modes, resulting in

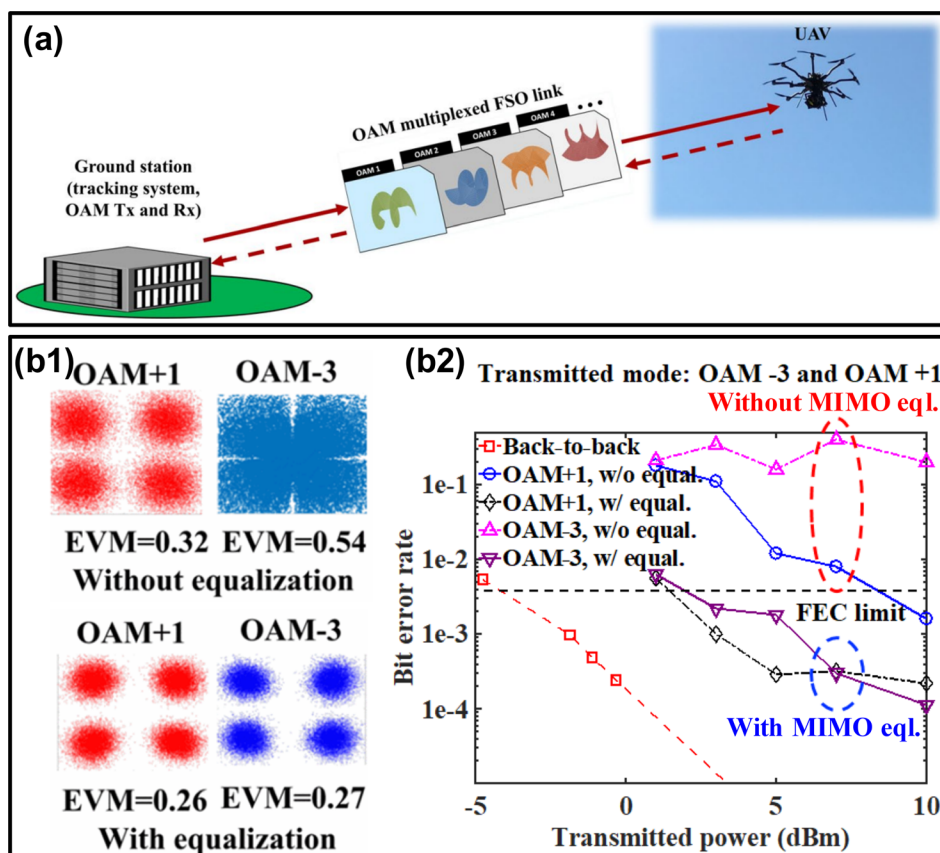


FIG. 32. (a) Concept of the OAM-multiplexed ground-to-UAV-to-ground FSO communication link. The OAM transmitter and receiver are located at the same ground station. A tracking system is employed to mitigate the misalignment at the ground station. The multiplexed OAM beams are reflected by a retro-reflector carried by the hovering UAV. Reproduced with permission from Li *et al.*, Sci. Rep. **7**, 17427 (2017).¹⁴⁰ Copyright 2017 Macmillan Publishers. (b-1) The constellations of the received QPSK signals carried by the two OAM beams and the corresponding EVMs. MIMO equalization is used to mitigate the atmospheric turbulence-induced channel crosstalk. (b-2) Measured BERs at different transmitted power for the two channels. The UAV is hovering ~ 50 m away. Cases without and with MIMO equalization are shown. Reproduced with permission from Li *et al.*, Opt. Lett. **44**, 5181 (2019). Copyright 2019 Optical Society of America.¹⁴⁴

inter-channel crosstalk. The atmospheric turbulence-induced channel crosstalk could be mitigated using the aforementioned MIMO equalization algorithm. It has been shown that a 2×2 MIMO equalization is utilized in an OAM-multiplexed communication link between a hovering UAV and the ground station with a 100-m link length. Figure 32(b-1) illustrates the constellations of the received QPSK signals carried by the two OAM beams. The EVMs could be reduced with the MIMO equalization. It is observed that the MIMO equalization can reduce the EVM from 32% and 54% to 26% and 27%, respectively, for OAM $\ell = +1$ and $\ell = -3$ beams. Figure 32(b-2) shows the received BERs with various the transmitted power. For both OAM channels, the BER is reduced by the MIMO equalization, which indicates that the turbulence-induced channel crosstalk could be mitigated. In addition to MIMO equalization, some other approaches for mitigating turbulence effects might also be helpful, such as the AO system or beam shaping.

To enable the OAM-based airborne communication links in the future, the corresponding challenges for different scenarios need to be investigated and mitigated. For satellite-to-satellite links, the beam diverges after the long-distance propagation. At the receiver, the received power can be reduced as the aperture size is often limited. Therefore, a highly sensitive detector at the receiver can benefit such communication links. In addition, mitigation methods such as transmitter lenses and partial receivers can also be potentially used to mitigate the loss and crosstalk in such ultralong links. For satellite-to-ground-station and airplane-to-ground-station links, both beam divergence and atmospheric turbulence need to be considered. Therefore, besides the methods for beam divergence, some aforementioned mitigation methods for turbulence effects might also help to improve the system performance.

Moreover, there are some common features favored for these types of FSO links. For example, (1) low size, weight, and power (SWaP) are desired, which might be achieved with photonic integrated circuits and will be discussed in Sec. VIII,¹⁴⁵ and (2) accurate pointing, acquisition, and tracking (PAT) systems are favored, which might mitigate the power coupling among the OAM modes.⁴⁸

E. OAM-based optical communications in underwater environments

In addition, the data capacity demand of underwater communication links has also been increasing because of the various applications.¹⁴⁶ Although acoustic waves can be utilized in such underwater links, the data rate transmitted could be quite limited due to the small bandwidth resources at a low carrier frequency.¹⁴⁷ In contrast, optical light waves can provide a higher bandwidth, allowing a higher data rate being transmitted. Specifically, the blue-green visible light region has a low attenuation in the underwater link, enabling high-capacity optical underwater communications.¹⁴⁸ In these communication systems, the OAM multiplexing technique could potentially further enhance the data capacity.

1. Propagation effects in underwater environments

There are several reports of OAM beam propagation through underwater environments with water currents, particle scattering, and turbulence.^{149,151} Figure 33(a) illustrates the schematic of an underwater OAM-multiplexing optical communication link. Data-carrying

OAM beams are multiplexed, transmitted through the underwater environment, and de-multiplexed at the receiver. Such links can be affected by various water conditions, as shown by the profiles of a Gaussian beam, OAM + 1 and + 3 beams in Fig. 33(b). Among these effects, (i) the tap water is not likely to distort the donut-shaped intensity profile of the OAM beams. (ii) The water current can slightly change the intensity profiles. (iii) The scattering effect is emulated by adding Maalox solution to water. It causes a dynamic change to the profiles over time as the particles move in the water. (iv) The turbulence effect in the water is emulated by mixing cold and hot water to create a thermal gradient. It tends to cause a large distortion to the beam profiles.¹⁴⁹

Besides the transmission of a single OAM beam, another work explored using combinations of concentric optical vortex beams for underwater links with scattering effects.¹⁵⁰ Figure 33(c) shows the intensity profiles of the “petal” pattern generated by the periodic constructive and destructive interference of the concentric vortices. The profiles are little affected by the clean water and slightly more distorted by the turbid water because of the underwater scattering effects.¹⁵⁰

2. OAM-multiplexed underwater communication links

Blue-green light underwater links with non-OAM beams have been reported over a ~100-m transmission distance.¹⁴⁸ Moreover, to further boost the data capacity, OAM-multiplexing has been demonstrated in underwater links with a transmission distance of a few meters^{149,151}

Generally, the signal could be modulated on the blue-green light by the internal modulation of the light source. For instance, an 1.5-Gbit/s OOK signal is directly modulated on the driving current of a 445-nm laser diode.¹⁵¹ By multiplexing two independent OOK data channels carried by two OAM modes, an underwater communication link with a 3-Gbit/s total capacity is achieved over a 2.96-m transmission distance.¹⁵¹

However, the direct modulation on commercial laser diodes might have a limited bandwidth. Therefore, the data rate of direct modulated data channels could be limited. To achieve higher data rates, a high-speed modulated blue-green light can be generated based on the second harmonic generation. For example, a 10-Gbit/s OOK signal can be first generated by using a commercial high-speed 1064-nm lithium niobite modulator. Subsequently, a module for a second harmonic generation is used such that the carrier wavelength of the signal is converted to 532 nm.¹⁴⁹ Figure 33(d) presents the BERs as a function of the received power for the two multiplexed OAM channels, each carrying a 10-Gbit/s OOK signal. As the link is affected by the turbulence in water, the BER is degraded to above the FEC limit. With the constant modulus algorithm (CMA)-based equalization, the BER can be reduced to below the FEC limit.¹⁴⁹

In addition to OAM-based links in underwater environments, there are applications where the OAM beams originate above the water and need to be in contact with a station below the water. In this scenario, the OAM beams may propagate through several “layers” at the air-water interface, including maritime turbulence, non-uniform aerosols above water, time-varying water curvatures, and underwater scattering/turbulence below the surface,^{152,153} as shown in Fig. 34. The combination of these issues could potentially cause power loss and modal coupling in an OAM-based optical link, which might be

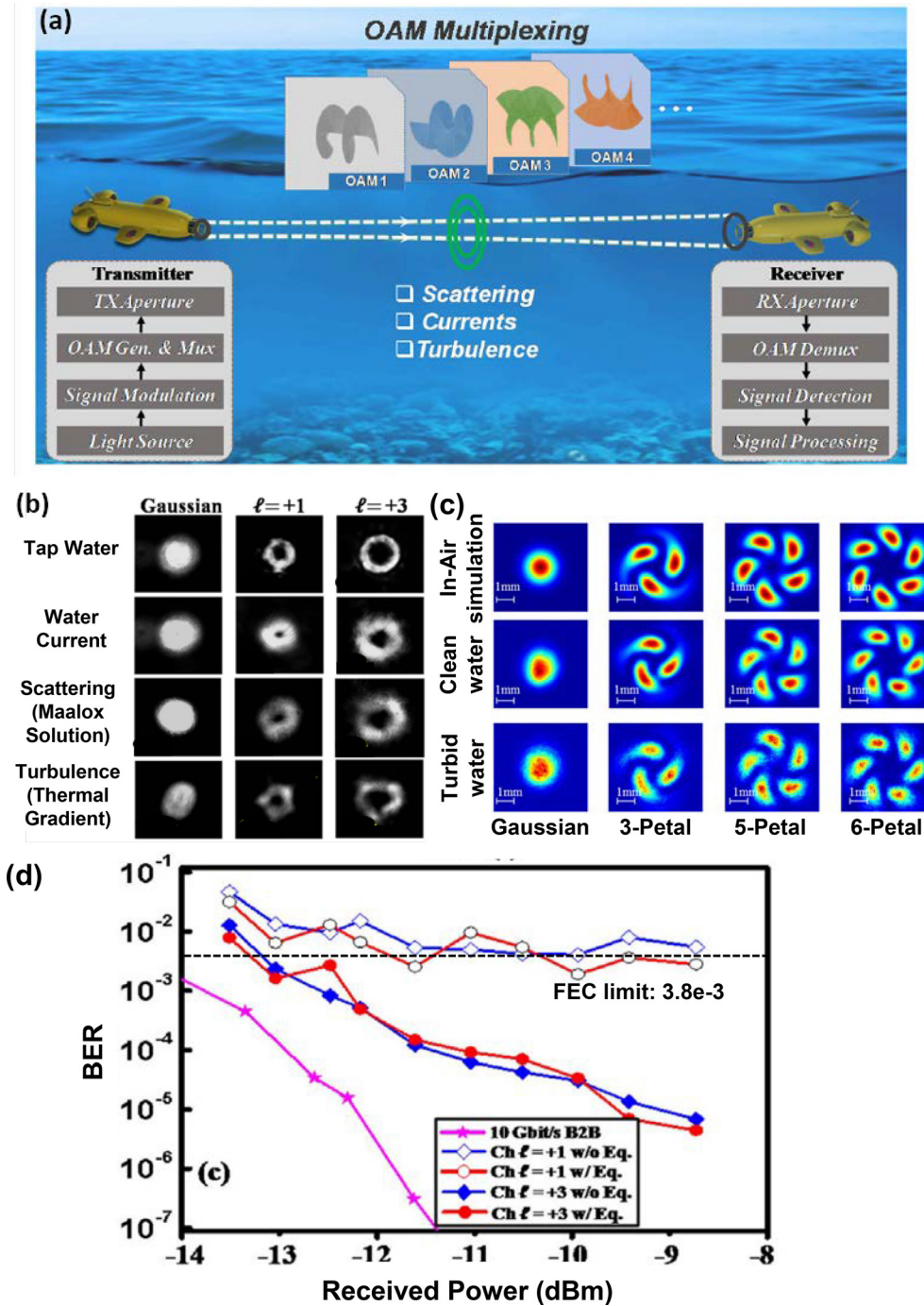


FIG. 33. (a) Concept of an underwater OAM-multiplexing optical communication link. Reproduced with permission from Ren *et al.*, Sci. Rep. **6**, 33306 (2016).¹⁴⁹ Copyright 2016 Macmillan Publishers. (b) Intensity profiles of the Gaussian beam and OAM $\ell = +1, +3$ beams under different conditions including tap water, water current, scattering, and turbulence. Reproduced with permission from Ren *et al.*, Sci. Rep. **6**, 33306 (2016).¹⁴⁹ Copyright 2016 Macmillan Publishers. (c) Intensity profiles of the beams with “petal” patterns for simulated propagation through air, experimental propagation through clean water, and experimental propagation through turbid water. Reproduced with permission from Morgan *et al.*, J. Opt. **18**, 104004 (2016).¹⁵⁰ Copyright 2016 IOP Publishing. (d) Measured BERs as a function of the received power for the two multiplexed OAM channels, each carrying a 10-Gbit/s OOK signal. As the link is affected by the turbulence in water, the BER is degraded to above the forward error correction (FEC) limit. With the constant modulus algorithm-based equalization, the BER can be reduced to below the FEC limit. Ch.: channel. Eq.: equalization. Reproduced with permission from Ren *et al.*, Sci. Rep. **6**, 33306 (2016).¹⁴⁹ Copyright 2016 Macmillan Publishers.

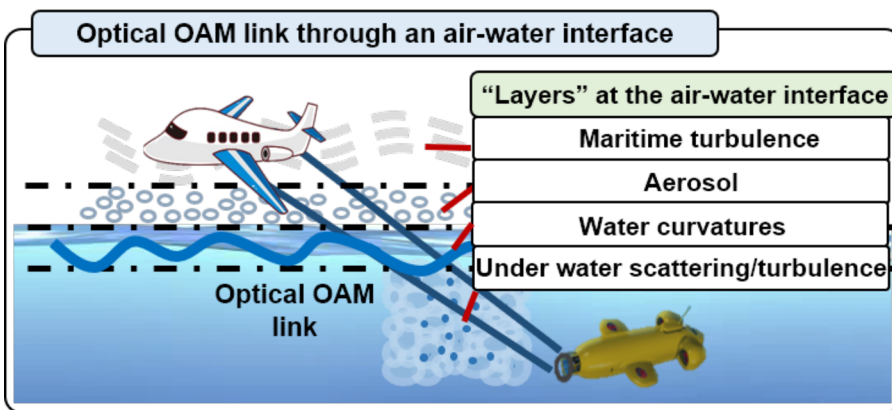


FIG. 34. Challenges for an optical OAM link through an air–water interface.

alleviated by using aforementioned mitigation approaches. Further investigations in this field could be an interesting challenge.

F. OAM-based diversity system

As mentioned above, atmospheric turbulence could lead to power fluctuation and link loss in a single-channel FSO system.⁴⁴ One way to mitigate the turbulence effects is to utilize AO, which generally consists of a wavefront sensor, a wavefront corrector, and a feedback control unit.^{155,156} Without using a feedback control loop for an AO system, diversity schemes could be employed to potentially provide system redundancy and thus reduce the outage probability of the FSO link.^{44,156,157} In a diversity scheme, multiple copies of the same data streams are simultaneously carried by multiple beams.^{44,158,159} Each beam experiences a different channel condition, which reduces the variance of the overall received power, and thus the outage probability of the link could be lower than that of the link without diversity.^{44,158,159} Specifically, spatial diversity can be realized by transmitting the same data stream with multiple apertures at the transmitter and/or receiver (i.e., aperture diversity).^{44,158,159} Instead of using multiple apertures that are physically separated, another form of spatial diversity, namely, mode diversity, can be employed utilizing coaxial spatial modes from different or the same spatial mode groups at the same Tx/Rx aperture.^{154,160–162}

Recently, a single-channel FSO link using mode diversity from different spatial mode basis sets has been experimentally demonstrated.¹⁵⁴ Specifically, two beams (i.e., $HG_{m=2,n=2}$ and $LG_{\ell=2,p=1}$) carrying the same data stream are combined and transmitted at a single aperture as shown in Fig. 35(a). Beams with the same mode order ($m + n = |\ell| + 2p$) have similar beam divergence after propagation, and thus they tend to have a similar field size at the receiver. In this case, the $HG_{m=2,n=2}$ and $LG_{\ell=2,p=1}$ beams are selected due to their mutual orthogonality. As these two orthogonal beams with different spatial profiles could potentially interact differently with the turbulent medium, the data channel carried by each data-carrying beam tends to have an independent outage probability. By receiving the combined beams at the receiver, the overall outage probability in the mode diversity scheme tends to be smaller compared to that in the single-mode scheme. As proof of concept, the BER performance of a 1-kbit/s FSO link under varying turbulence strength (r_0) are measured as shown in

Fig. 35(b). It is shown that employing mode diversity could help reduce the BER under different turbulence strength.

Furthermore, OAM-based mode diversity has also been experimentally implemented using the modes in the same mode group (e.g., multiple OAM modes).^{161,162} In addition, the mode diversity could also be potentially used in an OAM-multiplexing system to increase the system robustness.¹⁶⁰

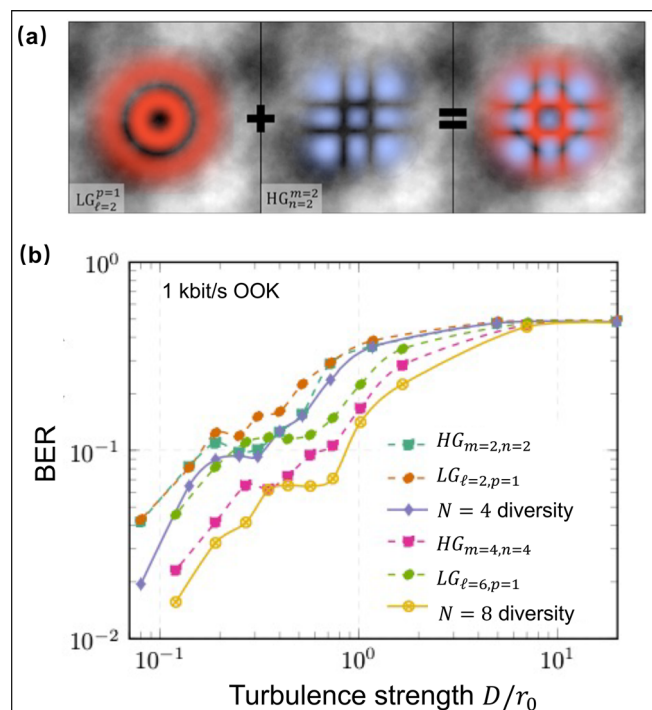


FIG. 35. (a) Concept of employing mode diversity in an FSO link. Different modes are used with half the original transmit power but with each traveling the same path: the separation is in mode space not physical space. (b) Measured bit error rate of data-carrying modes under varying turbulence strength. Reproduced with permission from Cox *et al.*, Phys. Rev. Appl. **10**, 024020 (2018).¹⁵⁴ Copyright 2018 American Physical Society.

G. Summary

In this section, some experimental demonstrations of FSO OAM multiplexing and encoding links are first presented. Subsequently, different potential challenges (beam divergence, misalignment, and turbulence) and the corresponding mitigation methods in OAM-based FSO communication systems are also discussed. Table I illustrates various experimental demonstrations mentioned in this section of OAM-based optical communication links in free space, in an underwater environment, and between a ground station and a UAV. Major parameters, including number of channels, total data rate, and transmission distance, are summarized. To further explore and develop the mitigation techniques for OAM-based communication links, one may need to consider several issues, including but not limited to: (1) scalability: for scaling the compensation scheme to the system that multiplexes a larger number of modes; (2) processing speed: for real-time mitigation of various environmental effects; and (3) cost and complexity: for enabling the deploy of a compensation scheme in a real OAM-based link.

V. OAM-BASED FIBER COMMUNICATION SYSTEMS

Optical fibers have been widely deployed in wired communications, providing a high data capacity. In order to further boost the data rate and spectral efficiency of fiber communication systems, OAM modes can be potentially facilitated in optical fibers that support multiple OAM modes.^{11,163} In this section, we will discuss several different types of the fibers that can allow the propagation of OAM beams. The random mode coupling is a key issue of the OAM-based fiber communication systems, and several mitigation methods will be introduced.

A. OAM modes in fibers

In general, a conventional multi-mode fiber (MMF) has a relatively large core diameter that can support multiple modes to be propagated. Theoretically, the optical beam in an MMF can be described with the Helmholtz equation,¹⁶⁴

$$\nabla^2 E + (nk_0)^2 E = 0, \quad (22)$$

where E is the electrical field of the optical beam, $k_0 = \omega/c = 2\pi/\lambda$, and n is the refractive index as a function of the location in the fiber cross section. Different types of MMFs can be characterized by different n distributions,^{165,166} such as step-index fibers, as shown in Fig. 36.¹⁶⁵

Equation (22) can be solved with the method of variable separation.¹⁶⁴ The exact solutions lead to the vector eigenmodes of the fiber, including the $HE_{\nu m}$ and $EH_{\nu m}$ modes. When the mode index $\nu = 0$, they are also referred to as the transverse-electric (TE) and transverse-magnetic (TM) modes. Applying the weakly guiding approximation,¹⁶⁷ the vector eigenmodes can be expressed as¹⁶⁸

$$\begin{cases} HE_{\ell+1,m}^e \\ HE_{\ell+1,m}^o \end{cases} = R_{\ell,m}(r) \exp(i\beta z) \begin{cases} \hat{x} \cos(\ell\theta) - \hat{y} \sin(\ell\theta) \\ \hat{x} \sin(\ell\theta) + \hat{y} \cos(\ell\theta) \end{cases}, \quad (23)$$

$$\begin{cases} EH_{\ell-1,m}^e \\ EH_{\ell-1,m}^o \end{cases} = R_{\ell,m}(r) \exp(i\beta z) \begin{cases} \hat{x} \cos(\ell\theta) + \hat{y} \sin(\ell\theta) \\ \hat{x} \sin(\ell\theta) - \hat{y} \cos(\ell\theta) \end{cases},$$

where $R_{\ell,m}(r)$ is the radial field distribution ($\ell = 0, 1, 2, \dots$; $m = 1, 2, \dots$ are two mode indices). In addition, (r, θ, z) is the cylindrical coordinate and refers to the radial, azimuthal position in a fiber

cross section, and propagation position along the fiber. \hat{x} and \hat{y} represent the unit vector of the X and Y polarizations, respectively. e and o denote the even and odd modes, respectively. Each mode solution has a propagation constant β , and the effective index n_{eff} is defined as $n_{\text{eff}} = \lambda\beta/2\pi$. The modes that have a similar propagation constant are generally classified into the same “mode group.”

Under the weakly guiding approximation, another set of mode solutions with linear polarizations can be obtained, which are referred to as the LP modes.¹⁶⁴ The $LP_{\ell,m}$ mode solution along one polarization (e.g., x polarization) is given as

$$\begin{cases} LP_{\ell,m,x}^e = \hat{x}R_{\ell,m}(r) \cos(\ell\theta) \exp(i\beta z), \\ LP_{\ell,m,x}^o = \hat{x}R_{\ell,m}(r) \sin(\ell\theta) \exp(i\beta z). \end{cases} \quad (24)$$

We note that the LP modes can be constructed by a linear superposition of vector eigenmodes,¹⁶⁸

$$\begin{cases} LP_{\ell,m,x}^e = EH_{\ell-1,m}^o + HE_{\ell+1,m}^o, \\ LP_{\ell,m,x}^o = EH_{\ell-1,m}^e - HE_{\ell+1,m}^e. \end{cases} \quad (25)$$

It is observed that, based on Eq. (24), OAM can be represented by a combination of the LP modes or vector eigenmodes, as shown in Fig. 37. For example, a combination of LP modes¹⁶⁹

$$LP_{\ell,m,x}^e + iLP_{\ell,m,x}^o = \hat{x}R_{\ell,m}(r) \exp(i\ell\theta) \exp(i\beta z) \quad (26)$$

can represent an OAM mode of order ℓ with a linear polarization. In order to increase the data capacity in a fiber-based MDM link, OAM modes can be potentially used as a modal basis in the MMFs.¹⁷⁰

B. Random mode coupling in the fiber

Although the fiber medium is quite different than free space, OAM-based fiber communication systems also have important mode-related challenges. For instance, while the beams could be excited into orthogonal modes (e.g., vector modes or LP modes) when launching into an MMF, they will often be coupled to other modes as a result of the temperature variation, different kinds of inhomogeneities, bends, and other non-idealities.¹⁷¹

In general, different modes in a fiber might have different β values. When the difference between the β values for two modes is smaller, intermodal power coupling gets higher. If the two modes have the same β , the power coupling becomes the highest.¹⁶⁴ Thus, the modes from the same mode group tend to have a relatively strong coupling (i.e., intra-modal-group power coupling) to each other during fiber transmission. In contrast, modes from different mode groups have large propagation constant differences such that they have a relatively weak mode coupling (i.e., inter-modal-group power coupling).¹⁷² It has been shown that an effective index difference of $\Delta n_{\text{eff}} > 10^{-4}$ ($n_{\text{eff}} = \lambda\beta/2\pi$) can potentially result in a low mode coupling between the modes and stable propagation for a certain transmission length.¹⁷³ As mentioned above, an OAM mode could propagate in conventional central-core fibers as a combination of the vector eigenmodes or LP modes within the same group. Moreover, these mode components (vector eigenmodes or LP modes) that have similar β (or n_{eff}) tend to randomly couple power into each other. Therefore, the OAM modes that are combination of these modes

TABLE I. Demonstrations of OAM-based free-space optical communication links mentioned in this section. The wavelengths are ~ 1550 nm if not specified.

Channel medium	Number of modes	Pol. number	Wavelength number	Type	Total data rate	Distance	Note	Year ^{Ref.}
Free space	8 OAM	1	1 (He-Ne laser)	Encoding	...	15 m	...	2004 ¹⁴
	Gaussian and 1 OAM	1	1	Multiplexing	20-Gbit/s OOK	2010 ⁹⁴
	4 OAM	1	1	Multiplexing	171.2-Gbit/s 16-QAM	2011 ⁹⁵
	4 OAM	2	1	Multiplexing	1.37-Tbit/s 16-QAM	1 m	...	2012 ¹²
	2 OAM	1	1	Multiplexing	200-Gbit/s QPSK	...	• Partial receiver aperture	2013 ¹¹³
	3 OAM	1	1	Multiplexing	300-Gbit/s QPSK	...	• Double partial receiver apertures	2014 ¹¹²
	12 OAM	2	42	Multiplexing	100.8-Tbit/s QPSK	1 m	...	2014 ³⁸
	26 OAM	2	368	Multiplexing	1.036-Pbit/s OFDM-8QAM	2014 ⁹⁶
	4 OAM	1	1	Multiplexing	80-Gbit/s QPSK	1 m	• Emulated turbulence • MIMO	2014 ¹²⁰
	Multiple OAM on one pol.; Gaussian on the other pol.		1	Multiplexing	Multiple 100-Gbit/s QPSK	...	• Bi-directional • Gaussian beam also as probe beam • Emulated turbulence • AO	2014 ¹²⁶
Free space	4 OAM, 2 pol. on wavelength 1; Gaussian, 2 pol. on wavelength 2			Multiplexing	1-Tbit/s QPSK	...	• Gaussian beam also as probe beam • Emulated turbulence • AO	2015 ¹²⁵
	4 OAM	1	1	Encoding	20-Gbit/s	1 m	...	2015 ¹⁵
	4 OAM	1	1	Multiplexing	400-Gbit/s QPSK	120 m	...	2016 ⁹⁷
	2 OAM	1	1	Multiplexing	80-Gbit/s 16-QAM	260 m	...	2016 ⁹⁸
	6 OAM	1	1 (532 nm)	Encoding	...	143 km	• Artificial neural network	2016 ¹⁶
	LG _{0,0} and LG _{0,1}	1	1	Multiplexing	200-Gbit/s QPSK	1 m	...	2016 ²⁰
	LG _{5,0} , LG _{2,1} , LG _{-2,1} , LG _{-5,0}	1	1 (633 nm)	Encoding	...	3.55 m	...	2016 ⁴³
	4 OAM	1	1	Multiplexing	400-Gbit/s QPSK	1 m	• Limited-size aperture • Transmitter lenses	2016 ¹¹¹
	2 OAM	1	1	Multiplexing and aperture diversity	40-Gbit/s QPSK	1 m	• 2 Tx apertures and 2 Rx apertures sending the same OAM-multiplexed data • Emulated turbulence • MIMO	2016 ¹⁵⁹

TABLE I. (Continued.)

Channel medium	Number of modes	Pol. number	Wavelength number	Type	Total data rate	Distance	Note	Year ^{Ref.}
Free space	4 OAM	1	1	Multiplexing	400-Gbit/s QPSK	1 m	• Limited-size aperture • Non-zero radial index LG modes	2017 ¹⁹
	LG _{1,0} , LG _{-1,0} , LG _{1,1} , LG _{-1,1}	1	1	Multiplexing	400-Gbit/s QPSK	1 m	...	2018 ¹³
	4 OAM	1	1	Multiplexing	400-Gbit/s QPSK	1 m	• Displacement • OAM-beam based tracking	2018 ¹¹⁶
	HG _{2,2} , LG _{2,1}	1	1 (660 nm)	Mode diversity	1-kbit/s OOK	...	• Emulated turbulence	2018 ¹⁵⁴
	4 multi-mode beams using LG modes	1	1	Multiplexing	400-Gbit/s QPSK	1 m	• Limited-size aperture • Displacement • SVD-based orthogonalization	2020 ¹¹⁵
	2 OAM	1	1	Multiplexing	200-Gbit/s QPSK	1 m	• Emulated turbulence • MPLC and AO	2020 ¹³⁰
	2 OAM	1	1	Multiplexing	200-Gbit/s QPSK	...	• Emulated turbulence • Adaptive wavefront shaping and diffusing	2020 ¹²⁹
	2 OAM	1	1	Multiplexing	200-Gbit/s QPSK	...	• Emulated turbulence • Pre-signal combining	2020 ¹²⁷
	Gaussian and 1 OAM	1	1	Aperture and mode diversity	10-Gbit/s QPSK	...	• 2 Tx apertures and 2 Rx apertures sending the same data • Displacement and emulated turbulence • MIMO	2020 ¹⁶¹
	2 OAM	1	1 (785 nm)	Multiplexing	40-Mbit/s OOK	340 m	• Phase conjugation	2021 ¹³¹
Underwater	Gaussian and 1 OAM	1	1	Aperture and mode diversity	100-Gbit/s QPSK	1 m	• 2 Tx apertures and 2 Rx apertures sending the same data • Emulated turbulence	2021 ¹⁶²
	2 OAM	1	1 (445 nm)	Multiplexing	3-Gbit/s OOK	2.96 m	• Direct modulation	2016 ¹⁵¹
	4 OAM	1	1 (532 nm)	Multiplexing	40-Gbit/s OOK	1.2 m	• Wavelength conversion	2016 ¹⁴⁹
	Ground station to UAV	2 OAM	1	Multiplexing	80-Gbit/s QPSK	100-m round trip	• Tracking with Gaussian beacon beam	2017 ¹⁴⁰
		2 OAM	1	Multiplexing	40-Gbit/s QPSK	100-m round trip	• Tracking with Gaussian beacon beam • Emulated turbulence • MIMO	2019 ¹⁴⁴

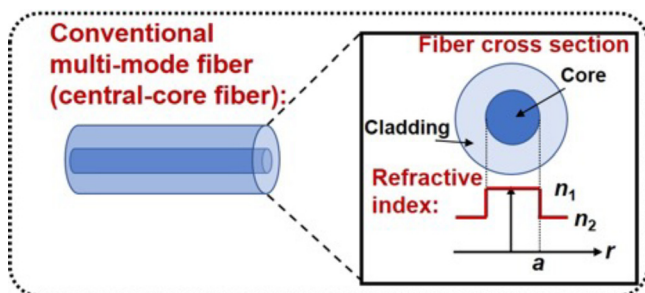


FIG. 36. The refractive index distribution of the conventional MMFs (central-core fibers). The dark blue part of the fiber cross section represents the fiber core with a higher refractive index (n_1). The light blue part represents the fiber cladding with a lower refractive index (n_2). a is the radius of the fiber core.

could be distorted, thus inducing mode coupling to other OAM modes.¹⁶⁸

C. Potential techniques for mitigating OAM mode coupling

Generally, the mode coupling effect in the fibers could induce channel crosstalk for an OAM-multiplexed fiber communication system.¹⁶³ Therefore, mitigation methods or novel designed fibers for the issue of the random mode coupling are often required to enable the OAM multiplexing.

1. MIMO equalization

The concept of MIMO equalization mentioned previously to compensate for turbulence effects in free-space links can be used to compensate the OAM channel crosstalk caused by the random mode coupling in central-core fibers without adding optical complexities. An example of the receiver configuration is shown in Fig. 38(a). In this scheme, two PDM QPSK signals are carried by OAM +1 and -1. The two OAM beams are transmitted through a 5-km few-mode fiber (FMF) and demultiplexed to two single-mode fibers (SMF). A local oscillator is split to four branches to be mixed with the four data signals. Subsequently, the four data channels are detected and sampled simultaneously. Offline DSP is used to perform a 4×4 MIMO

equalization.¹⁷⁰ Figure 38(b) shows the received constellations of the 20-Gbit/s QPSK signals carried by the four multiplexed OAM beams, which have the corresponding EVMs below 25%. It should be noted that this approach might also be potentially used for simultaneous mitigation of both inter- and intra-group mode couplings.^{122,174} However, the MIMO equalization could have high electrical complexity when the number of modes increases.

2. Adaptive optics

In some applications, it might be desired to use an optical approach to compensate for the modal crosstalk without increasing the electrical DSP complexity. The AO system introduced previously for the turbulence mitigation can be used to compensate the mode crosstalk in MDM fiber communication systems.

The schematic of intra-group mode coupling mitigation in an FMF utilizing AO is shown in Fig. 39(a). The mode coupling of the OAM +1 and -1 modes in an FMF can be described with a complex 2×2 transmission matrix H . The amplitude and phase components indicate the power coupling and phase change between the two OAM modes, respectively. An inverse matrix S can be applied to the received beams with mode coupling¹⁷⁵

$$S = H^{-1} = \begin{bmatrix} s_{11} & s_{12} \\ s_{21} & s_{22} \end{bmatrix} = \begin{bmatrix} s_1^T \\ s_2^T \end{bmatrix}, \quad (27)$$

where $s_1^T = [s_{11} \ s_{12}]$ and $s_2^T = [s_{21} \ s_{22}]$ are the row vectors of matrix S . A phase pattern can be generated as a superposition of the demultiplexing phase patterns of the two OAM modes. The complex weights are determined by the row vectors (s_1^T and s_2^T) for the OAM +1 and -1 channels, respectively. By applying such a superposed phase pattern at the receiver, the crosstalk between the two OAM channels can be mitigated. Figure 39(b) shows the measured crosstalk as a function of time for the $\ell = +1$ channel. The crosstalk is reduced to a relatively low level (< -11 dB) when the AO is applied. The AO is applied again when the crosstalk increases to a threshold. In addition, a similar “optical equalization” approach, called digital optical phase conjugation, has also been used for the mitigation of the inter-group mode coupling.¹⁷⁶ However, these optical approaches might require a feedback loop, which would increase the complexity of the optical system.

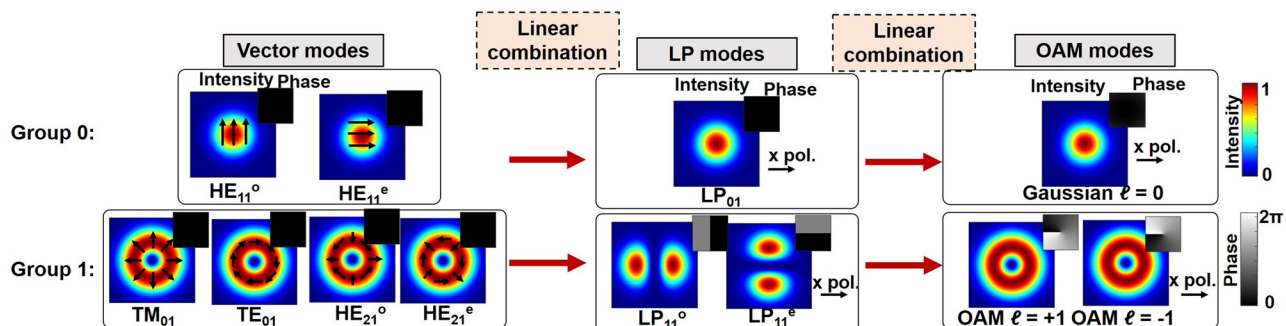


FIG. 37. Intensity and phase profiles of the vector modes, LP modes, and the corresponding OAM modes of two mode groups (group 0 and group 1) in conventional MMFs. The arrows in the vector mode intensity profiles represent the polarizations. LP and OAM modes on the x-polarization are shown as an example.

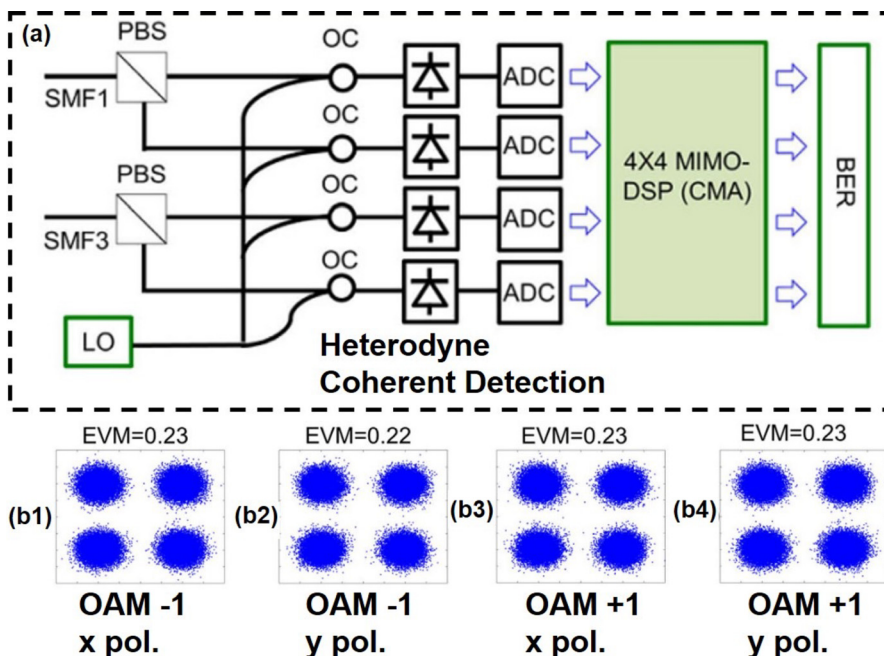


FIG. 38. (a) Receiver configuration of a 4x4 MIMO to compensate for the modal crosstalk of an OAM-multiplexed fiber communication system. SMF: single-mode fiber; PBS: polarization beam splitter; OC: optical coupler; ADC: analogue-to-digital converter; LO: local oscillator; CMA: constant modulus algorithm; MIMO DSP: multi-input–multi-output digital signal processing. (b) Received constellations of 20-Gbit/s QPSKs on the OAM beams after MIMO. Reproduced with permission from Huang *et al.*, Sci. Rep. 5, 14931 (2015).¹⁷⁰ Copyright 2015 Macmillan Publishers.

3. Novel fibers

Without increasing system complexity, one can consider to designing novel fibers to support the transmission of OAM modes.^{11,178–180} In order to reduce the OAM mode coupling, the design of such fibers generally has two goals: (1) large effective index

difference between the vector eigenmodes and (2) a fiber profile that is compatible with the donut-shaped OAM beams.¹⁸¹ One potential candidate might be the ring-core fiber of which the typical refractive index distributions are shown in Fig. 40(a).

An example of such ring-core fibers for OAM mode propagation is shown in Fig. 40(b). The measured (dots) and numerically

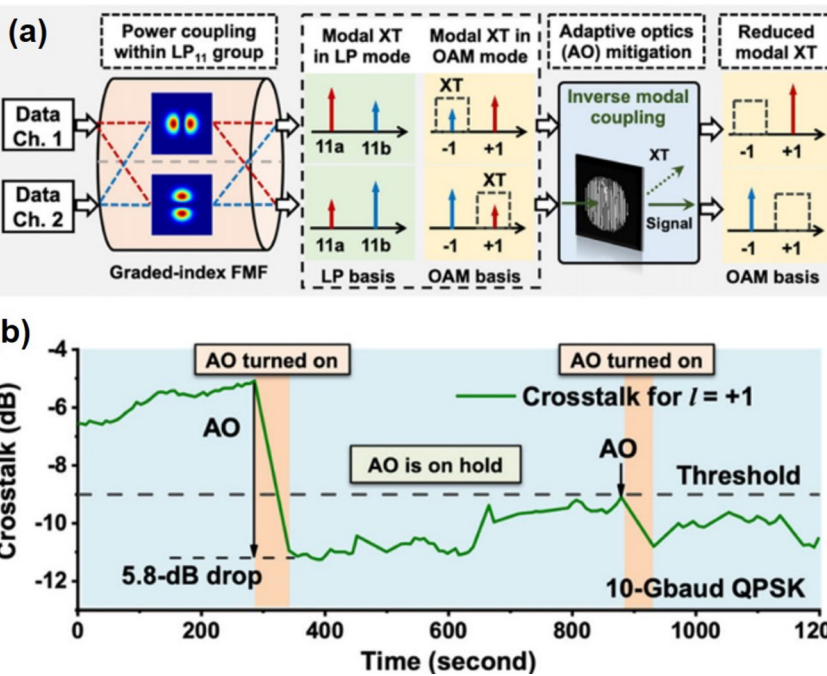


FIG. 39. (a) Concept diagram for the intra-group mode coupling mitigation in an FMF utilizing AO. The crosstalk is reduced by applying an inverse transmission matrix of the two modes at the receiver. (b) Measured time-varying crosstalk for the OAM +1 channel. Reproduced with permission from Zhang *et al.*, Opt. Lett. 45, 3577 (2020).¹⁷⁵ Copyright 2020 Optical Society of America.

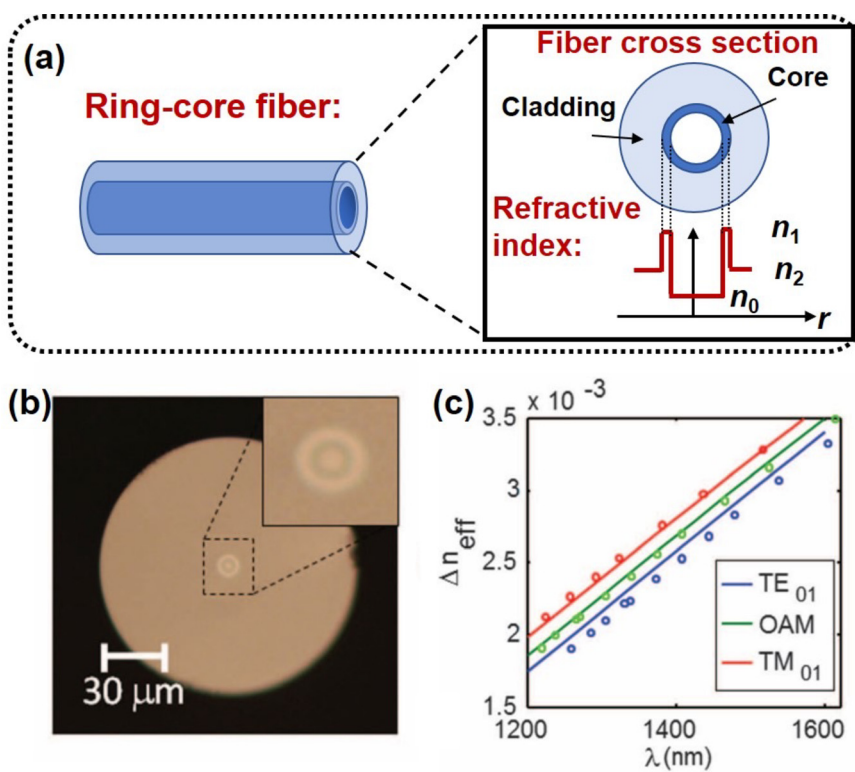


FIG. 40. (a) The refractive index distribution of the ring-core fibers. The white part represents the inner core with the refractive index of n_0 . The dark blue part of the fiber cross section represents the ring-shaped core with a higher refractive index of n_1 . The light blue part represents the fiber cladding with a refractive index of n_2 . (b) Microscope image of the vortex fiber cross section. (c) Measured and numerically calculated effective index differences of the first-order modes with respect to the fundamental LP_{01} mode. Reproduced with permission from Bozinovic *et al.*, Science 340, 1545 (2013).¹¹ Copyright 2013 American Association for the Advancement of Science.

calculated (lines) effective index differences of the first-order modes with respect to the LP_{01} are shown in Fig. 40(c).¹¹ The result shows separation among the effective index of the OAM mode, the TE_{01} mode, and the TM_{01} mode, which indicates that this OAM mode would be preserved within a certain transmission distance. Moreover, 1.6-Tbit/s data capacity with two OAM beams on ten wavelengths have been achieved through such a fiber over 1.1 km.¹¹

Furthermore, to increase the number of supported modes, a high refractive index difference between the ring-shaped core and the inner core is preferred.¹⁸² For example, the air–core fiber has been proposed with the air as the inner–core medium.^{177,183} As shown in Fig. 41(a), the simulated effective indices of a specially designed air–core fiber have a relatively large difference between most of the OAM modes. As a result, MIMO-free data transmission of 12 OAM modes over 1.2-km

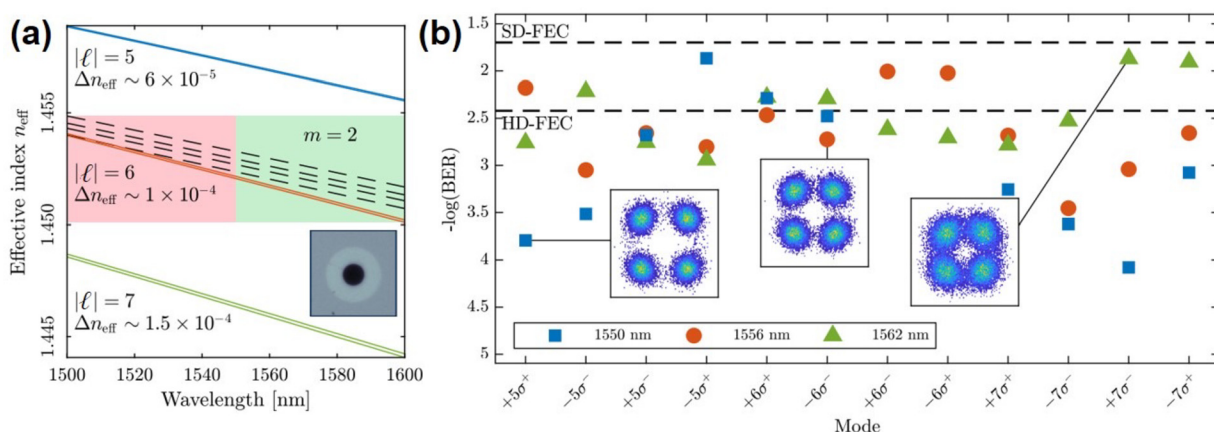


FIG. 41. (a) Simulated effective indices as a function of the wavelength. The inset shows a microscope image of the air–core fiber. The red-shaded area denotes the bandwidth where the $|\ell| = 6$ modes experience accidental degeneracies with double-ringed $m = 2$ modes. (b) Measured BERs after the fiber transmission. σ^{\pm} denote two circular polarizations. SD-FEC: soft-decision forward error correction. HD-FEC: hard-decision forward error correction. Reproduced with permission from Ingerslev *et al.*, Opt. Express 26, 20225 (2018).¹⁷⁷ Copyright 2018 Optical Society of America.

air-core fiber is achieved with 60 WDM channels, each carrying 10-Gbaud QPSK signals.¹⁷⁷ The received BERs of all the OAM modes on three wavelengths are shown in Fig. 41(b). However, such novel fibers have different structures compared to the current deployed fibers. In order to broadly deploy them in the actual links, more resolve might be needed.

D. OAM fiber amplifiers

In addition to random mode coupling, the power loss caused by fiber attenuation might be another challenge for OAM-based fiber communication systems, which may limit the transmission distance. In order to achieve long-distance OAM-based fiber transmission links, the inline OAM fiber amplifiers might help us to compensate for the power loss in the fiber link. For an OAM-based fiber communication system, a desired OAM fiber amplifier might have features, including high gain and small gain difference on different OAM modes and different wavelengths.

As similar to the case of conventional single-mode fiber amplifiers, there are generally two types of OAM fiber amplifiers, including the OAM erbium-doped fiber amplifiers (EDFA)^{184,186} and OAM Raman amplifiers,¹⁸⁵ as shown in Fig. 42. The OAM EDFA uses the specially designed erbium-doped fiber (EDF) as the gain medium,

which has a central air hole and a ring-shaped erbium-doped core in its cross section,¹⁸⁴ as shown in Fig. 42(a-1). The OAM beams can be amplified by launching them to the EDF along with a 976-nm pump laser. The measured gain spectrum has a gain peak of ~15.7 dB located at ~1565 nm, as shown in Fig. 42(a-2). Figure 42(a-3) shows the interferograms of the amplified OAM +1 and -1 beams at the output of the EDFA.¹⁸⁴ This OAM EDFA shows a gain of >10 dB with a uneven curve in the ~20-nm wavelength range. Recently, this type of OAM amplifier has been utilized in a two-OAM-multiplexed communication link with each OAM carrying 10-Gbaud 16-QAM signals on four wavelengths.¹⁸⁶

The OAM Raman amplifier uses the normal ring-core fiber for both transmitting and amplifying the OAM modes, as shown in Fig. 42(b-1). In this example, to amplify the OAM beams, two 1455-nm pump lasers are launched along with them in the forward Raman pumping configuration. Another two 1455-nm pump lasers and a 1360-nm pump laser are launched in the other direction in the backward pumping configuration.¹⁸⁵ The measured gain spectra for OAM +4 and +5 modes are shown in Fig. 42(b-2). The intensity profiles of the output OAM modes after the Raman amplifier are shown in Fig. 42(b-3). In contrast to the EDFA example, this OAM Raman amplifier achieves a ~3-dB gain with a relatively even curve in the ~30-nm wavelength range.

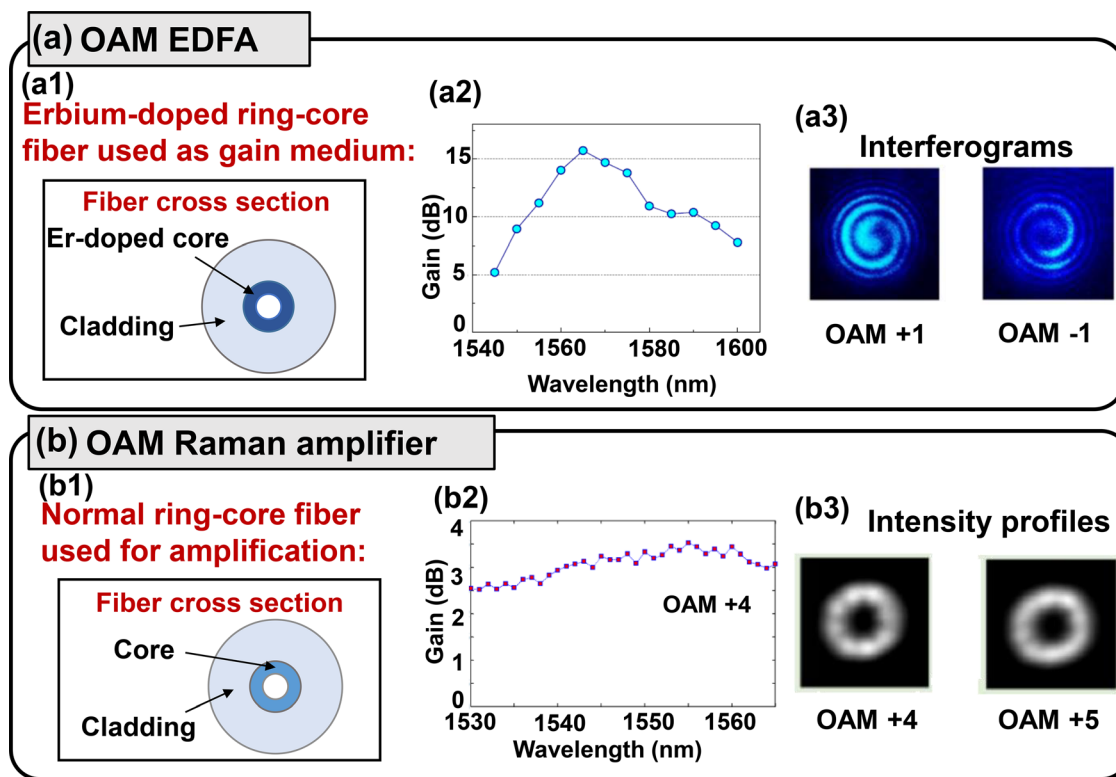


FIG. 42. Two examples of the OAM fiber amplifiers. (a-1) The OAM erbium-doped fiber amplifier (EDFA) uses an erbium-doped fiber with a central air hole and a ring-shaped core as the gain medium. (a-2) Measured gain spectrum of the OAM EDFA with an input signal power of -4 dBm and a launched pump power of 0.57 W. (a-3) Measured interferograms of the amplified OAM +1 and -1 beams at the output of the EDFA. Reproduced with permission from Jung *et al.*, J. Lightwave Technol. **35**, 430 (2017). Copyright 2017 IEEE. (b-1) The OAM Raman amplifier uses the normal ring-core fiber for amplification. (b-2) Measured gain spectra of the OAM +4 and +5 modes of the OAM Raman amplifier. (b-3) Measured intensity profiles of the amplified OAM +4 and +5 beams at the output of the OAM Raman amplifier.¹⁸⁵

E. Summary

In this section, we first discuss the propagation of OAM modes and random mode coupling in fibers. Subsequently, different approaches and novel fibers for mitigating mode-coupling-induced channel crosstalk in OAM-based links are presented. In addition, different types of inline OAM fiber amplifiers are discussed to compensate for the power loss caused by the fiber attenuation. Table II illustrates the experimental demonstrations mentioned in this section of the OAM-based fiber communication systems. Major parameters of each experiment, including the number of channels, total data rate, fiber type, and fiber length, are summarized. In order to further deploy OAM modes in fiber-based communication links, novel fibers with more complex designs, more advanced OAM fiber amplifiers, or other techniques might be needed to improve system performance in fibers over a long transmission distance.¹⁶⁸

VI. OAM IN QUANTUM COMMUNICATIONS

Quantum optical communication links have attracted much interest since they could potentially enhance the system security.^{187–189} In order to increase the photon efficiency (i.e., bits/photon), OAM modes can be potentially used in quantum communication links.^{190–193} In this section, we will first illustrate the basic concept of the OAM-based quantum encoding system. Subsequently, the quantum key distribution (QKD) systems based on OAM modes are introduced. In addition, experimental demonstrations of OAM-based QKD systems in different scenarios are presented. Some practical challenges and corresponding mitigation methods are discussed.

A. OAM-based quantum encoding

Conventionally, data could be encoded on two orthogonal quantum states of the photon, for example, polarizations.¹⁹⁴ In such a quantum scheme, only one bit of information is encoded on each photon. In order to improve photon efficiency, a larger number of orthogonal states might be utilized.^{190–193} As mentioned above, OAM is another property of photons that can also be potentially used in communication links. The experimental accumulated intensity structure of single photons with OAM +1 is shown in Fig. 43.¹⁹⁵ For single photons, the intensity profiles gives the probability of detecting a photon at a certain point. If a triggered single-photon camera is used to detect

many heralded OAM photons, the donut-shaped intensity profile of the OAM mode emerges.¹⁹⁵ Generally, the OAM occurs in discrete steps of $\ell\hbar$, where ℓ is an integer.⁵ Therefore, if multiple orthogonal OAM states are used for encoding, such a high-dimensional quantum link could potentially improve the photon efficiency. Figure 43 presents the concept of a quantum link by encoding data on OAM modes. In each symbol period, a single Gaussian photon is converted to and occupies one of the M OAM states, inducing a photon efficiency of up to $\log_2 M$ bit/photon.¹⁹⁶

B. Free-space OAM-based quantum key distribution (QKD)

Quantum cryptography, such as the QKD, implements a cryptographic protocol and, thus, enables secure communication links between many parties.¹⁸⁷ Typically, QKD systems utilize polarization states of photons for data encoding.^{197–199} For example, in the BB84 protocol,¹⁸⁷ two pairs of orthogonal polarization states are usually used, which are two mutually unbiased bases (MUBs). The usual polarization state pairs used are the rectilinear basis [vertical (0°) and horizontal (90°)] and the diagonal basis (45° and 135°). The sender (Alice) creates a random bit (0 or 1) and randomly chooses one of the two bases.²⁰⁰ Therefore, she randomly prepares a photon based on the bit and chosen basis. Subsequently, she transmits the photon to the receiver (Bob) using the quantum channel. Since Bob does not know which basis the photon is encoded in, he randomly chooses a basis for the photon measurement.²⁰⁰ After Bob has measured all the photons, he communicates with Alice about the selected bases over a public classical channel. In this way, this QKD protocol establishes a secure key between Alice and Bob. This is due to the fact that, if an eavesdropper selects the incorrect basis, he or she might obtain no meaningful information but instead introduce a disturbance in the system, which results in its detection by Alice and Bob.¹⁸⁷

1. Basic concept of OAM-based QKD

Although MUBs based on polarization states offer security against eavesdropping, only a maximum of one bit of information per photon can be transmitted, resulting in a limited key generation rate. As another degree of freedom, the OAM state could be potentially utilized for achieving higher-dimensional QKD schemes.^{17,202,203}

TABLE II. Demonstrations of OAM-based optical fiber communication systems mentioned in this section. The wavelengths are ~ 1550 nm.

Fiber type	Number of modes	Wavelength number	Total data rate	Distance	Note	Year ^{Ref.}
Conventional central-core fiber	4 OAM	1	80-Gbit/s QPSK	5-km FMF	• 4 × 4 MIMO	2015 ¹⁷⁰
	6 OAM	1	120-Gbit/s QPSK	8.8-km OM4 MMF	• 4 × 4 and 2 × 2 MIMO	2018 ¹⁷⁴
	2 LP	1	200-Gbit/s QPSK	0.6-km FMF	• AO using OAM basis	2020 ¹⁷⁵
Ring-core fiber	2 OAM	10	1.6-Tbit/s 16-QAM	1.1-km vortex fiber	...	2013 ¹¹
	12 OAM	60	10.56-Tbit/s QPSK	1.2-km air-core fiber	...	2018 ¹⁷⁷
	2 OAM	112	8.5-Tbit/s 8-QAM	18-km ring-core fiber	...	2018 ¹⁷⁹
	2 OAM	16	640-Gbit/s QPSK	18-km ring-core fiber	• OAM Raman amplification	2018 ¹⁸⁵
	2 OAM	4	320-Gbit/s 16-QAM	1-m ring-core EDF	• OAM EDFA	2020 ¹⁸⁶

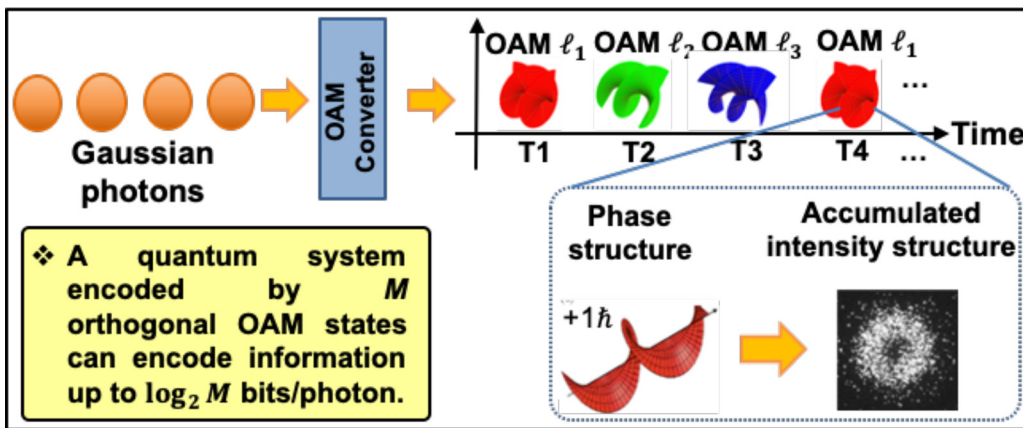


FIG. 43. Concept of quantum link by encoding data on OAM modes. In each symbol period, a Gaussian photon is converted to one of the M OAM states, inducing a photon efficiency of up to $\log_2 M$ bit/photon. Reproduced with the permission from Willner *et al.*, APL Photonics **6**, 030901 (2021).⁴⁰ Copyright 2021 of AIP Publishing.

Figure 44 presents the experimental setup and the two MUBs for a seven-dimensional OAM-based QKD system. In this scheme, Alice randomly chooses photons from two MUBs for information encoding. One base is a set of OAM modes, whose phase profiles can be characterized by $\psi_{\text{OAM}}^{\ell} = e^{i\ell\theta}$, where $\ell \in \{-3 : +3\}$. Moreover, the other basis is constructed by a linear combination of these OAM modes based on the following formula:¹⁷

$$\psi_{\text{ANG}}^n = \frac{1}{\sqrt{M}} \sum_{\ell=-3}^3 \psi_{\text{OAM}}^{\ell} \exp\left(\frac{i2\pi n\ell}{M}\right), \quad (28)$$

where dimension $M=7$ in the experiment. These modes are referred to as the ANG modes, as shown in Fig. 44(b). The ANG modes form a MUB with respect to the OAM basis,¹⁷

$$|\langle \psi_{\text{ANG}}^n | \psi_{\text{OAM}}^{\ell} \rangle|^2 = 1/M \quad \forall \{n, \ell\}. \quad (29)$$

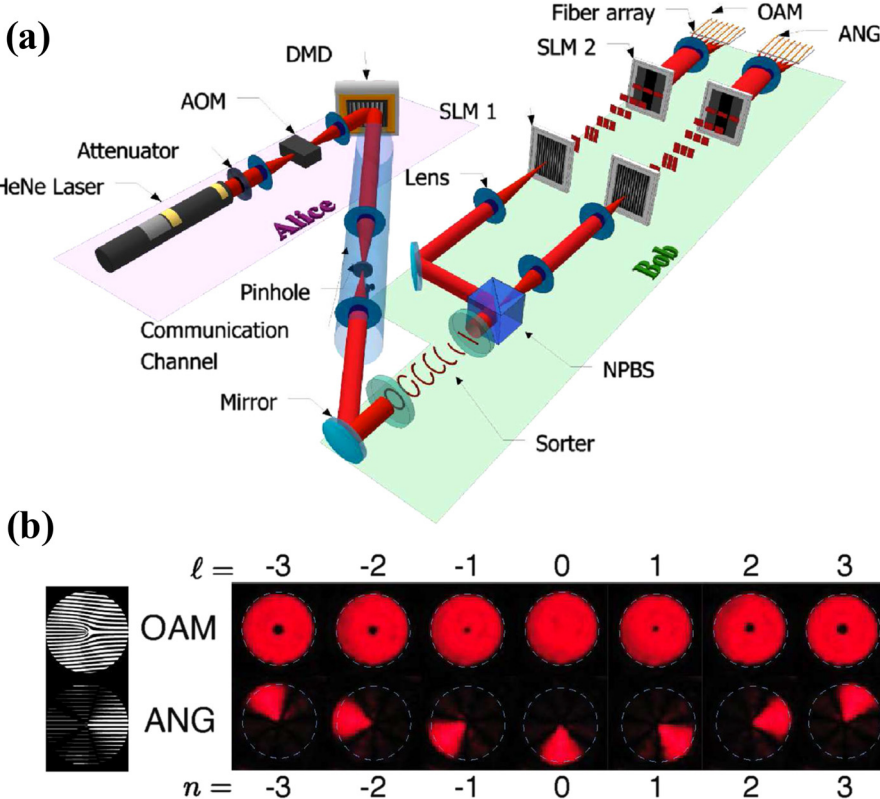


FIG. 44. (a) Experimental setup for a seven-dimensional OAM-based QKD system. At the Alice side, photons with modes are prepared using a He-Ne laser and an acousto optic modulator. The spatial modes are generated by a digital micro-mirror device. At Bob side, single photons are efficiently separated by a mode sorter based on their OAM/ANG states and subsequently collected by an array of fibers. (b) (Left side) Two holograms used for the generating OAM and ANG modes, respectively. (Right side) The measured intensity profiles of the produced light field in OAM and ANG bases ($M=7$). Reproduced with permission from Mirhosseini *et al.*, New J. Phys. **17**, 033033 (2015).¹⁷ Copyright 2015 IOP Publishing.

At Alice's side, photons with OAM and ANG states are generated by shining the attenuated pulse on a digital micro-mirror device. At Bob's side, single photons are efficiently separated by a mode sorter based on their OAM/ANG states and subsequently collected by an array of fibers. As similar to the case of the polarization-based MUBs, an eavesdropper who measures a photon in the OAM basis might not obtain useful information about its ANG state and vice versa. Based on such a seven-dimensional alphabet, a channel capacity of 2.05 bits per sifted photon is achieved with an average symbol error rate (SER) of 10.5%.

2. OAM-based QKD systems beyond laboratory distances

In general, OAM-based QKD links in the laboratory have been experimentally demonstrated over only several meters. However, when OAM photons are used in a long-distance quantum link outside the laboratory, the system performance might be degraded due to several potential issues, such as beam divergence, system misalignment, and atmospheric turbulence effects.

For example, a high-dimensional FSO OAM-based QKD link has been demonstrated between two buildings over 300 m, as shown in Fig. 45.²⁰¹ Four-dimensional quantum states were utilized based on two OAM modes and two vector modes. Under moderate turbulence without active wavefront correction, a BB84 protocol was performed, and a quantum bit error rate of 11% was achieved with a secret key rate of 0.65 bits per sifted photon.

3. Adaptive optics for OAM-based quantum links

As mentioned before, atmospheric turbulence distorts the phase front of light in the classical domain, thus inducing both power loss and crosstalk. Similarly, in the quantum domain, atmospheric turbulence is also a key challenge for OAM-based quantum FSO links. Since it would distort the phase front of photons, intermodal crosstalk might be induced.

One potential method for mitigating the turbulence effect is performing an AO system in an OAM-based quantum communication link. This approach has been experimentally demonstrated in an

OAM-based encoding link with emulated turbulence effects, as shown in Fig. 46.²⁰⁴ A classical Gaussian probe beam (λ_2 , Pol. 2) is transmitted coaxially with the quantum channel (λ_1 , Pol. 1). A wavefront sensor and wavefront corrector are used for phase detection and correction, respectively. Subsequently, a PBS, wavelength filter, and OAM converter are used to efficiently separate the classical and quantum channels due to their different polarizations, wavelengths, and OAM orders.

Figure 47 shows the channel transfer matrices (upper line) between OAM modes $\{\ell = -3, \dots, +3\}$, and the photon count ratio (lower line) on the received OAM modes when sending only OAM $\ell = +1$ photons in different cases. The results show that, under atmospheric turbulence distortion, the mode purity of photons carrying OAM $\ell = +1$ is reduced from $\sim 57\%$ to $\sim 31\%$. With AO compensation, the mode purity of photons is improved from $\sim 31\%$ to $\sim 52\%$. Consequently, quantum symbol error rates (QSERs) are reduced by $\sim 76\%$ in such a 10-Mbit/s OAM-based quantum encoding link. In addition, registered photon rates are also improved by $\sim 64\%$. Since OAM-based encoding might be performed in the QKD protocols, the AO approach could be potentially used for mitigating turbulence effects in an OAM-based QKD system.²⁰⁶

C. OAM-based QKD in underwater environments

As mentioned before, there is growing interest in high-capacity underwater communications. In the classical domain, OAM multiplexing has been investigated and demonstrated in order to increase the capacity of underwater communications.^{149,151,207} In the quantum domain, there have been several studies demonstrating quantum communications based on polarization states,^{208,209} motivated by the goal of secure communication in underwater environments. In order to increase the photon efficiency and the secret key rate, OAM-based high-dimensional QKD would be one scheme that can be implemented.^{205,210}

As similar to the atmospheric environment, turbulence is also one of the key issues for underwater quantum channels, which could be induced by local changes in the refractive index of water from temperature variations. The effects of the turbulence on a 3-m underwater

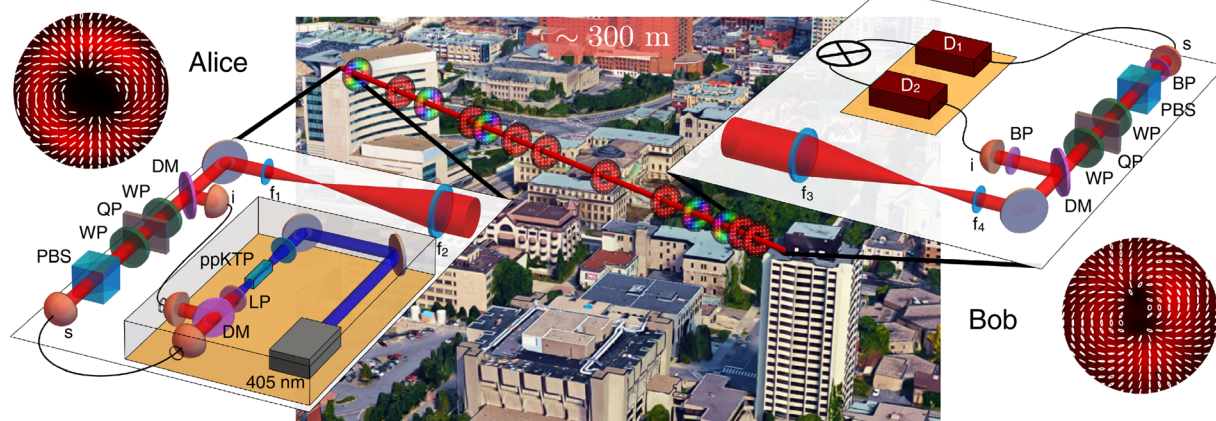


FIG. 45. The quantum communication link between two buildings over 300 m. ppKTP: periodically poled KTP crystal; LP: long-pass filter; WP: waveplate; BP: bandpass filter; DM: dichroic mirror. Reproduced with permission from Sit et al., Optica 4, 1006 (2017).²⁰¹ Copyright 2017 Optical Society of America.

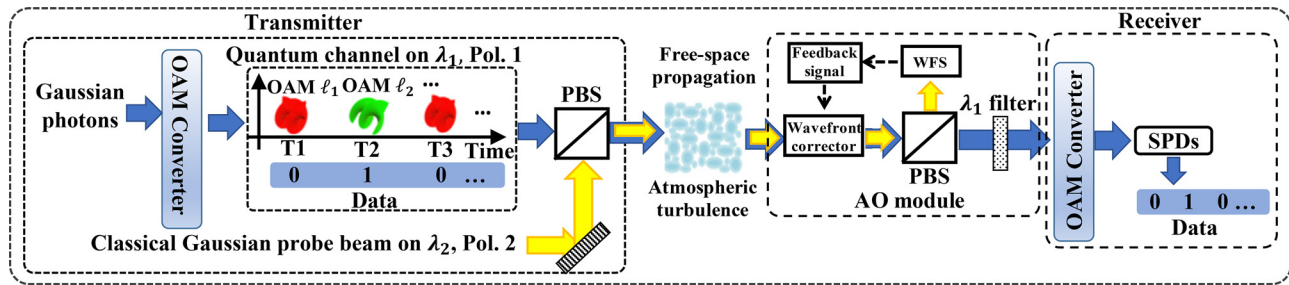


FIG. 46. The concept of AO method for mitigating atmospheric turbulence effects in an OAM-encoded quantum link. A classical Gaussian beam (λ_2 , Pol. 2) as a probe is coaxially transmitted with the quantum channel (λ_1 , Pol. 1). A wavefront sensor and wavefront corrector are used for the phase detection and correction, respectively. Subsequently, a PBS, wavelength filter, and OAM converter are used to efficiently separate the classical and quantum channel at the receiver. SPD: single photon detector, Pol.: polarization, AO: adaptive optics, WFS: wavefront sensor, and PBS: polarizing beam splitter. Reproduced with permission from Willner et al., *APL Photonics* **6**, 030901 (2021). Copyright 2021 AIP Publishing.

quantum channel using OAM photons have been experimentally investigated.²⁰⁵ Figure 48 presents the experimental setup and state crosstalk measurements for such a quantum channel. Photon pairs are generated at the Alice side. A single signal photon with a particular OAM state is prepared using SLM-A then sent to Bob through the 3-m underwater link. At the receiver side, the received OAM states of the single photons are measured using SLM-B and single photon detectors. The crosstalk matrix is measured, as shown in Fig. 48(b). It is observed that the crosstalk of higher-order OAM states is higher than that of lower-order OAM states. Finally, the 2-, 3-, and 4-

dimensional BB84 protocol based on OAM states $\{\ell = \pm 1\}$, $\{\ell = 0, \pm 1\}$, and $\{\ell = \pm 1, \pm 2\}$ are performed, respectively. The QSER for these three cases are 6.57%, 11.73%, and 29.77%. To mitigate the turbulence effects and reduce the QSER, one potential method might be the AO system.

Moreover, another underwater quantum link of up to 30 m has been also explored.²¹⁰ Since the length of the quantum link is relatively longer, the beam wandering caused by the turbulence might introduce a significant challenge to the system alignment and coupling to the SMF. Therefore, in order to achieve an underwater quantum channel

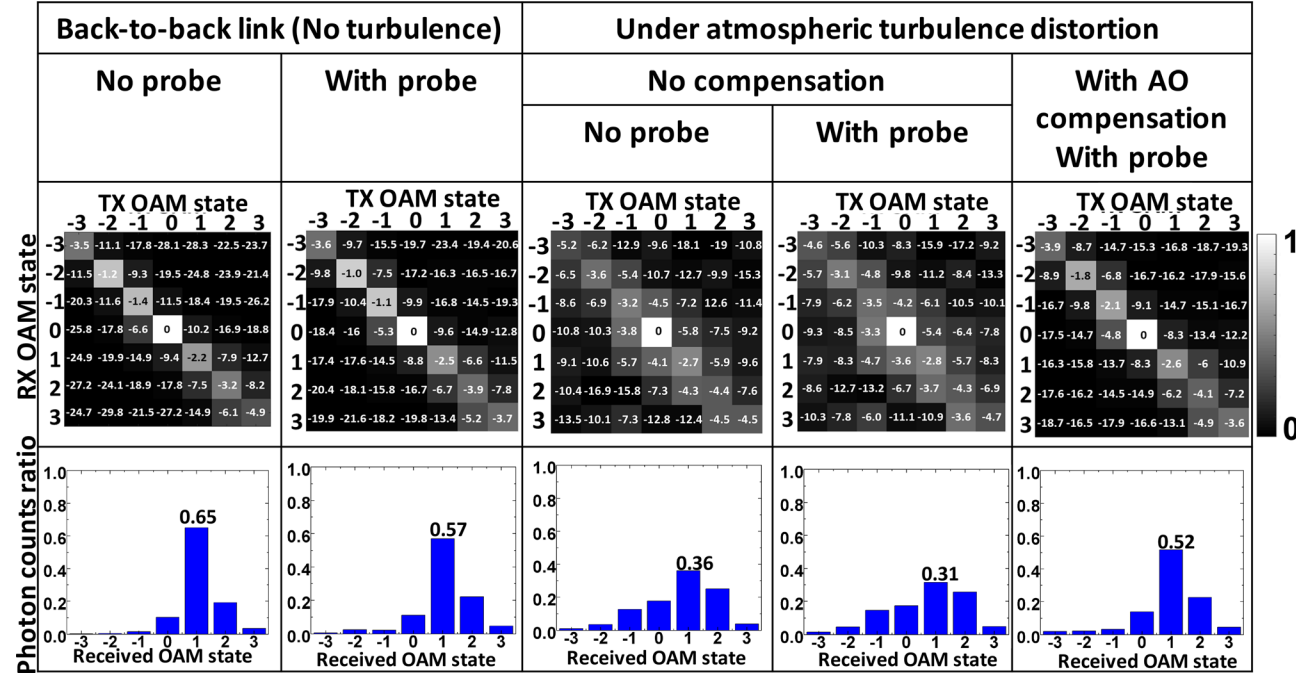


FIG. 47. The performance of AO compensation for turbulence effects in an OAM-encoded quantum link. The measured transfer matrices between OAM modes $\ell = -3, \dots, +3$ in different cases are shown in the top row. The measured photon counts ratio on received OAM modes $\ell = -3, \dots, +3$ when sending only OAM $\ell = +1$ photons in different cases are shown in the bottom row. Reproduced with permission from Research **2019**, 8326701 (2019).²⁰⁴ Copyright 2019 American Association for the Advancement of Science.

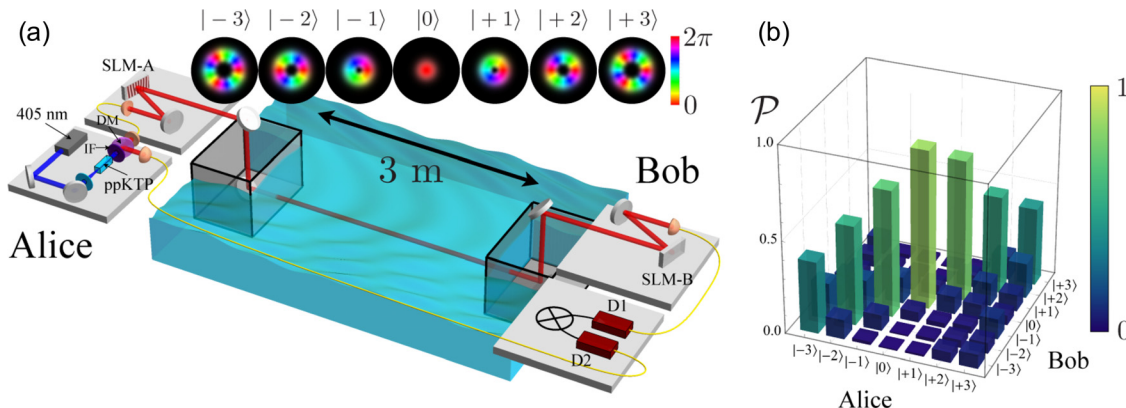


FIG. 48. Experimental setup for an OAM-based underwater quantum link and state crosstalk measurements. (a) Photon pairs are generated at the Alice side. A single signal photon with a particular OAM state is prepared by using SLM-A, then sent to Bob through the 3-m underwater link. At Bob side, the received OAM states of the single photons are measured by using SLM-B and single photon detectors. (b) Experimental crosstalk matrix for OAM states $\ell = -3$ to $+3$. Reproduced with permission from Bouchard *et al.*, Opt. Express **26**, 22563 (2018).²⁰⁵ Copyright 2018 Optical Society of America.

over a long distance, the implementation of both automated beam tracking and AO system might be needed.

D. Fiber-based OAM QKD links

OAM-based QKD links can also be achieved in the fiber. As mentioned before, due to various inhomogeneities, mode coupling might occur among modes within a specific mode group or between mode groups. However, this effect might be potentially reduced by using specialty fibers. A 1.2-km air-core fiber has been utilized in QKD links, as shown in Fig. 49(a).²¹¹ This type of fiber could help us to preserve the mode orthogonality, and thus leading to a low mode coupling between the OAM modes. Using such an air-core fiber, 2-dimensional (2D), 4-dimensional (4D), and two times ($2 \times$) multiplexed 2D (2×2 D) QKD protocols are implemented. As a result, the secret key rates of the 2D,

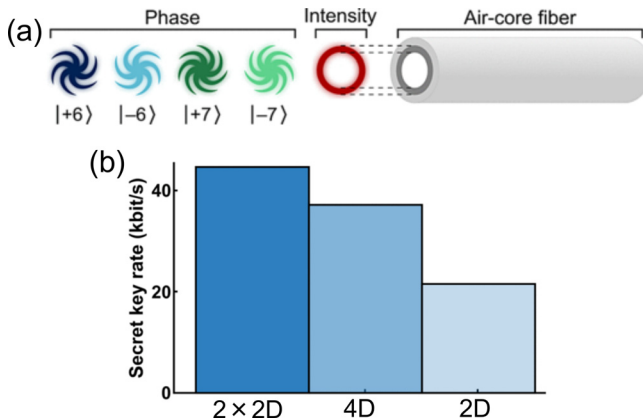


FIG. 49. (a) Schematic of the air-core fiber for transmission of OAM modes. Four different OAM modes and their spiraling phases are shown. The designed air-core fiber could help to preserve OAM orthogonality, thus avoiding mode coupling. (b) The secret key rates of the 2D, 4D, and 2×2 D QKD protocols are 22.81, 37.85, and 42.3 kbit/s, respectively. Reproduced with permission from Cozzolino *et al.*, Phys. Rev. Appl. **11**, 064058 (2019).²¹¹ Copyright 2019 American Physical Society.

4D, and 2×2 D QKD protocols are 22.81 kbit/s, 37.85 kbit/s, and 42.3 kbit/s, respectively, as shown in Fig. 49(b).

E. OAM-based quantum secret sharing among multiple parties

In general, a typical QKD link enables secure key sharing between two parties.²⁰⁰ In recent years, quantum secret sharing (QSS) protocols have been developed to securely share keys among multiple parties.²¹³ Conventionally, the polarizations of photons were utilized for the experimental realizations of single photon QSS schemes, which are limited to two dimensions.²¹⁴ As mentioned before, OAM is a property of photons that can potentially provide a large number of orthogonal states. Therefore, OAM can also be potentially utilized to achieve a high-dimensional QSS schemes among multiple parties.²¹⁵

Recently, there was an experimental demonstration of a QSS scheme for ten participants in $d = 11$ dimensions based on OAM states.²¹² Figure 50(a) presents the concept and experimental setup of such a QSS scheme using OAM states. First, single photons are prepared and emitted by an attenuated laser. Subsequently, the distributor (R_1) generates a photon comprising a number of concentric rings using SLM. Then, each participant (R_2 to R_{10}) applies their own unitary transformation using the phase pattern on the SLM. The last participant (R_{10}) sends the qudit state back to the distributor (R_1), who measures the state in a specific MUB with an avalanche photodiode (APD). As a result, through a collaboration of the remaining participants (R_2 to R_{10}), the distributor's secret can be determined. Figure 50(b) and 50(c) show the simulated and experimentally measured $11^2 \times 11^2$ detection probability matrices for the 11-dimensional QSS scheme. It is observed that there is good agreement between the simulated and experimental results. Moreover, based on the experimental probability matrix, a quantum bit error rate of 6.6% can be obtained.

F. Summary

In this section, we discuss the utilization of OAM modes in quantum communication links. OAM modes have the potential to improve

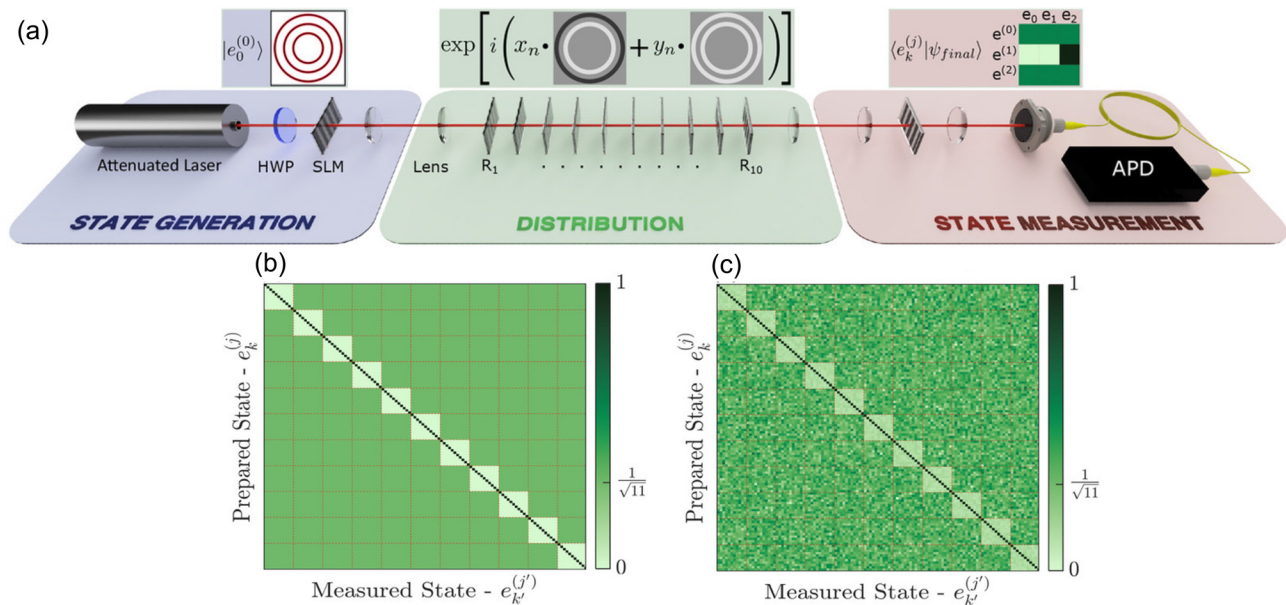


FIG. 50. (a) Concept and experimental setup of an 11-dimensional QSS scheme using OAM states. First, single photons are prepared and emitted by an attenuated laser. Subsequently, the distributor (R_1) generates a photon that is a combination of 11 OAM states using SLM. Then each participant (R_2 to R_{10}) applies their own unitary transformation using the phase pattern on the SLM. The last participant sends the qudit state back to the distributor (R_1), who measures the state in the Jth MUB with an avalanche photodiode (APD). As a result, through a collaboration of the remaining participants (R_2 to R_{10}), the distributor's secret can be determined. The (b) simulated and (c) experimentally measured $11^2 \times 11^2$ detection probability matrices for the 11-dimensional QSS scheme. Reproduced with permission from Pinnell *et al.*, *Laser Photonics Rev.* **14**, 2000012 (2020).²¹² Copyright 2020 Wiley.

02 July 2024 13:55:29

the photon efficiency of quantum communication links in various scenarios such as free space, underwater, and fiber. Table III illustrates the experimental demonstrations mentioned in this section of OAM-based quantum communication links in various scenarios. Some major parameters of each experiment, including the wavelength, number of modes, and transmission distance, are summarized. There are different challenges for different environments, which might increase the QSER and reduce the secret key rate. To overcome these challenges, much research is needed, such as (i) reducing coupling between

orthogonal quantum states in different scenarios and (ii) developing transmitters for rapidly generating single photons with different spatial states.

VII. OAM-BASED COMMUNICATION SYSTEMS IN DIFFERENT FREQUENCY RANGES

In addition to the optical region, free-space communication links could also use MDM to increase the channel capacity for many other different frequency regimes. As an orthogonal modal set, OAM modes

TABLE III. Demonstrations of OAM-based quantum communication links mentioned in this section.

Channel medium	Type of quantum link	Wavelength	Number of modes	Distance	Note	Year ^{Ref.}
Free space (in lab)	QKD	632.8 nm	7 OAM modes + 7 ANG modes	...	<ul style="list-style-type: none"> • Capacity: 2.05 bits per sifted photon • Average SER: 10.5% 	2015 ¹⁷
Free space (outdoor)	QKD	850 nm	2 OAM modes	300 m	<ul style="list-style-type: none"> • Capacity: 0.65 bits per sifted photon • Average SER: 11% 	2017 ²⁰¹
Free space (in lab with emulated turbulence)	Encoding	850 nm	2 OAM modes	1.5 m	<ul style="list-style-type: none"> • Bit rate: 10 Mbit/s • QSERs are reduced by ~76% with AO 	2019 ²⁰⁴
Free space (in lab)	QSS	...	11 OAM modes	...	<ul style="list-style-type: none"> • QBER = 6.6% 	2020 ²¹²
Under water (outdoor)	QKD	710 nm	7 OAM modes	3 m	<ul style="list-style-type: none"> • Capacity: 0.395 bits per sifted photon • QBER = 6.35% 	2018 ²⁰⁵
Under water (water tank)	QKD	532 nm	2 vector vortex modes	30 m	<ul style="list-style-type: none"> • Capacity: 0.84 bits per sifted photon • QBER = 0.96% 	2020 ²¹⁰
Fiber (air-core fiber)	QKD	1550 nm	4 OAM modes	1.2 km	<ul style="list-style-type: none"> • The secret key rates: 42.3 kbit/s 	2019 ²¹¹

can be manifest in many types of electromagnetic (EM) and mechanical waves and have been recently explored in acoustic, radio, millimeter, and THz waves for wireless communication links.^{51–64} For OAM-based communication links operated in different frequency ranges, there tends to be a trade-off between the effects of beam divergence and wave-matter interaction, as shown in Fig. 51:

- (i) Divergence: The OAM beams at lower frequencies have larger beam divergence. When the receiver's aperture size is limited, it becomes more difficult to capture enough of the beam for data channel recovery. Such a problem might be more serious when a higher-order OAM mode is used.
- (ii) Interaction with matter: There tends to be much more wave-matter interaction at higher frequencies. For example, optical waves suffer more atmospheric-turbulence-induced distortion and modal power coupling than radio waves in OAM-based links.

For different application scenarios or link conditions, it might be desired to use OAM multiplexing in different frequency regimes. In this section, we review the exploration of using OAM for free-space communication links in millimeter and THz waves. Key techniques for OAM generation and detection, and recent demonstrations for OAM-based communication systems are introduced. Moreover, several unique properties and existing challenges are discussed when using OAM in these frequency ranges.

A. OAM-multiplexed links in the millimeter-wave range

The bandwidth shortage experienced by wireless communications has especially motivated the use of the underutilized millimeter-wave bands, which could offer a large amount of spectra. To further improve the spectral efficiency (bit/s/Hz) and data capacity (bit/s) of the system, MDM using multiple OAM beams in millimeter-wave

bands is being actively investigated. Recently, there have been exciting advances in utilizing OAM-based techniques in millimeter-wave frequency ranges, and some industrial labs are conducting investigations using OAM multiplexing to potentially increase the capacity of millimeter-wave wireless links.^{51,55–58}

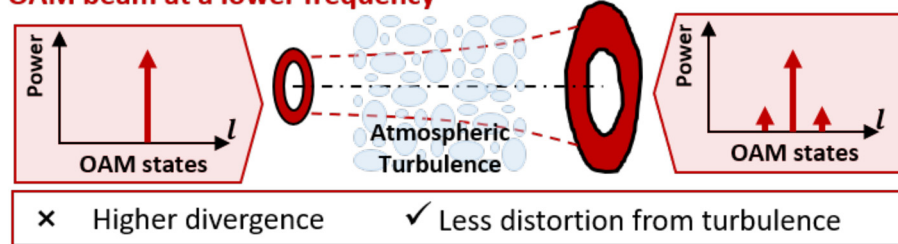
One of the important research topics is the generation and detection of millimeter-wave OAM beams in OAM multiplexing communication systems. Similar to the methods of the optical OAM generation and detection, there are several popular approaches that can be used to generate and detect millimeter-wave OAM beams. Typical methods include the spiral phase plate (SPP), metasurface, and uniform circular array (UCA).

SPP:⁵¹ The SPP has a linear changing thickness along the azimuthal direction for OAM generation and detection. Such a structure can generate different phase delays along the azimuthal direction, which can convert a Gaussian beam to an OAM beam or an OAM beam back to a Gaussian beam. In general, the SPP has the advantage of low attenuation. However, it might be hard to generate multiple coaxial OAM beams simultaneously using a single SPP.

Metasurface:^{216,217} A metasurface structure could shape the wavefronts of EM waves to generate an OAM beam by regulating the phase shift to the incoming waves. Such a scheme has the advantages of small mass, low profile, and low manufacturing cost. However, it might have a lower conversion efficiency compared with SPP.²¹⁶

UCA:⁵⁹ The UCA is an antenna array in which different antenna elements are uniformly distributed in a ring. It can generate a millimeter-wave OAM beam when the antenna elements are selectively excited with a differential phase delays. The phase information of each antenna element of a UCA is linearly changed by $2\pi\ell/N$, where N is the number of elements and ℓ is the OAM order. By using a single ring, multiple OAM beams could be generated simultaneously. Moreover, the UCAs comprising multiple concentric rings can generate many multiplexed OAM beams with different beam radii simultaneously.⁵⁵ An example of the UCA prototype is shown in Fig. 54(a).

OAM beam at a lower frequency



OAM beam at a higher frequency

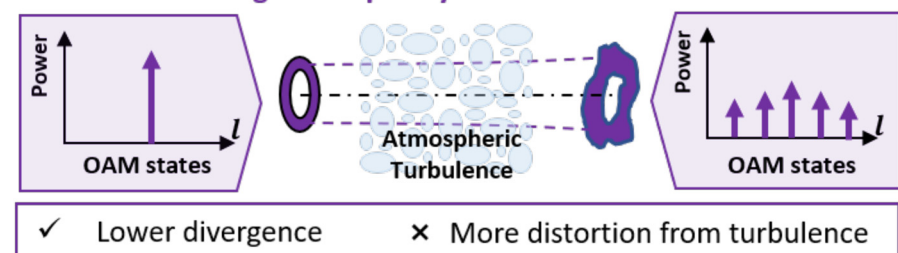


FIG. 51. There tends to be a trade-off in OAM-based communication links for different frequency ranges. OAM beams at lower frequencies have much larger divergence but are less affected by atmospheric-turbulence-induced beam distortion and modal coupling than higher frequencies.

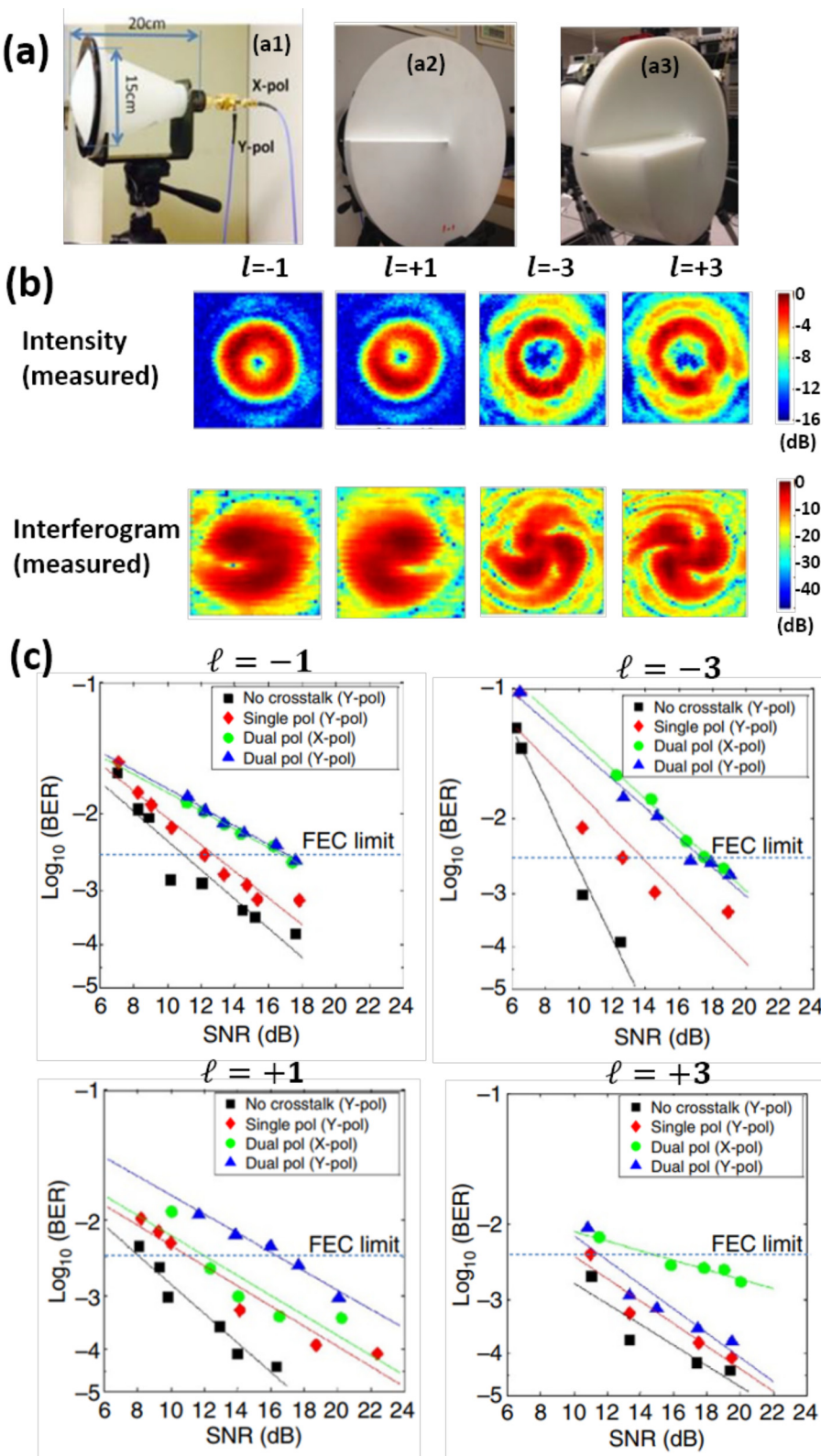


FIG. 52. Experimental results for a 32-Gbit/s millimeter-wave communication link using four multiplexed OAM modes and two polarizations at 28 GHz. (a-1) Horn antenna and fabricated SPPs for generating (a-2) OAM $+1$ and (a-3) OAM $+3$. (b) Measured intensity profiles and interferograms for generated millimeter-wave OAM beams with $\ell = -3, -1, +1, +3$. (c) Measured BER performance of data channels carried by different OAM beams under different cases: (i) a single OAM channel (w/o crosstalk), (ii) multiplexing four OAM channels on a single-polarization (w/ crosstalk), and (iii) multiplexing eight channels on four OAM modes and two polarizations (w/ crosstalk). Reproduced with permission from Yan et al., Nat. Commun. 5, 4876 (2014).⁵¹ Copyright 2014 Macmillan Publishers.

A 32-Gbit/s PDM and OAM-multiplexed millimeter-wave link has been experimentally demonstrated by multiplexing eight OAM beams (four OAM beams on each polarization) with a carrier frequency of 28 GHz. As shown in Fig. 52, SPPs are used to convert Gaussian beams to different OAM beams for two polarizations (X-pol. and Y-pol.). Four OAM beams with OAM orders of $\ell = -3, -1, +1$, and $+3$ are generated on each of the polarizations. Figure 52(b) shows the measured intensity profiles and interferograms of the generated OAM beams. The interferograms are measured by interfering the OAM beams with a Gaussian beam. The eight generated OAM beams are spatially multiplexed using specially designed beam splitters at the transmitter. After propagating through a 2.5-m free-space link simultaneously, the multiplexed beams are separated and converted back to Gaussian beams using corresponding conjugated SPPs at the receiver. Subsequently, eight data channels are detected and recovered one at a time. With each beam carrying a 4-Gbit/s 16-QAM signal, a millimeter-wave link with a total capacity of 32 Gbit/s and a spectral efficiency of approximately 16 bit/s/Hz has been demonstrated. Figure 52(c) shows the measured BER performance of the 1-Gbaud 16-QAM signal for a single OAM channel, four multiplexed OAM channels on a single polarization, and eight multiplexed channels on four OAM modes and two polarizations. It is observed that all channels can achieve below-FEC-limit BER performance. In addition, based on a similar scheme, an OAM-multiplexed millimeter-wave link with a carrier frequency of 60 GHz has also been demonstrated with a data capacity of 32-Gbit/s.²¹⁸

By utilizing metasurfaces to generate and detect millimeter-wave OAM beams, an OAM-multiplexed link in the millimeter-wave range has been demonstrated in a more compact fashion.²¹⁶ As shown in Fig. 53(a), the metasurface is designed by arranging a rectangular aperture array on a printed circuit board (PCB). By designing the spatial distribution and orientation angle of rectangular apertures, millimeter-wave OAM beams with different orders could be generated. Figure 53(b) compares the structure and thickness of the metasurface plate and a normal SPP for generating OAM $\ell = +1$ at 28 GHz. The metasurface plate, which is much thinner than the SPP, might be more favorable in a compact OAM system. The designed metasurface plate has been demonstrated in a 16-Gbit/s OAM-multiplexed millimeter-wave link for OAM generation and detection. Two OAM beams are generated, multiplexed, and transmitted at a carrier frequency of 28 GHz, with each beam carrying a 2-Gbaud 16-QAM signal. As shown in Fig. 53(c), the measured BERs for both OAM channels $\ell = +1$ and $\ell = +3$ can be achieved below the level of the FEC limit.

As a type of SDM, OAM multiplexing could be combined with conventional spatial multiplexing. Recently, a 100-Gbit/s millimeter-wave communication link has been demonstrated by combining these two techniques at 28 GHz.^{54,55} As shown in Fig. 52(a), the transmitter consists of four concentric UCAs and a single antenna at the center. Each UCA generates five data channels carried by five OAM beams ($\ell = 0, \pm 1, \pm 2$). The OAM beams generated by different UCAs have different beam radii, which enable the conventional spatial multiplexing. The single antenna in the center transmits a data channel carried by a Gaussian beam. Thus, in total, 21 ($4 \times 5 + 1$) data channels are transmitted simultaneously by the transmitter. As shown in Fig. 54(b), after propagating through a distance of 10 m, data channels carried by different beams are detected by another set of UCAs at the receiver. A more recent demonstration utilizing similar UCAs is a

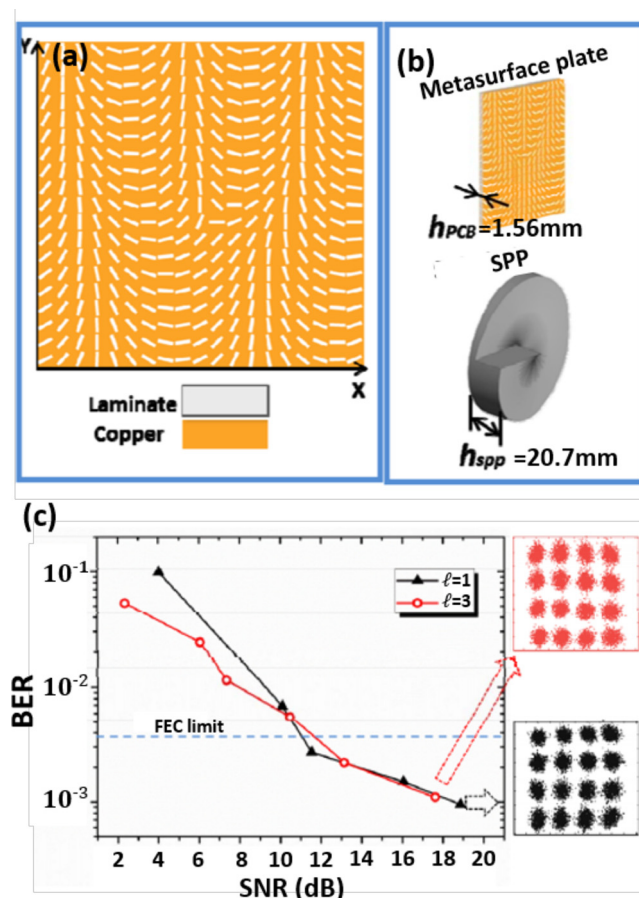


FIG. 53. (a) The structure of the designed metasurface plate. (b) The thicknesses of a metasurface plate and an SPP for generating OAM $\ell = +1$ at 28 GHz. (c) Measured BER performance of 2-Gbaud 16-QAM signals carried by OAM $\ell = +1$ and $\ell = +3$. Reproduced with permission from Zhao *et al.*, in 2015 IEEE International Conference on Communications (ICC) (IEEE, 2015), p. 1392.²¹⁶ Copyright 2015 IEEE.

100-Gbit/s link over 100 m at a frequency of 40 GHz by combining PDM, OAM multiplexing, and conventional spatial multiplexing.²¹⁹

B. THz links using OAM multiplexing

Recently, there has been growing interest in using the 0.1–1 THz carrier-frequency range to increase the available bandwidth for wireless communication systems. A goal of THz communication systems might be to further increase the capacity of the system. As a subset of SDM, OAM multiplexing could also be potentially utilized to increase the capacity of THz wireless links by transmitting multiple OAM beams.

One widely used approach for OAM mode generation and detection in the THz band is utilizing SPPs.⁶¹ Compared with SPPs used for millimeter-wave OAM generation and detection, SPPs for THz OAM are usually thinner since THz waves have smaller wavelengths.

A subterahertz frequency regime at ~ 300 GHz has gained much interest due to low atmospheric transmission loss, and most

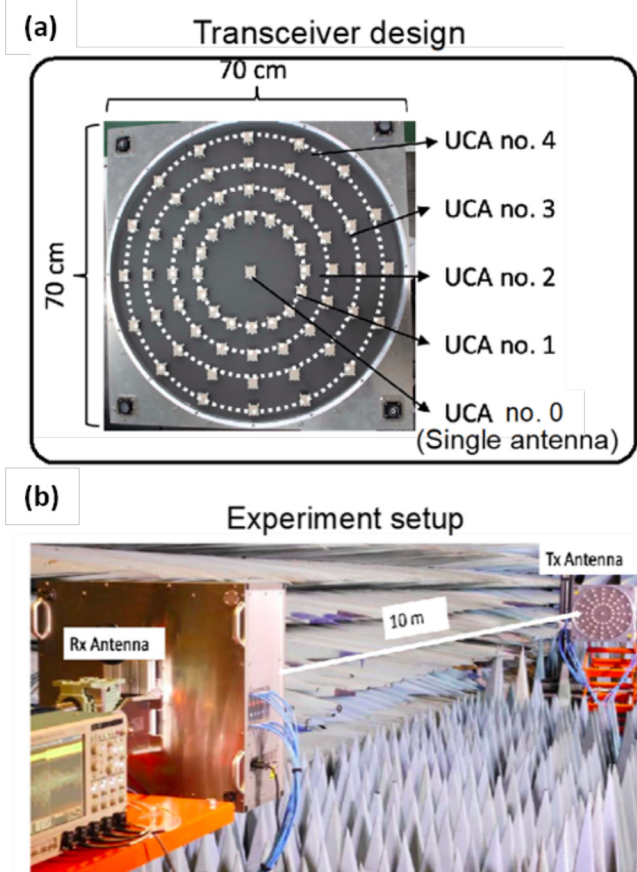


FIG. 54. (a) The structure of multiple concentric UCAs, comprising four circular antenna arrays and a single antenna element at the center. (b) Experimental setup of a 100-Gbit/s OAM-multiplexed millimeter-wave communication link over a distance of 10 m using the UCAs to generate and detect OAM beams. Reproduced with permission from Lee *et al.*, Appl. Sci. 9, 1729 (2019).⁵⁴ Copyright 2019 MDPI.

demonstrations of communication links in this frequency regime usually utilize beams without carrying OAM.^{221–224} Using OAM for a high-speed communication system in the THz regime is still fairly new. Recently, there is a report that has demonstrated 8-Gbit/s QPSK communications using two multiplexed OAM beams in the 0.27–0.33 THz range.²²⁰ As shown in Fig. 55(a), a THz data channel is generated by mixing two lasers in a positive-intrinsic-negative photodiode (PIN-PD) based THz emitter with one of them modulated with a data signal. Two PIN-PDs and two different SPPs are used to generate two THz-OAM beams. At Rx, corresponding inverse SPPs are used to convert the THz-OAM beam back to a THz-Gaussian beam, which can be received by an antenna. A down-converter can convert the THz data channel to an intermediate-frequency (IF) band for off-line processing. By multiplexing two OAM beams, an 8-Gbit/s data rate is achieved in a 0.2-m THz wireless link with each channel carrying a 2-Gbaud QPSK signal. Figure 55(b) shows the normalized received IF power of different OAM components (OAM mode spectrum). The results show that, for OAM +1 and OAM -2 beams, the maximum relative power of received undesired modes is ~ -10 dB

and ~ -9 dB, respectively. Figure 55(c) shows the BER performance of the OAM-multiplexed THz link. The results show that both two multiplexed channels (Muxed OAM +1 and Muxed OAM -2) could be below the FEC limit. The power penalty compared to a single Gaussian channel is ~ 2 dB and ~ 4 dB for OAM +1 and -2 channels, respectively. More recently, there was an experimental demonstration that combines PDM, FDM, and OAM multiplexing and achieves an 8-data channel multiplexing with a total data rate of 32 Gbit/s at a carrier wave of ~ 300 GHz.²²⁵

C. Challenges for millimeter-wave/THz OAM-multiplexed systems

Many challenges for optical OAM-multiplexed systems also exist in OAM-multiplexed systems using millimeter-wave/THz frequency ranges, for example, atmospheric turbulence, misalignment, and beam divergence. Although they share many similarities, different degradation might be observed for millimeter-wave/THz communication systems due to their much lower carrier frequencies. In this section, we review some recent explorations for the turbulence effects and multi-path effects on OAM-multiplexed systems in these frequency ranges.

1. Turbulence-induced system degradation for THz-OAM links

THz waves have longer wavelengths (lower frequencies) than optical waves and shorter wavelengths (higher frequencies) than millimeter waves. Therefore, atmospheric turbulence might affect THz OAM beams in its own manner. In general, there tends to be much less wave-matter interaction at longer wavelengths (lower frequencies). Specifically, THz waves with lower frequencies would be less affected by atmospheric turbulence. Recently, the fundamental system degrading effects caused by turbulence have been numerically explored in simulations for OAM-based THz wireless links.²²⁶ As shown in Fig. 56(b), the results indicate that THz OAM beams at higher frequencies might experience larger distortion and power coupling induced by atmospheric turbulence. For example, an OAM beam at 0.1 THz suffers little beam distortion and modal power coupling under stronger turbulence, while an OAM beam at 10 THz is significantly distorted even under weaker turbulence.

Moreover, the dependence of the crosstalk performance on the frequency over a 0.1–10 THz range is investigated in simulation.²²⁶ Turbulence-induced OAM modal crosstalk is simulated considering the same transmitted beam size D and the Fried parameter r_0 of a fixed value for different frequencies. Thus, the ratio D/r_0 , which represents the strength of phase front distortion, is the same for different frequencies. Under this condition, the strength of phase front distortion during the beam propagation only depends on the beam size, and the influence of r_0 is isolated. Figure 57(a) shows that, with the same value of D/r_0 for transmitted beams, the crosstalk to neighboring modes decreases when the frequency becomes higher. This might be because, at a lower frequency, the beam size D of the OAM beam increases faster during propagation (i.e., larger beam divergence). Therefore, the D/r_0 of the beam becomes larger at a lower frequency, resulting in a more distorted phase front and larger modal power coupling.

In addition, the crosstalk performance is also investigated in simulation with the same atmospheric structure constant C_n^2 . In this case, the value of r_0 is smaller for a higher frequency according to Eq. (17).

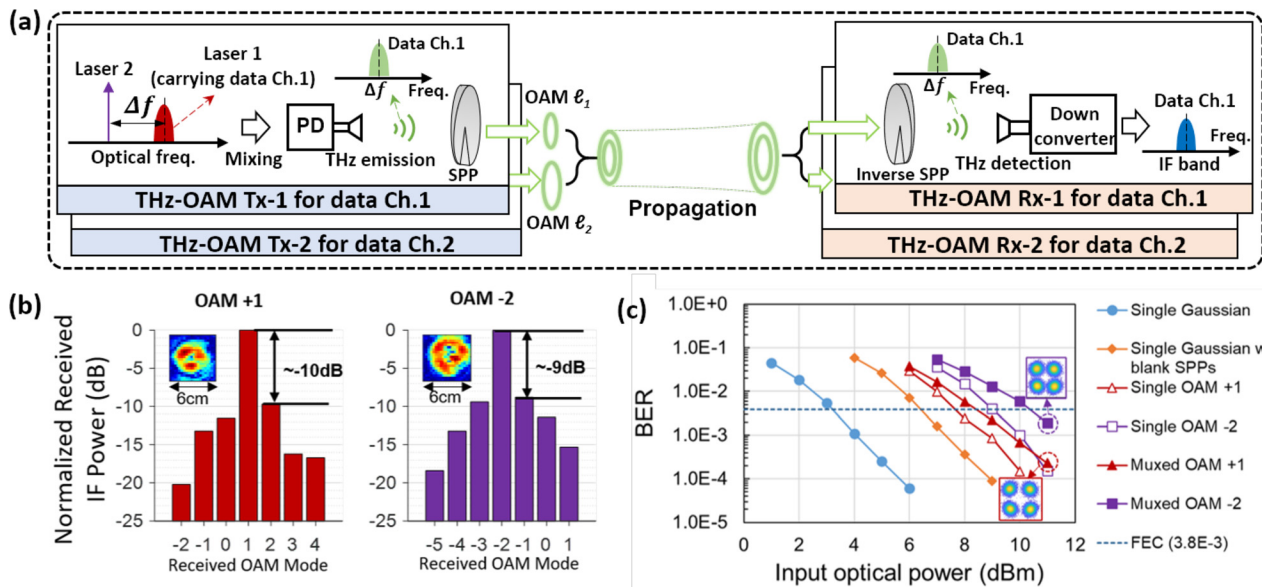


FIG. 55. (a) Concept of an OAM-multiplexed THz communication link, including photonics-assisted tunable THz data channel generation, OAM beam generation and detection using SPPs, and THz detection using THz to IF downconversion. SPP: spiral phase plate; Ch: channel. (b) Measured mode spectrum of generated OAM beams for OAM +1 and OAM -2 at 0.3 THz. Insets are measured THz-OAM beam intensity profiles using the X-Z scanning approach. (c) Measured BER performance of the OAM-multiplexed THz link.²²⁰

Thus, the strength of phase distortion D/r_0 is related to both beam size and r_0 during the beam propagation. Simulation results indicate that, with the same value of C_n^2 , the OAM beam at a higher frequency suffers a larger distortion effect and modal crosstalk, as shown in Fig. 57(b). At a higher frequency, although the beam has a smaller divergence (smaller D after a given propagation distance), the r_0 also becomes much more smaller [see Eq. (17)]. As a result, considering

both of these two frequency-dependent parameters, the value of D/r_0 increases with increased frequencies, and thus, the beam experiences larger phase front distortion and modal coupling. Consequently, there might be a trade-off between the influence of frequency-dependent beam divergence and the influence of frequency-dependent turbulence effects (r_0) on a turbulence-affected THz OAM link.

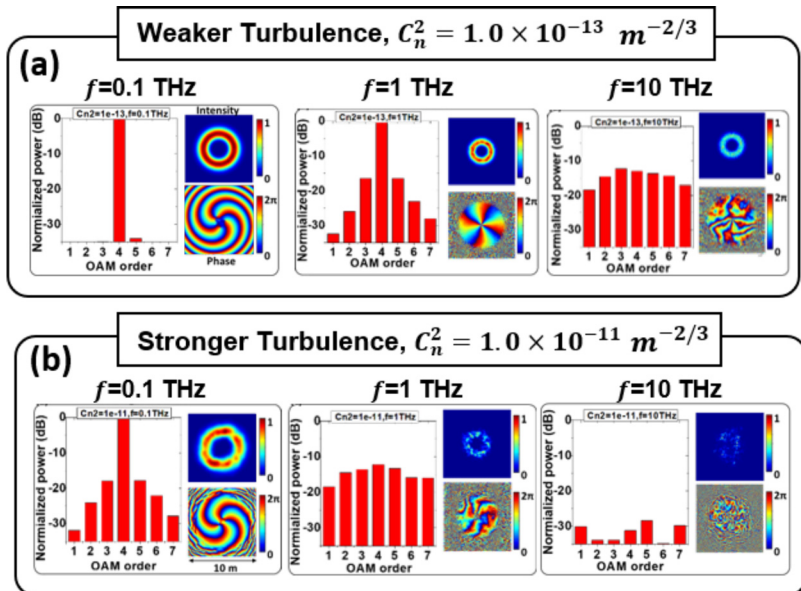


FIG. 56. Simulated power distribution and beam profiles for different THz OAM beams under turbulence effects. An OAM beam with an OAM order of $\ell = +4$ and a beam waist of $w_0 = 1$ m is transmitted through a 1-km link for all the cases. Weaker turbulence: $C_n^2 = 1 \times 10^{-13} m^{-2/3}$; stronger turbulence: $C_n^2 = 1 \times 10^{-11} m^{-2/3}$. Reproduced with permission from Zhao et al., Sci. Rep. 11, 1 (2021).²²⁶ Copyright 2021 Macmillan Publishers.

Modal crosstalk induced by the phase distortion (D/r_0) for different frequency

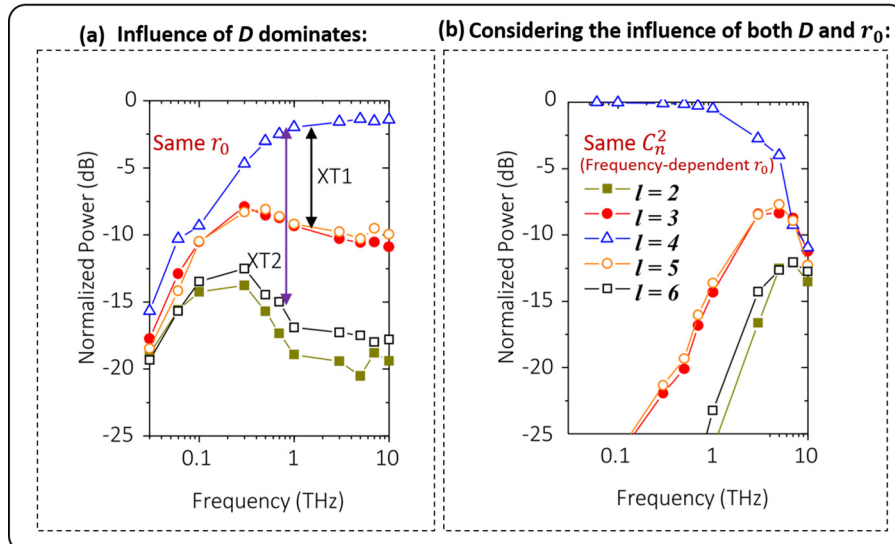


FIG. 57. Simulated normalized power distribution on different OAM modes for different frequencies under turbulence effects, (a) considering fixed $D/r_0 = 0.224$ at the transmitter side, and (b) considering fixed $C_n^2 = 1 \times 10^{-11} \text{ m}^{-2/3}$. An OAM beam ($\ell = +4$) with a beam waist of $w_0 = 0.1 \text{ m}$ is transmitted over a distance of 200 m for all the cases. XT1: modal crosstalk to the right-(higher)-nearest mode. XT2: modal crosstalk to the second-nearest mode. Reproduced with permission from Zhao *et al.*, Sci. Rep. 11, 1 (2021).²²⁶ Copyright 2021 Macmillan Publishers.

2. Multi-path and receiver aperture effects

In conventional millimeter-wave wireless links using Gaussian beams, the transmitted beam could be partially reflected by some surrounding objects due to its divergence during the propagation. The reflected beam would propagate in a different path and interfere with the direct beam at the receiver, which could cause multipath effects and degrade the performance of the system.²²⁸ In general, since OAM beams have larger divergence than Gaussian beams,²²⁷ they are more likely to be reflected by the objects. Thus, the issue of multipath effects could be more serious in an OAM-based millimeter-wave wireless link. The concept of multipath effects in an OAM-based millimeter-wave link is shown in Fig. 58(a). At the transmitter, an OAM beam with an order of ℓ_1 is generated by an SPP. During propagation, due to the increased beam size caused by the divergence, a part of the beam is reflected by a reflector placed in parallel with the propagation path.²²⁷ The reflected beam could be treated as an OAM beam generated from an imaging aperture and an imaging SPP with an opposite order of $-\ell_1$. After propagation, the received beam is a coherent superposition of beams coming from the direct path and the reflected path. SPPs with different orders of ℓ_2 are used to measure the OAM spectrum of the received beam at the receiver. Since the reflected beam is relatively displaced with the desired beam coming from the direct path, these two beams are not orthogonal with each other, which could induce intra-and inter-channel crosstalk.

Figure 58(b) shows the simulated intensity profiles, phase profiles, and OAM power spectrum of the direct-path beam, reflected beam, and superposed beam. In this simulation, the reflector is considered to be ideal with a 100% reflection coefficient. As shown in the left column, the direct-path beam is a pure OAM beam and carries a single OAM component $\ell = +3$. In the middle column, the reflected beam is an off-axis OAM beam with an opposite OAM order $\ell = -3$. When measuring the OAM spectrum of the reflected beam along the direct path, the result shows a spread spectrum covering a range of

OAM components, which induce inter-channel crosstalk to other OAM modes and intra-channel crosstalk to the desired OAM mode $\ell = +3$. The right column shows the results for the superposed beam. There is a fringing pattern in the intensity profile and a distorted phase profile, which are caused by the interference between the direct-path beam and the reflected beam. Recently, multipath effects have also been investigated in THz OAM communication systems by simulation.²²⁹ In general, in addition to the modal coupling to other ℓ modes, multipath effects might also potentially cause modal coupling to other p modes, which may affect system performance in millimeter-wave/THz wireless links based on LG modes.²²⁹

D. Summary

In this section, we discuss the exploration of using OAM for free-space communication links in millimeter and THz waves, including the OAM generation/detection, link demonstrations, and potential challenges. Based on different OAM generation/detection techniques and combinations with other multiplexing schemes (e.g., PDM and conventional SDM), various experimental demonstrations mentioned in this section of OAM-multiplexed millimeter-wave and THz communication links are summarized in Table IV. The performance of OAM-based free-space systems in different frequencies tends to follow a trade-off between beam divergence and wave-matter interaction. Therefore, OAM-based systems might benefit from hybrid technologies over different frequency domains to accommodate different link requirements and conditions,^{230–232} as shown in Fig. 59. In such a system, one of the challenges is to dynamically select and switch the frequency bands for different link conditions. Moreover, broadband components may also need to be further investigated to support such heterogeneous OAM-multiplexed systems, including but not limited to signal emitters/detectors and frequency converters covering a large frequency range.

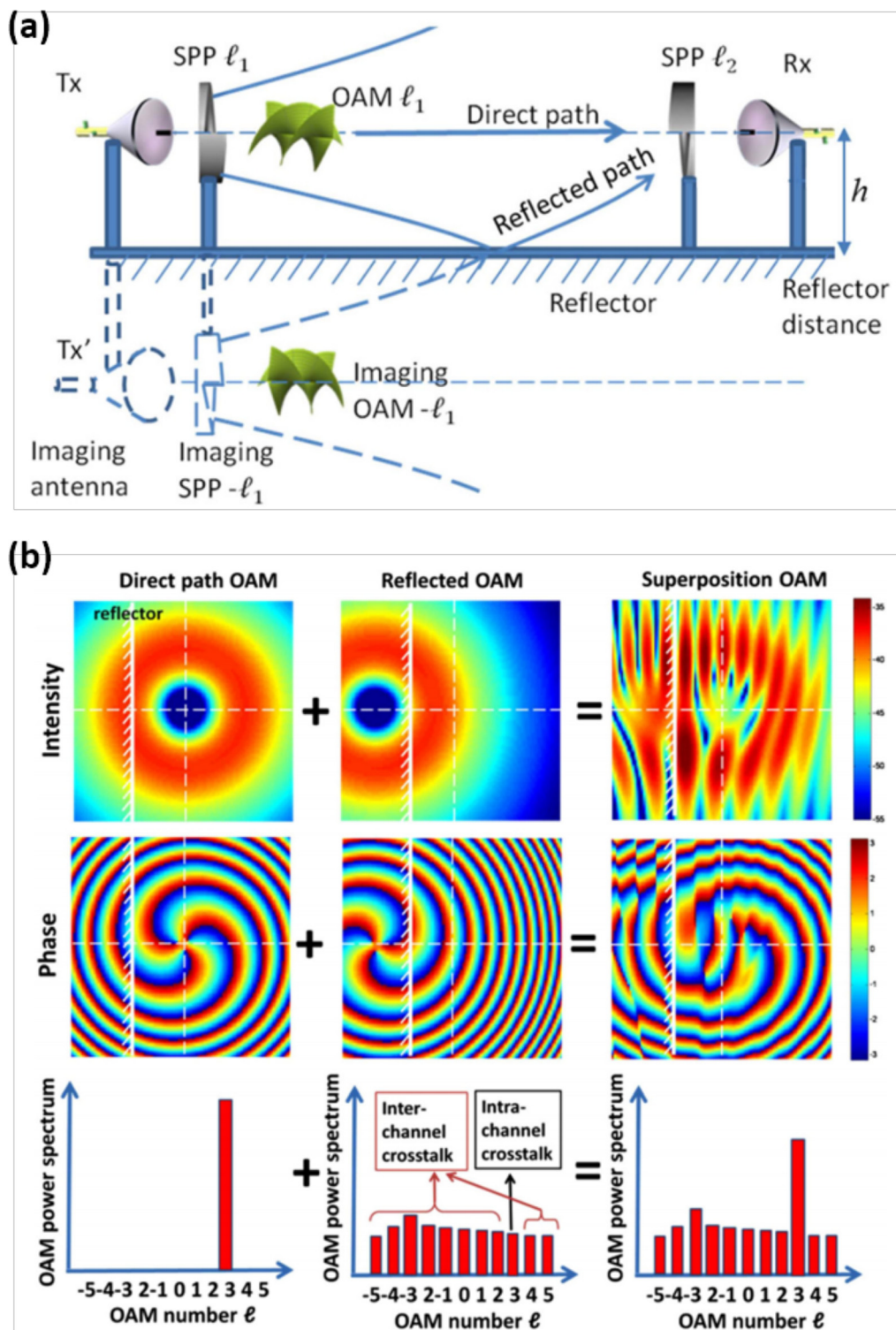


FIG. 58. (a) Concept of multipath effects for an OAM channel. During propagation, a part of the transmitted OAM beam is reflected by a parallel reflector. The reflected beam could be treated as a displaced OAM beam with an opposite order. (b) Simulated intensity profiles, phase profiles, and OAM power spectrum of the direct-path beam, reflected beam, and superposed beam. Reproduced with permission from Yan *et al.*, Sci. Rep. **6**, 33482 (2016).²²⁷ Copyright 2016 Macmillan Publishers.

TABLE IV. Demonstrations of OAM-multiplexed millimeter-wave and THz communication links mentioned in this section.

Frequency bands	Carrier frequency	Multiplexing scheme	Multiplexed channel number	OAM generation	Total data rate	Distance	Year ^{Ref.}
Millimeter waves	28 GHz	PDM + OAM mux	8 (2 pol. × 4 OAM modes)	SPP	32-Gbit/s 16 QAM	2.5 m	2014 ⁵¹
	60 GHz	OAM mux	4 (4 OAM modes)	SPP	32-Gbit/s 16 QAM	2.5 m	2016 ²¹⁸
	28 GHz	OAM mux	2 (2 OAM modes)	Metasurface	16-Gbit/s 16 QAM	1 m	2015 ²¹⁶
	28 GHz	SDM + OAM mux	21 (4 UCAs × 5 OAM +1 Gaussian)	Multiple UCAs	100-Gbit/s 16 QAM	10 m	2018 ⁵⁵
	40 GHz	PDM + OAM mux	14 (2 Pol. × 7 OAM modes)	UCA	100-Gbit/s 16 QAM	100 m	2020 ²¹⁹
	300 GHz	OAM mux	2 (2 OAM modes)	SPP	8-Gbit/s QPSK	0.3 m	2020 ²²⁰
THz	300 GHz	FDM + PDM +OAM mux	8 (2 pol. × 2 freq. × 2 OAM modes)	SPP	32-Gbit/s QPSK	0.3 m	2021 ²²⁵

VIII. INTEGRATED DEVICES FOR OAM COMMUNICATIONS

For a WDM communication system, developed WDM integration technology with lower cost played an essential role in the system deployment. However, the devices utilized in MDM optical communications experiments were bulky, expensive, and not originally designed for MDM communication. To enable the future deployment of MDM communication, cost-efficient integration technology would be likely important. In an OAM-based communication system, there are some desirable features of the integrated OAM devices, including large number of modes, high mode purity, large bandwidth, fast tunability, and high conversion efficiency, as shown in Fig. 60.

Recently, there have been some efforts on integrated devices for OAM generation and detection.^{233–237} In this section, different structural designs of the integrated devices for OAM-based communications will be discussed, including ring-resonator-based OAM emitter/receiver,^{233,238–242} circular-phase-array OAM emitter,^{234,243–246} and subwavelength optical OAM antenna,^{235,247–249} as shown in Fig. 61. We will also review the typical features of different structures and their applications for OAM-based communications.

A. Ring-resonator-based OAM emitter/receiver

The development of an integrated device for tunable OAM generation and detection is of importance to an OAM-based communication link.^{36,239} One way to generate a tunable OAM beam is to utilize a ring-resonator-based structure.^{233,250,251} The ring-resonator-based OAM emitter consists of a micro-ring resonator and angular grating structures with a periodic modulation of the refractive index in the azimuthal direction. The structure of the ring-resonator-based OAM emitter is analogous to that of the grating coupler used in a straight waveguide.²³³ In a conventional straight waveguide, the modes carrying no OAM could be extracted from the waveguide to free space using grating structures. The wavefront of the radiated light is tilted at the angle in which constructive interference occurs, as shown in Fig. 62(a-1). In a regular ring optical resonator, the supported whispering gallery modes (WGMs) could carry OAM.²⁵² To extract OAM modes from the micro-ring waveguide into free space, the ring resonator structure is embedded with angular gratings. The wavefront twists in the azimuthal direction, and the output light is transformed into a beam carrying OAM, as shown in Fig. 62(a-2). The generated OAM order is given by²³³

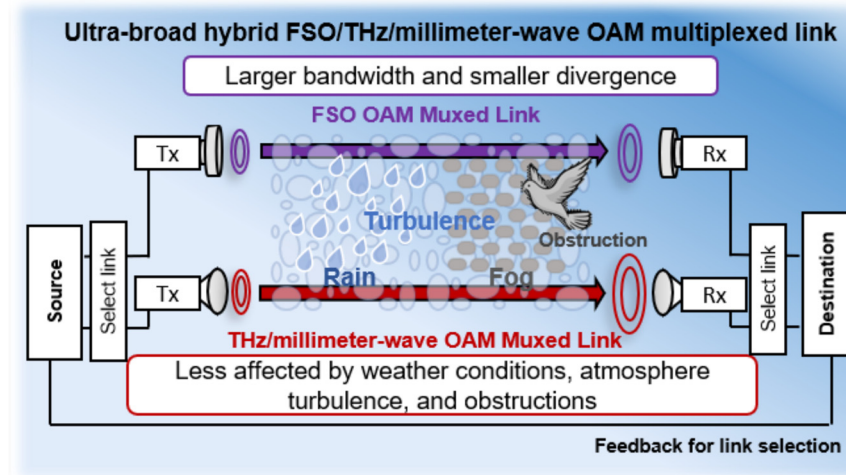


FIG. 59. An FSO OAM-multiplexed link could be potentially co-installed with a millimeter-wave/THz OAM-multiplexed link. Such a hybrid system might be able to increase the reliability of the link under various complex environment conditions.

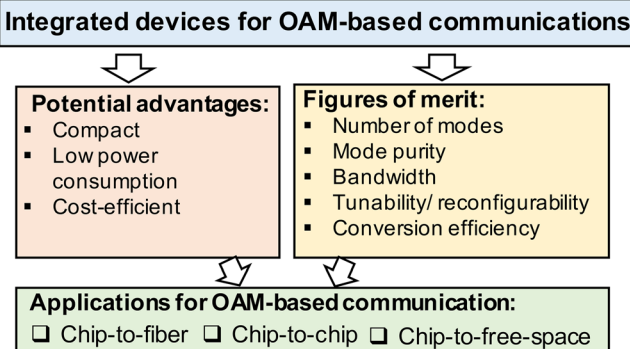


FIG. 60. Potential advantages, key figures of merit, and potential applications of using integrated devices for OAM-based communications.

$$\ell = m - q = \frac{n_e L_c}{\lambda_R} - q, \quad (30)$$

where m is the number of optical periods around the resonator, which is dependent on the effective index n_e , geometric round trip length of the ring L_c and resonant wavelength λ_R , and q is the number of grating elements around the resonator. It should be noted that the OAM beams are generated at some specific discrete resonant wavelengths λ_R , when the angular phase matching condition is satisfied, as shown in Fig. 62(b). By tuning the input wavelength to fit different resonant wavelengths of the structure, the generated OAM order could be changed. In addition, by tuning the refractive index using a thermal²³⁹ or carrier-induced effect, the generated OAM order could be tuned at the same wavelength. Moreover, this type of the ring-resonator-based device could also be potentially used as an OAM receiver.²⁵³

Furthermore, there are various efforts to apply the ring-resonator-based OAM emitter/receiver in OAM-multiplexed communication systems. In order to generate/detect multiple OAM beams efficiently, there are different variants of ring-resonator-based

structures. One is to design a multi-mode waveguide ring-resonator, as shown in Fig. 63(a-1). As the number of m is different for different WGMs at the same wavelength, OAM beams of different OAM orders could be generated simultaneously. A chip-to-chip four-OAM-multiplexed link has been demonstrated using the multi-mode-ring-resonator-based OAM emitters,²⁴¹ as shown in Fig. 63(a-2). Each OAM beam carried a 16-Gbit/s QPSK signal whose BER could be achieved below the 3.8×10^{-3} FEC limit, as shown in Fig. 63(a-3). The OAM orders of these four generated OAM beams could be potentially tuned simultaneously at the same wavelength using this structure. In order to independently control generated OAM orders for different wavelengths, one way is to design multiple concentric-omega-shaped OAM emitters, as shown in Figs. 63(b-1) and 63(b-2). Each omega-shaped waveguide could be independently tuned for generating different OAM orders.^{242,254} By utilizing the tunability of the structure, a similar BER performance of a 30-Gbaud OOK channel is achieved for different omega-shaped waveguides when tuning OAM orders or changing input wavelengths, as shown in Fig. 63(b-3).²⁴² Moreover, since the beam generated by a ring-resonator-based emitter could be directly coupled to the fiber, a chip-to-fiber two-mode-multiplexing link has been demonstrated.^{238,240}

B. Circular phase array OAM emitter/receiver

In order to increase the scalability of the integrated devices for generating multiple OAM beams, one could use a circular phase array based on multiple optical antennas. The working principle of the circular phase array is based on coherent beam combining, as mentioned in Sec. III A. As an example, the structure could be composed of a star coupler, length-matched waveguide, and circularly distributed single-mode antennas,^{234,245} as shown in Fig. 64(a). Fed at a different input port, each input beam evolves into a plane wave with a different linear phase tilt. Subsequently, the beam is collected by multiple waveguides with a matched path length. After propagating through the waveguides, the phase-tilted fields inside different waveguides are emitted

OAM generation, multiplexing, demultiplexing and detection

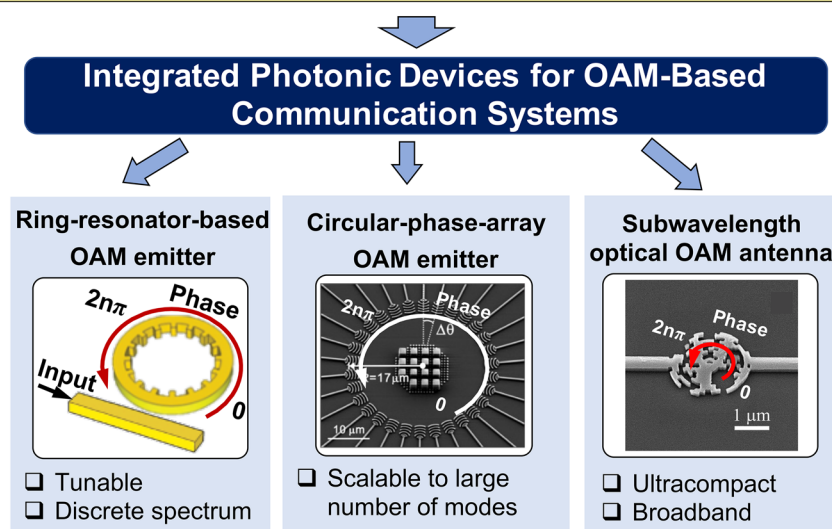


FIG. 61. Different structures of the integrated devices for OAM-based communications and their typical features.^{233,235,244} Reproduced with permission from Shams et al., Science 338, 363 (2012).²³³ Copyright 2012 American Association for the Advancement of Science. Reproduced with permission from Xie et al., Light 7, 18001 (2018).²³⁵ Copyright 2018 Macmillan Publishers.

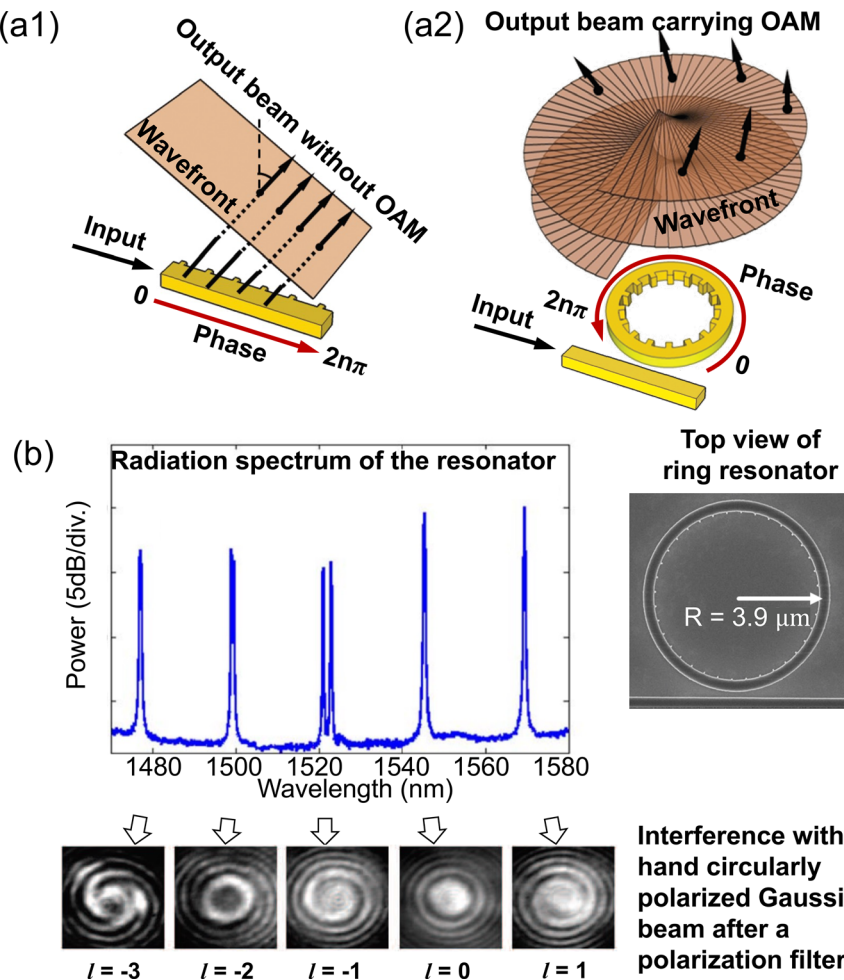


FIG. 62. (a-1) and (a-2) Concept of the ring-resonator-based OAM emitter. (b) Radiation spectrum at different wavelengths and corresponding output OAM beams of the ring-resonator-based OAM emitter. Reproduced with permission from Shams *et al.*, Science 338, 363 (2012).²³³ Copyright 2012 American Association for the Advancement of Science.

by the circular distributed single-mode antennas and coherently combined in free space. In theory, a device composed of N antennas could simultaneously generate N different OAM beams with the mode order ranging from $-N/2$ to $N/2 - 1$.^{234,245}

The scalability of the structure makes it feasible to support more modes by increasing the number of the optical antennas. It has been reported that up to 15 OAM modes could be supported based on this circular phase array structure.²⁴⁵ In addition, due to the optical reciprocity of the device, the OAM multiplexer could be also be used as an OAM demultiplexer. A chip-to-chip OAM-multiplexing communication link²⁴⁵ with two OAM beams ($\ell = -2, +1$), each carrying a 20-Gbit/s QPSK signal, has been demonstrated using a pair of circular phase arrays, as shown in Fig. 64(b). Furthermore, a chip-to-fiber OAM-multiplexing communication link²⁵⁵ with three OAM beams ($\ell = +5, +6, +7$), each carrying a 10-Gbit/s OOK signal, has also been demonstrated using the circular phase array.

Different from the ring-resonator-based OAM emitter, the wavelength spectrum of the generated OAM beams by the circular phase array device is continuous, which might be compatible with a WDM system.²⁴⁶ However, the bandwidth of the star coupler and length

matching of the waveguides should be taken into consideration to make it WDM-compatible.²⁴⁶ Furthermore, the OAM order generated by this structure is tunable by tuning the relative phase between different waveguides.^{243,244} However, the phase error induced by the waveguide mismatch makes it necessary to add phase controllers into the device.^{234,245,246}

C. Subwavelength optical OAM antenna

Even though a circular phase array OAM emitter of multiple antennas could generate a large number of modes, its relatively large footprint might limit its applications in large-scale integration.²³³ In addition, the compact micro-ring-resonator-based structure could also be limited by its discrete wavelength spectrum. To achieve broadband OAM generation by a relatively compact structure, one way is to utilize a specifically designed subwavelength optical antenna. Different types of designing principles have been reported, including (i) superimposed binary fork gratings and (ii) joint phase control of the optical path and local resonance.

As similar to the fork grating hologram discussed in Sec. III, a fork grating could be fabricated in an optical antenna to generate

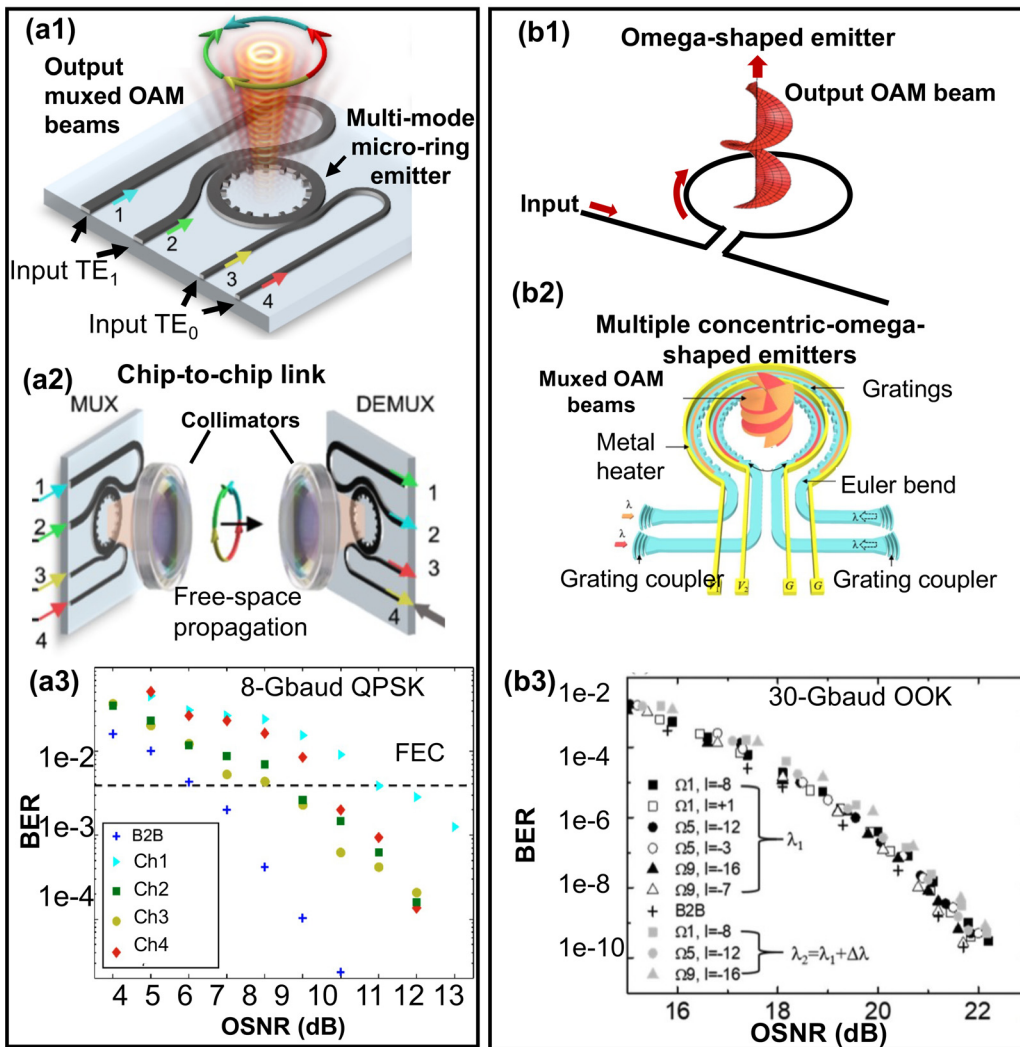


FIG. 63. (a-1) Concept of the multi-mode micro-ring emitter. (a-2) An example of a chip-to-chip link using a pair of the multi-mode micro-ring emitters. (a-3) BER performance for the four OAM-multiplexed channels. Reproduced with permission from Li *et al.*, Opt. Express **26**, 29895 (2018).²⁴¹ Copyright 2018 Optical Society of America. Concept of (b-1) a single omega-shaped emitter and (b-2) multiple concentric-omega-shaped emitters. (b-3) BER performance for different omega-shaped waveguides (Ω_1 , Ω_5 , and Ω_9) by tuning the generated OAM modes or changing the input wavelengths ($\lambda_1 = 1557.55\text{ nm}$ and $\lambda_2 = 1561.39\text{ nm}$). Reproduced with permission from Zhang *et al.*, arXiv:2008.00680 (2020). Copyright 2020 Author(s).

OAM beams from the waveguide input.²⁴⁷ A fork grating is designed based on the coupled interference between the vertically backpropagating OAM mode $E_{\text{OAM}} = A_{\text{OAM}} \exp(i\ell\theta)$ and the waveguide mode $E_{\text{waveguide}} = A_{\text{waveguide}} \exp(ikx)$, as shown in Figs. 65(a-1) and 65(a-2). The distribution of the fork grating hologram could be expressed as follows:²⁴⁷

$$\Psi_{\text{fork}} = |E_{\text{OAM}} + E_{\text{waveguide}}|^2 = A_{\text{OAM}}^2 + A_{\text{waveguide}}^2 + 2A_{\text{OAM}}A_{\text{waveguide}} \cdot \cos(kx - \ell\theta). \quad (31)$$

In order to transfer the fork grating onto the silicon waveguide, the grating pattern should be converted into a binary phase hologram. The binary hologram could be expressed as²⁴⁷

$$\begin{aligned} \Psi_{\text{biphase}} = & T_{\text{biphase}} \exp \{-i(A_{\text{OAM}}^2 + A_{\text{waveguide}}^2 \\ & + 2A_{\text{OAM}}A_{\text{waveguide}} \cdot \text{binary}(\cos(kx - \ell\theta)))\}. \end{aligned} \quad (32)$$

T_{biphase} is the transmission coefficient of the binary phase hologram and binary is a binary function.²⁴⁷

When the binary phase hologram is illuminated with the waveguide mode from the left input $E_{\text{left}} = A_{\text{waveguide}} \exp(ikx)$ as an example, the output field ($E_{\text{out}} = E_{\text{left}}\Psi_{\text{biphase}}$) is emitted in the vertical direction, as shown in Fig. 65(a-3). The output field contains a term of $\exp(i\ell\theta)$, which indicates that it carries OAM with an order of ℓ . The measured beam profiles of generated OAM beams at different wavelengths are shown in Fig. 65(a-5), which indicates the broadband

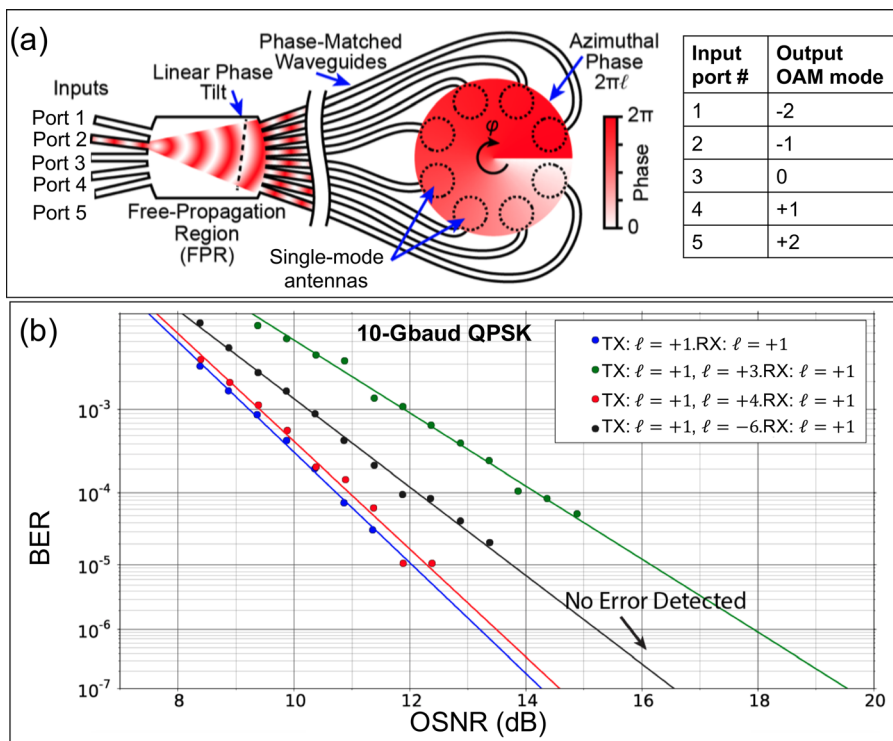


FIG. 64. (a) Concept of the integrated circular phase array for OAM multiplexing. The integrated circular phase array is composed of a star coupler with free-propagation region, phase-matched waveguides, and multiple optical antennas. (b) BER performance for a 10-Gbaud QPSK signal carried by an OAM beam with $\ell = +1$ in a chip-to-chip link without and with the other mode transmitted. Reproduced with permission from Guan et al., Opt. Express **22**, 145 (2014).²⁴⁵ Copyright 2013 Optical Society of America.

property of the structure. In addition, an output beam with an opposite OAM order (i.e., $-\ell$) could be generated from the right waveguide input. Furthermore, by superimposing two fork gratings as shown in Fig. 65(a-4), OAM beams with two orthogonal polarization directions could be simultaneously generated.

The second method to design the subwavelength optical antenna is based on joint phase control of the optical path and local resonances in a specifically designed structure,²³⁵ as shown in Fig. 65(b-1). In general, the phase delay at each location is composed of both the propagating phase ϕ_1 and the resonance phase ϕ_2 . Both ϕ_1 and ϕ_2 are related to the refractive index distribution of the subwavelength structure $N(r, \theta)$. By applying a global optimization algorithm to design $N(r, \theta)$, ϕ_1 and ϕ_2 could be jointly controlled, resulting in an output optical field with a term of $\phi = \phi_1 + \phi_2 = \ell\theta$. As a result, Fig. 65(b-2) shows the conversion efficiency of the generated OAM beams at different wavelengths ranging from 1450 to 1650 nm.²³⁵ It should be noted that the broadband property of this device might be due to a relatively small Q factor (<15) of the local resonator.

Based on the broad bandwidth of the designed OAM emitter, a chip-to-free-space link^{235,247} has been demonstrated combining OAM multiplexing ($\ell = \{+1, -1\}$) and WDM. A set of 30 frequency comb lines with each wavelength channel carrying a 20-Gbit/s QPSK signal are generated and fed into the chip. The total data rate for the emitter associated with the two multiplexed OAM modes is achieved to be 1.2 Tbit/s, as shown in Figs. 65(b-3) and 65(b-4).

One interesting challenge is to increase the tunability of such a broadband subwavelength optical OAM antenna. A potential way is utilizing the phase delay of different waveguide inputs.^{248,249,256}

In addition, to support higher-order OAM modes, increasing designing area and fabrication resolution could be considered.^{235,249}

D. Summary

In this section, we discuss different integrated devices for OAM-based communication links. Table V summarizes the experimental demonstrations mentioned in this section of different integrated structures for various types of communication links (e.g., chip-to-free space, chip-to-fiber, and chip-to-chip) and their bandwidth and tunability properties. For the future deployment of the OAM-based communication system, an ecosystem of integrated devices would potentially play an important role. In addition to the aforementioned devices, it would be beneficial to investigate various system components, including (i) multi-mode amplifiers with a flat gain curve and (ii) multi-mode waveguides with low mode-dependent loss and inter-modal crosstalk.

IX. NOVEL STRUCTURED BEAMS FOR MDM COMMUNICATIONS

The advantages and excitement of MDM communication systems largely rely on the ability to multiplex the spatial orthogonal beams and utilize them to transmit multiple data channels simultaneously. Recently, in addition to the aforementioned OAM beams and LG beams, there is much interest in other novel types of spatially structured beams (e.g., Airy and Bessel types). Some of these concepts have been reported and explored in various applications, and a partial “wish list” (Fig. 66) for novel structured beams in free-space communications systems includes beams

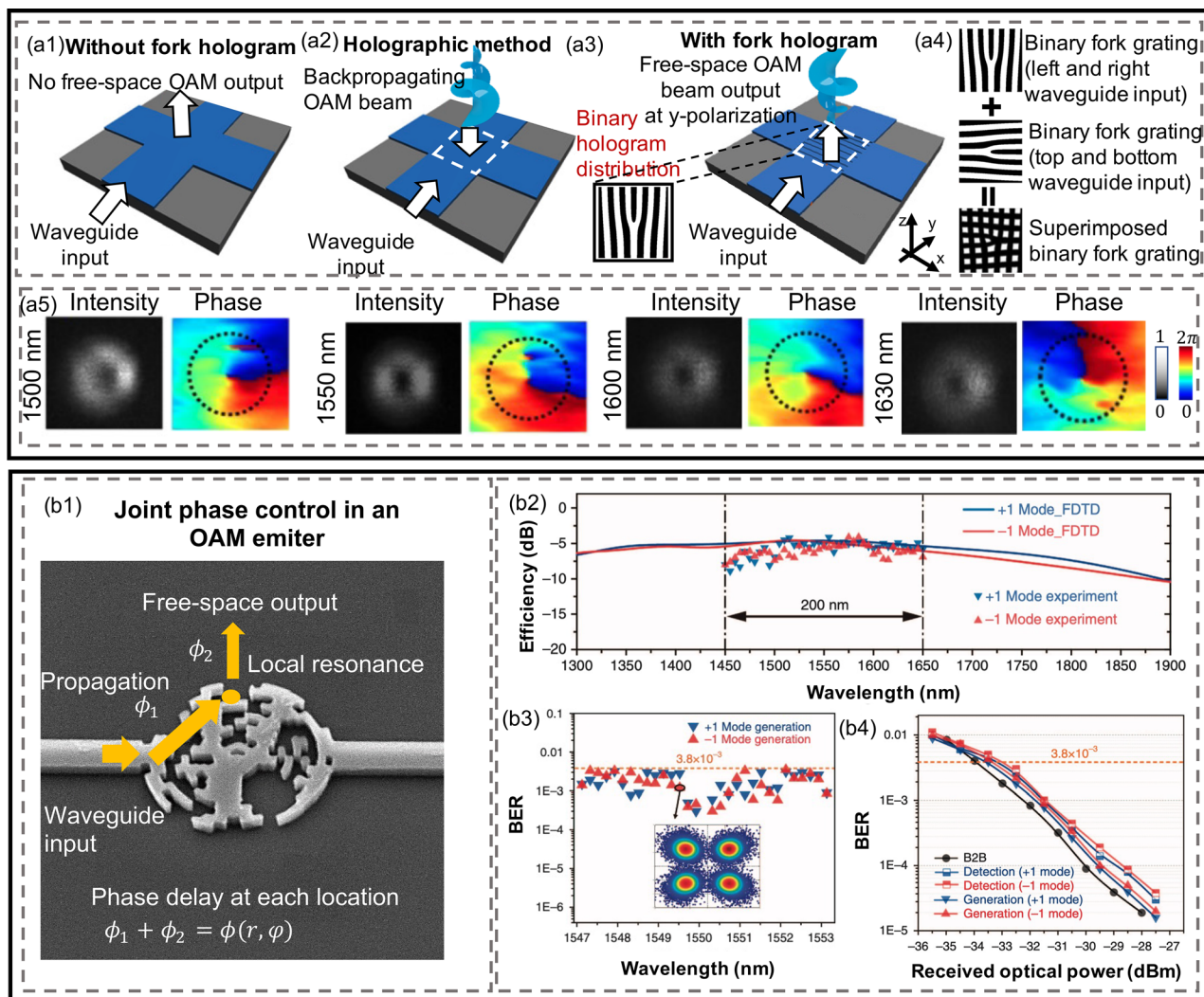


FIG. 65. (a-1)–(a-5) OAM generation using a fork-hologram-based subwavelength optical antenna. (a-1) Bare waveguide crossing without fork hologram. (a-2) Concept of the holographic method based on the interference between the waveguide input and the backpropagating OAM beam. (a-3) OAM beam generated by optical antenna with the binary fork hologram. (a-4) Superposition of two fork holograms to generate OAM beams with two polarizations. (a-5) Intensity and phase profiles of the generated OAM beam (y -pol, $\ell = +1$) at different wavelengths. Reproduced with permission from Zhou *et al.*, Sci. Adv. 5, eaau9593 (2019).²⁴⁷ Copyright 2019 American Association for the Advancement of Science. (b-1)–(b-4) OAM generation utilizing the joint phase control in the subwavelength OAM emitter designed by a global optimization algorithm. (b-1) The measured BERs of the $\ell = +1$ OAM mode and $\ell = -1$ OAM mode in an MDM + WDM link (30 wavelengths and two OAM modes). The total received powers for all 30 wavelengths are -18 dBm ($\ell = -1$) and -17.3 dBm ($\ell = +1$), respectively. (b-4) BER performance of the cases using this device for detection and generation at 1550 nm. B2B: back to back. Reproduced with permission from Xie *et al.*, Light 7, 18001 (2018).²³⁵ Copyright 2018 Macmillan Publishers.

- (a) that have low divergence, which may benefit a long-distance free-space link with a limited-size receiver aperture;
- (b) that can be less affected when propagating in a partially obstructed link. For example, their spatial structures can “self-heal” after the obstruction, or they can circumvent the obstruction;
- (c) that are more resilient to turbulence-induced distortion, which may improve the performance and robustness of the system in a turbulence link.

In this section, fundamental concepts and properties of three types of novel beams that could carry OAM will be introduced,

including Bessel-type, Airy-type, and pin-like beams. In addition, we will also review several system-level examples of applying these beams to minimize the link/system degradation effects, such as beam divergence, obstruction, and atmospheric turbulence.

A. Bessel-type beams

Bessel beams are solutions to the Helmholtz equation in the cylindrical coordinates.^{22–24} They have several unique proprieties, of which two are interesting: (1) they are theoretically diffraction-free during the propagation and (2) their beam shapes are “self-heal” after

TABLE V. Demonstrations of different integrated structures for various optical communication links mentioned in this section. The wavelengths are ~ 1550 nm.

Integrated structure		Link type	Number of muxed modes	Total data rate	Bandwidth	Note	Year ^{Ref.}
Micro-ring emitter	Single ring	w/o data transmission	• Different OAM orders (-4 to $+4$) at different wavelengths	2012 ²³³
	Single ring	w/o data transmission	• Tunable OAM orders from -10 to $+10$ by thermal tuning	2014 ²³⁹
	Multi-mode ring	Chip to chip	4 OAM modes	64-Gbit/s QPSK	2018 ²⁴¹
	Two separate rings	Chip to fiber	2 vector vortex modes	40-Gbit/s 16 QAM	...	• 2-km large-core fiber	2018 ²⁴⁰
	Ω -shaped rings	Chip to free space	10 OAM modes	1-Tbit/s 16 QAM	0.24 nm	• 16 WDM channels	2021 ²⁴²
		Chip to chip	2 OAM modes	20-Gbit/s QPSK	2012 ²⁴⁵
Circular array of antennas		w/o data transmission	• Tunable OAM orders from -4 to $+4$ by thermal tuning	2015 ²⁴⁴
		w/o data transmission	17 nm	• Compatible with PDM and WDM	2020 ²⁴⁶
		Chip to fiber	3 OAM modes	30-Gbit/s OOK	...	• 800-m ring-core fiber	2021 ²⁵⁵
	Subwavelength optical antenna	Chip to free space	2 OAM modes	1.2-Tbit/s QPSK	200 nm	• 30 WDM channels	2018 ²³⁵
		w/o data transmission	2 OAM modes	...	130 nm	• Support 2 pol.	2019 ²⁴⁷
		Pixel-array pattern	2 OAM modes	400-Gbit/s QPSK	6.4 nm	• 2 WDM channels • Tunable OAM orders from -1 to $+1$ by thermal tuning	2021 ²⁵⁶

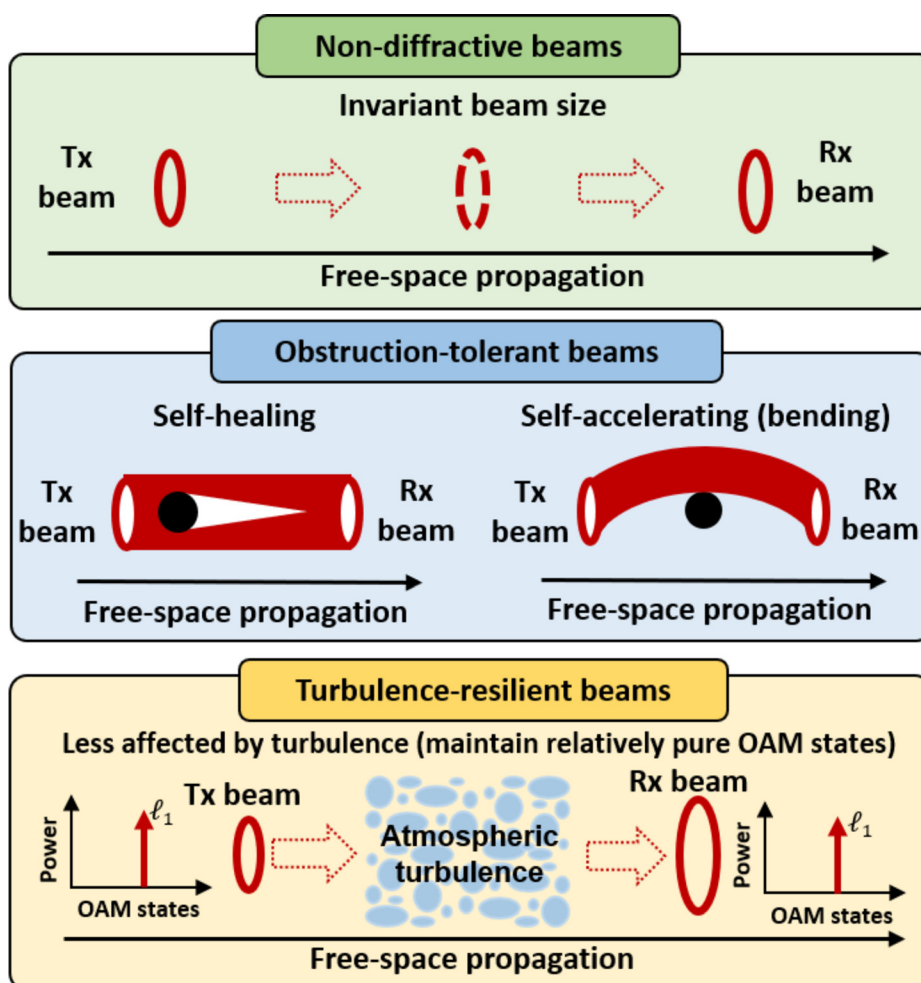


FIG. 66. A partial “wish list” for novel beams, including (a) beams with low divergence, (b) beams that are tolerant to partial obstructions, and (c) turbulence-resilient beams.

being disrupted by a partial obstruction. Due to these features, Bessel beams have attracted much attention in various research fields.²⁴ Recently, there is growing interest in using Bessel beams as a carrier to transmit data information in communication links with lower beam divergence and increased obstruction tolerance.^{24,257–259}

Theoretically, the electric field for the n -th-order Bessel beam [in the cylindrical coordinates (r, θ, z)] is of the following form:²⁶⁰

$$E(r, \theta, z) = a_0 J_n(k_z r) \exp[i(k_z z \pm n\theta)], \quad (33)$$

where J_n is the n -th-order Bessel function of the first kind. k_z and k_r are the longitudinal and transverse wave number, respectively. It can be seen from Eq. (33) that the transverse electrical field follows a Bessel function in the radial coordinate. High-order ($n > 0$) Bessel beams have helical phase fronts in the azimuthal direction, which means that they carry OAM of order n or $-n$. Figure 67(a) shows intensity and phase profiles for Bessel beams with different orders. Theoretically, the intensity and phase profiles of Bessel beams can be characterized by an azimuthal index n and a continuous radial wave vector k_r .²⁴

An ideal Bessel beam needs to have infinite extent in the transverse direction and requires an infinite amount of energy, which is impractical to be generated in laboratory.²⁶¹ One typical way to create a Bessel beam is using an axicon (a cone-shaped lens),^{24,259} as shown in Fig. 67(b). The axicon can structure the incoming wavefront and bend it in a cone-shape fashion. Thus, after the axicon, a set of plane waves would intersect with each other, and interfere to generate a Bessel-type beam in the intersection region. If the incoming wave is a Gaussian beam, a Bessel-Gaussian (BG) beam could be generated. As an approximation to Bessel beams, BG beams keep the properties of “diffraction-free” and “self-healing” over a limited range.²⁵⁹ Moreover, a higher-order BG beam could be created by illuminating an LG beam on the axicon. In the intersection region, the shape and intensity of the beam is invariant during the propagation, representing a “diffraction-free” property. In addition, Bessel beams could re-form themselves within a short distance when an obstruction blocks some part of the beams. As shown in Fig. 67(c), this “self-healing” property results from the fact that the light that is not blocked by the obstruction could still reach the axis and interfere

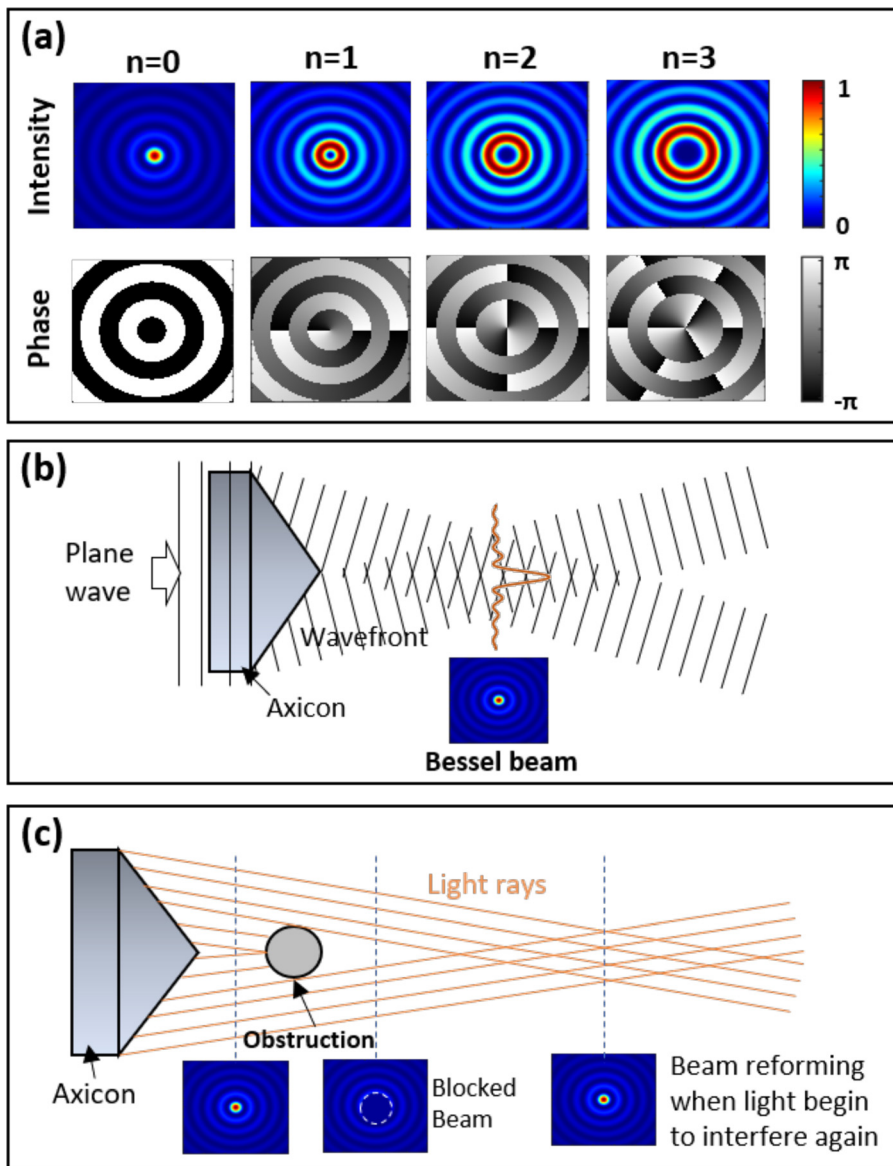


FIG. 67. (a) Intensity and phase profiles for Bessel beams with different orders. (b) An axicon (a cone-shaped lens) can be used to produce Bessel-type beams. By passing a Gaussian beam through the axicon, a Bessel–Gaussian (BG) beam could be generated. If the input beams are LG beams, the generated beams would be higher-order BG beams. (c) Self-healing of the Bessel beam after an obstacle. The light that is not blocked by the obstruction could still interfere after the obstruction to “re-generate” the Bessel beam.

after the obstruction to “re-generate” the Bessel beam with less energy than before.

Recently, by taking advantages of the self-healing property, BG beams have been utilized in an MDM FSO link to mitigate the obstruction-induced degradation effects.²⁵⁹ Figure 68(a) shows the concept of the MDM link using BG beams. At the transmitter, N data-carrying OAM beams are generated and spatially multiplexed. All multiplexed data-carrying OAM beams propagate through an axicon to generate multiple multiplexed higher-order BG beams. These BG beams could keep invariant beam profiles and “self-heal” themselves after being partially obstructed by an opaque disk during propagation within a “Bessel region.” At the receiver, another axicon with an opposite cone angle is used to convert the BG beams back to OAM beams, and an OAM mode demultiplexer is used to separate different beams

to demultiplex different data channels. In this demonstration, a total data rate of 200 Gbit/s has been achieved by transmitting two multiplexed BG beams carrying OAM $\ell = +1$ and $\ell = +3$. Figure 68(b) shows the beam profiles of a BG beam at different locations with and without the obstruction, which indicates that the BG beams are self-healing after the obstruction. Figure 68(c) shows the measured BER performance for the two multiplexed data channels. The results show that the BERs of both channels could be achieved below the FEC limit with an obstruction of 1.5-mm radius.²⁵⁹

B. Other types of structured beams

In addition to Bessel-type beams, other types of structured beams have also been explored to mitigate system degradation effects of

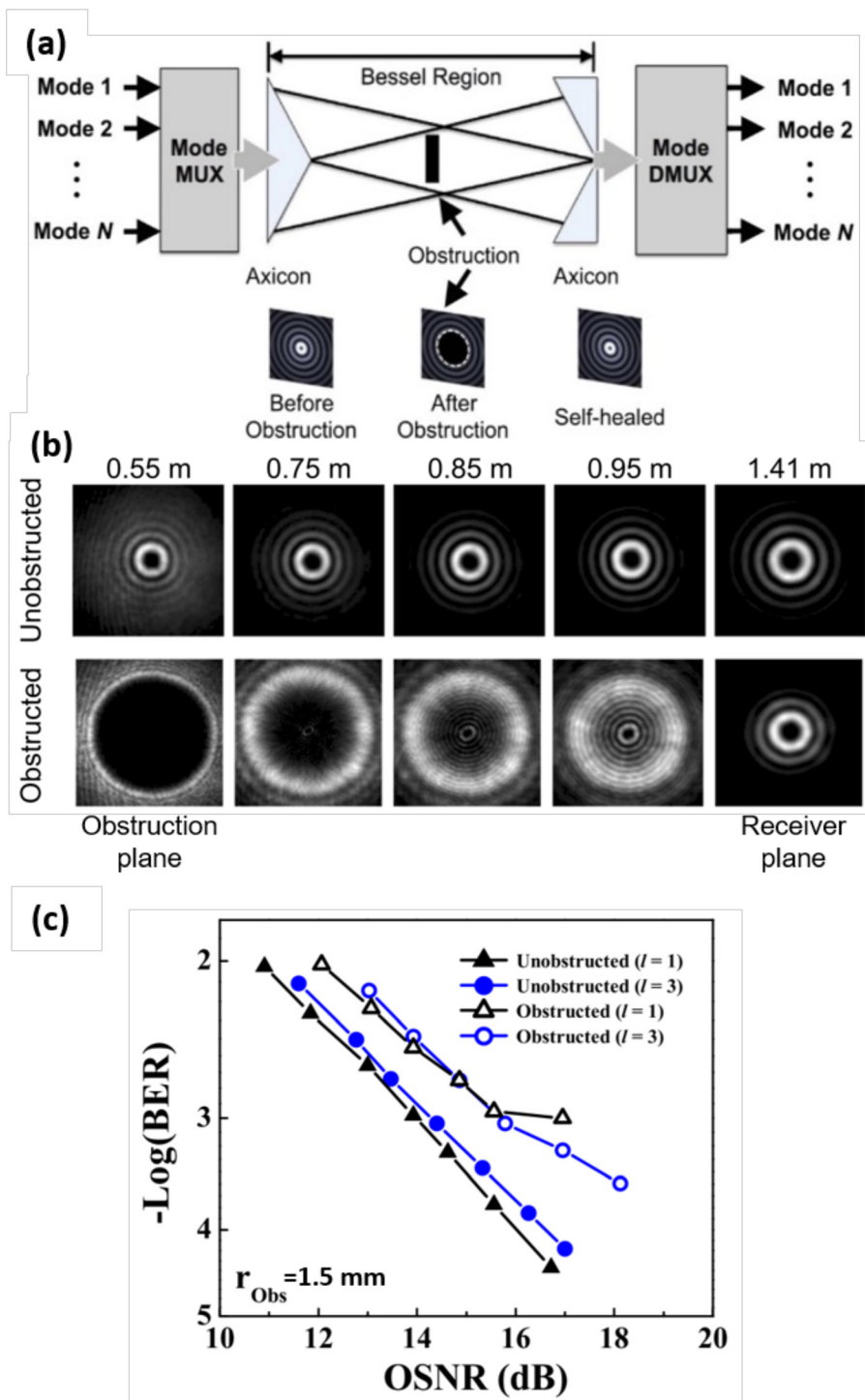


FIG. 68. (a) Concept of utilizing the self-healing property of higher-order BG beams to mitigate obstruction-induced degradation effects in an MDM FSO link. The insets show the intensity profiles of a BG beam before and after an opaque disk. (b) Measured intensity profiles of a BG beam ($\ell = +3$) at different locations with and without the obstruction. The radius of the obstruction is 1.5 mm. (c) Measured BER performance for the multiplexed data channels with and without an obstruction of 1.5 mm radius. Reproduced with permission from Ahmed *et al.*, Sci. Rep. 6, 22082 (2016).²⁵⁹ Copyright 2016 Macmillan Publishers.

free-space optical systems. For example, the Airy beam could propagate following a “bendable” trajectory.^{25–27} Such a property has been demonstrated in FSO communication systems to avoid obstructions that are located between the transmitter and receiver.^{262–264} More

recently, another type of structured beam has been proposed, which is the pin-like beam.²⁸ Such a beam has been demonstrated to have low divergence over kilometers of distance, and its intensity profile experiences relatively less distortion compared to a Gaussian beam under

atmospheric turbulence.^{28,29} Although such different types of beams have been originally investigated without carrying OAM, it is possible to generate these beams carrying OAM (e.g., Airy vortex beams^{265,266} and pin-like vortex beams²⁶⁷) and potentially utilize them in OAM-based FSO communication links.

C. Summary

In this section, we present different types of novel structured beams. The potential applications of these novel beams for OAM-based communications are also discussed. Although many realizations and applications of novel beams are originally explored in the fields of optics and photonics, their basic concepts could be extended to different frequency regimes.^{268–271} In future, more types of novel structured beams might be explored and used to improve the robustness of free-space communication systems either using a single beam or multiple orthogonal beams.

X. SUMMARY AND PERSPECTIVE

This paper reviews the advances and perspectives of OAM utilization for communications. We discussed different aspects, including (a) generation/detection and (de)multiplexing of the OAM beams, (b) classical FSO communication links, (c) fiber-based communication links, (d) quantum communication links, (e) OAM-multiplexed communications for different frequency ranges, (f) OAM-based communications using integrated devices, and (g) novel structured beams for MDM communications.

As one type of structured beam, OAM has been gaining much interest in various significant fields. Indeed, there are some important and valuable advances that could be potentially beneficial for the applications of OAM. In future, it is quite possible that OAM will be widely adopted in communication systems.

Moreover, it is likely that SWaP issues will be essential for many types of applications. Currently, many devices utilized in OAM-based communication systems are bulky, expensive, and slow (e.g., SLMs). In order to deploy the OAM-based communication systems widely and commercially in future, novel and cost-efficient integration technology (e.g., photonic integrated circuits) would likely be important.

Furthermore, in addition to the aforementioned scenarios in this paper, it remains a challenge for OAM-based communication links to operate under more complicated conditions and harsher environments. Such conditions and environments might cause more serious degradation effects, such as more distorted beams, larger power loss, and modal power coupling. Thus, investigating and evaluating system performance under such conditions and environments could be a valuable task. In addition, it is also important to develop techniques to increase the reliability and robustness of the OAM-based link, such as more resilient link designs and more effective mitigation approaches.

ACKNOWLEDGMENTS

We gratefully acknowledge the special collaboration over many years and many projects with Professors Robert W. Boyd, Andreas F. Molisch, Moshe Tur, and Jian Wang. We thank many current and former members of USC Optical Communications Laboratory who contributed to many of the projects.

We also acknowledge the generous support from the Vannevar Bush Faculty Fellowship (VBFF) sponsored by the Basic Research Office of the Assistant Secretary of Defense (ASD) for Research and Engineering (R&E) and funded by the Office of Naval Research (ONR) (N00014-16-1-2813), the Office of Naval Research through a MURI (N00014-20-1-2558), the Office of Naval Research through a MURI (N00014-20-1-2789), the Air Force Research Laboratory (FA8650-20-C-1105), the Defense Security Cooperation Agency (DSCA) (4440646262 and 4441006051), the Naval Information Warfare Center Pacific (NIWCP) (N6600120C4704), the Qualcomm Innovation Fellowship (QIF), the Airbus Institute for Engineering Research, the Nippon Telegraph and Telephone Corporation (NTT).

DATA AVAILABILITY

Data sharing is not applicable to this article as no new data were created or analyzed in this Review.

REFERENCES

- ¹H. Rubinsztein-Dunlop, A. Forbes, M. V. Berry, M. R. Dennis, D. L. Andrews, M. Mansuripur, C. Denz, C. Alpmann, P. Banzer, T. Bauer, E. Karimi, L. Marrucci, M. Padgett, M. Ritsch-Marte, N. M. Litchinitser, N. P. Bigelow, C. Rosales-Guzmán, A. Belmonte, J. P. Torres, T. W. Neely, M. Baker, R. Gordon, A. B. Stilgoe, J. Romero, A. G. White, R. Fickler, A. E. Willner, G. Xie, B. McMorran, and A. M. Weiner, “Roadmap on structured light,” *J. Opt.* **19**, 013001 (2016).
- ²K. I. Willig, S. O. Rizzoli, V. Westphal, R. Jahn, and S. W. Hell, “STED microscopy reveals that synaptotagmin remains clustered after synaptic vesicle exocytosis,” *Nature* **440**, 935 (2006).
- ³Y. Shen, X. Wang, Z. Xie, C. Min, X. Fu, Q. Liu, M. Gong, and X. Yuan, “Optical vortices 30 years on: OAM manipulation from topological charge to multiple singularities,” *Light: Sci. Appl.* **8**, 90 (2019).
- ⁴A. Forbes, M. de Oliveira, and M. R. Dennis, “Structured light,” *Nat. Photonics* **15**, 253 (2021).
- ⁵L. Allen, M. W. Beijersbergen, R. J. C. Spreeuw, and J. P. Woerdman, “Orbital angular momentum of light and the transformation of Laguerre–Gaussian laser modes,” *Phys. Rev. A* **45**, 8185 (1992).
- ⁶A. M. Yao and M. J. Padgett, “Orbital angular momentum: Origins, behavior and applications,” *Adv. Opt. Photonics* **3**, 161 (2011).
- ⁷A. E. Willner, H. Huang, Y. Yan, Y. Ren, N. Ahmed, G. Xie, C. Bao, L. Li, Y. Cao, Z. Zhao, J. Wang, M. P. J. Lavery, M. Tur, S. Ramachandran, A. F. Molisch, N. Ashrafi, and S. Ashrafi, “Optical communications using orbital angular momentum beams,” *Adv. Opt. Photonics* **7**, 66 (2015).
- ⁸A. Mair, A. Vaziri, G. Weihs, and A. Zeilinger, “Entanglement of the orbital angular momentum states of photons,” *Nature* **412**, 313 (2001).
- ⁹R. L. Phillips and L. C. Andrews, “Spot size and divergence for Laguerre–Gaussian beams of any order,” *Appl. Opt.* **22**, 643 (1983).
- ¹⁰H.-C. Kim and Y. H. Lee, “Hermite–Gaussian and Laguerre–Gaussian beams beyond the paraxial approximation,” *Opt. Commun.* **169**, 9 (1999).
- ¹¹N. Bozinovic, Y. Yue, Y. Ren, M. Tur, P. Kristensen, H. Huang, A. E. Willner, and S. Ramachandran, “Terabit-scale orbital angular momentum mode division multiplexing in fibers,” *Science* **340**, 1545 (2013).
- ¹²J. Wang, J.-Y. Yang, I. M. Fazal, N. Ahmed, Y. Yan, H. Huang, Y. Ren, Y. Yue, S. Dolinar, M. Tur, and A. E. Willner, “Terabit free-space data transmission employing orbital angular momentum multiplexing,” *Nat. Photonics* **6**, 488 (2012).
- ¹³K. Pang, H. Song, Z. Zhao, R. Zhang, H. Song, G. Xie, L. Li, C. Liu, J. Du, A. F. Molisch, M. Tur, and A. E. Willner, “400-Gbit/s QPSK free-space optical communication link based on four-fold multiplexing of Hermite–Gaussian or Laguerre–Gaussian modes by varying both modal indices,” *Opt. Lett.* **43**, 3889 (2018).
- ¹⁴G. Gibson, J. Courtial, M. J. Padgett, M. Vasnetsov, V. Pas’ko, S. M. Barnett, and S. Franke-Arnold, “Free-space information transfer using light beams carrying orbital angular momentum,” *Opt. Express* **12**, 5448 (2004).

- ¹⁵A. J. Willner, Y. Ren, G. Xie, Z. Zhao, Y. Cao, L. Li, N. Ahmed, Z. Wang, Y. Yan, P. Liao, M. Mirhosseini, R. W. Boyd, M. Tur, and A. E. Willner, "Experimental demonstration of 20 Gbit/s data encoding and 2 ns channel hopping using orbital angular momentum modes," *Opt. Lett.* **40**, 5810 (2015).
- ¹⁶M. Krenn, J. Handsteiner, M. Fink, R. Fickler, R. Ursin, M. Malik, and A. Zeilinger, "Twisted light transmission over 143 km," *Proc. Natl. Acad. Sci. U.S.A.* **113**, 13648 (2016).
- ¹⁷M. Mirhosseini, O. S. Magaña-Loaiza, M. N. O'Sullivan, B. Rodenburg, M. Malik, M. P. J. Lavery, M. J. Padgett, D. J. Gauthier, and R. W. Boyd, "High-dimensional quantum cryptography with twisted light," *New J. Phys.* **17**, 033033 (2015).
- ¹⁸L. Mandel and E. Wolf, *Optical Coherence and Quantum Optics* (Cambridge University Press, 1995).
- ¹⁹L. Li, G. Xie, Y. Yan, Y. Ren, P. Liao, Z. Zhao, N. Ahmed, Z. Wang, C. Bao, A. J. Willner, S. Ashrafi, M. Tur, and A. E. Willner, "Power loss mitigation of orbital-angular-momentum-multiplexed free-space optical links using nonzero radial index Laguerre-Gaussian beams," *J. Opt. Soc. Am. B* **34**(1), 1 (2017).
- ²⁰G. Xie, Y. Ren, Y. Yan, H. Huang, N. Ahmed, L. Li, Z. Zhao, C. Bao, M. Tur, S. Ashrafi, and A. E. Willner, "Experimental demonstration of a 200-Gbit/s free-space optical link by multiplexing Laguerre-Gaussian beams with different radial indices," *Opt. Lett.* **41**, 3447 (2016).
- ²¹G. Xie, C. Liu, L. Li, Y. Ren, Z. Zhao, Y. Yan, N. Ahmed, Z. Wang, A. J. Willner, C. Bao, Y. Cao, P. Liao, M. Ziyadi, A. Almaiman, S. Ashrafi, M. Tur, and A. E. Willner, "Spatial light structuring using a combination of multiple orthogonal orbital angular momentum beams with complex coefficients," *Opt. Lett.* **42**, 991 (2017).
- ²²J. Durnin, J. J. Miceli, Jr., and J. H. Eberly, "Diffraction-free beams," *Phys. Rev. Lett.* **58**, 1499 (1987).
- ²³J. Durnin, "Exact solutions for nondiffracting beams. I. The scalar theory," *J. Opt. Soc. Am. A* **4**, 651 (1987).
- ²⁴A. Dudley, M. Lavery, M. Padgett, and A. Forbes, "Unraveling Bessel beams," *Opt. Photonics News* **24**, 22 (2013).
- ²⁵N. K. Efremidis, Z. Chen, M. Segev, and D. N. Christodoulides, "Airy beams and accelerating waves: An overview of recent advances," *Optica* **6**, 686 (2019).
- ²⁶G. A. Siviloglou and D. N. Christodoulides, "Accelerating finite energy Airy beams," *Opt. Lett.* **32**, 979 (2007).
- ²⁷G. A. Siviloglou, J. Broky, A. Dogariu, and D. N. Christodoulides, "Observation of accelerating Airy beams," *Phys. Rev. Lett.* **99**, 213901 (2007).
- ²⁸Z. Zhang, X. Liang, M. Goutsoulas, D. Li, X. Yang, S. Yin, J. Xu, D. N. Christodoulides, N. K. Efremidis, and Z. Chen, "Robust propagation of pin-like optical beam through atmospheric turbulence," *APL Photonics* **4**, 076103 (2019).
- ²⁹D. Li, D. Bongiovanni, M. Goutsoulas, S. Xia, Z. Zhang, Y. Hu, D. Song, R. Morandotti, N. K. Efremidis, and Z. Chen, "Direct comparison of anti-diffracting optical pin beams and abruptly autofocusing beams," *OSA Continuum* **3**, 1525 (2020).
- ³⁰A. E. Willner, "OAM light for communications," *Opt. Photonics News* **32**, 34 (2021).
- ³¹A. H. Gnauck, P. J. Winzer, S. Chandrasekhar, X. Liu, B. Zhu, and D. W. Peckham, "Spectrally efficient long-haul WDM transmission using 224-Gb/s polarization-multiplexed 16-QAM," *J. Light. Technol.* **29**, 373 (2011).
- ³²X. Zhou, J. Yu, M.-F. Huang, Y. Shao, T. Wang, L. Nelson, P. Magill, M. Birk, P. I. Borel, D. W. Peckham, R. Lingle, and B. Zhu, "64-Tb/s, 8 b/s/Hz, PDM-36QAM transmission over 320 km using both pre- and post-transmission digital signal processing," *J. Light. Technol.* **29**, 571 (2011).
- ³³A. Sano, H. Masuda, T. Kobayashi, M. Fujiwara, K. Horikoshi, E. Yoshida, Y. Miyamoto, M. Matsui, M. Mizoguchi, H. Yamazaki, Y. Sakamaki, and H. Ishii, "Ultra-high capacity WDM transmission using spectrally-efficient PDM 16-QAM modulation and C-and extended L-band wideband optical amplification," *J. Light. Technol.* **29**, 578 (2011).
- ³⁴T. Richter, E. Palushani, C. Schmidt-Langhorst, R. Ludwig, L. Molle, M. Nolle, and C. Schubert, "Transmission of single-channel 16-QAM data signals at terabaud symbol rates," *J. Light. Technol.* **30**, 504 (2011).
- ³⁵X. Liu, S. Chandrasekhar, X. Chen, P. J. Winzer, Y. Pan, T. F. Taunay, B. Zhu, M. Fishteyn, M. F. Yan, J. M. Fini, E. M. Monberg, and F. V. Dimarcello, "1.12-Tb/s 32-QAM-OFDM superchannel with 8.6-b/s/Hz intrachannel spectral efficiency and space-division multiplexed transmission with 60-b/s/Hz aggregate spectral efficiency," *Opt. Express* **19**, B958 (2011).
- ³⁶D. J. Richardson, J. M. Fini, and L. E. Nelson, "Space-division multiplexing in optical fibres," *Nat. Photonics* **7**, 354 (2013).
- ³⁷P. J. Winzer, "Making spatial multiplexing a reality," *Nat. Photonics* **8**, 345 (2014).
- ³⁸H. Huang, G. Xie, Y. Yan, N. Ahmed, Y. Ren, Y. Yue, D. Rogawski, M. J. Willner, B. I. Erkmen, K. M. Birnbaum, S. J. Dolinar, M. P. J. Lavery, M. J. Padgett, M. Tur, and A. E. Willner, "100 Tbit/s free-space data link enabled by three-dimensional multiplexing of orbital angular momentum, polarization, and wavelength," *Opt. Lett.* **39**, 197 (2014).
- ³⁹M. Smit, J. Van der Tol, and M. Hill, "Moore's law in photonics," *Laser Photonics Rev.* **6**, 1 (2012).
- ⁴⁰A. E. Willner, Z. Zhao, C. Liu, R. Zhang, H. Song, K. Pang, K. Manukyan, H. Song, X. Su, G. Xie, Y. Ren, Y. Yan, M. Tur, A. F. Molisch, R. W. Boyd, H. Zhou, N. Hu, A. Minoofar, and H. Huang, "Perspectives on advances in high-capacity, free-space communications using multiplexing of orbital-angular-momentum beams," *APL Photonics* **6**, 030901 (2021).
- ⁴¹R. Ryf, S. Randel, A. H. Gnauck, C. Bolle, A. Sierra, S. Mumtaz, M. Esmaeelpour, E. C. Burrows, R.-J. Essiambre, P. J. Winzer, D. W. Peckham, A. H. McCurdy, and R. Lingle, "Mode-division multiplexing over 96 km of few-mode fiber using coherent 6 × 6 MIMO processing," *J. Light. Technol.* **30**, 521 (2011).
- ⁴²B. Ndagano, R. Brüning, M. McLaren, M. Duparré, and A. Forbes, "Fiber propagation of vector modes," *Opt. Express* **23**, 17330 (2015).
- ⁴³A. Trichili, A. B. Salem, A. Dudley, M. Zghal, and A. Forbes, "Encoding information using Laguerre Gaussian modes over free space turbulence media," *Opt. Lett.* **41**, 3086 (2016).
- ⁴⁴L. C. Andrews and R. L. Phillips, *Laser Beam Propagation through Random Media* (SPIE, 2005).
- ⁴⁵G. A. Tyler and R. W. Boyd, "Influence of atmospheric turbulence on the propagation of quantum states of light carrying orbital angular momentum," *Opt. Lett.* **34**, 142 (2009).
- ⁴⁶Y. Ren, H. Huang, G. Xie, N. Ahmed, Y. Yan, B. I. Erkmen, N. Chandrasekaran, M. P. J. Lavery, N. K. Steinhoff, M. Tur, and A. E. Willner, "Atmospheric turbulence effects on the performance of a free space optical link employing orbital angular momentum multiplexing," *Opt. Lett.* **38**, 4062 (2013).
- ⁴⁷S. Fu and C. Gao, "Influences of atmospheric turbulence effects on the orbital angular momentum spectra of vortex beams," *Photonics Res.* **4**, B1 (2016).
- ⁴⁸G. Xie, L. Li, Y. Ren, H. Huang, Y. Yan, N. Ahmed, Z. Zhao, M. P. J. Lavery, N. Ashrafi, S. Ashrafi, R. Rock, M. Tur, A. F. Molisch, and A. E. Willner, "Performance metrics and design considerations for a free-space optical orbital-angular-momentum-multiplexed communication link," *Optica* **2**, 357 (2015).
- ⁴⁹X. Zhong, Y. Zhao, G. Ren, S. He, and Z. Wu, "Influence of finite apertures on orthogonality and completeness of Laguerre-Gaussian beams," *IEEE Access* **6**, 8742 (2018).
- ⁵⁰Z. Mei and D. Zhao, "The generalized beam propagation factor of truncated standard and elegant Laguerre-Gaussian beams," *J. Opt. A: Pure Appl. Opt.* **6**, 1005 (2004).
- ⁵¹Y. Yan, G. Xie, M. P. J. Lavery, H. Huang, N. Ahmed, C. Bao, Y. Ren, Y. Cao, L. Li, Z. Zhao, A. F. Molisch, M. Tur, M. J. Padgett, and A. E. Willner, "High-capacity millimetre-wave communications with orbital angular momentum multiplexing," *Nat. Commun.* **5**, 4876 (2014).
- ⁵²C. Shi, M. Dubois, Y. Wang, and X. Zhang, "High-speed acoustic communication by multiplexing orbital angular momentum," *Proc. Natl. Acad. Sci. U. S. A.* **114**, 7250 (2017).
- ⁵³W. Cheng, H. Zhang, L. Liang, H. Jing, and Z. Li, "Orbital-angular-momentum embedded massive MIMO: Achieving multiplicative spectrum-efficiency for mmwave communications," *IEEE Access* **6**, 2732 (2017).
- ⁵⁴D. Lee, H. Sasaki, H. Fukumoto, Y. Yagi, and T. Shimizu, "An evaluation of orbital angular momentum multiplexing technology," *Appl. Sci.* **9**, 1729 (2019).
- ⁵⁵H. Sasaki, D. Lee, H. Fukumoto, Y. Yagi, T. Kaho, H. Shiba, and T. Shimizu, "Experiment on over-100-Gbps wireless transmission with OAM-MIMO

- multiplexing system in 28-GHz band," in *2018 IEEE Global Communications Conference (GLOBECOM)* (IEEE, 2018), p. 1.
- ⁵⁶H. Sasaki, Y. Yagi, T. Yamada, and D. Lee, "Field experimental demonstration on OAM-MIMO wireless transmission on 28 GHz band," in *2019 IEEE Globecom Workshops (GC Wkshps)* (IEEE, 2019), p. 1.
- ⁵⁷Z. Zhao, Y. Yan, L. Li, G. Xie, Y. Ren, N. Ahmed, Z. Wang, C. Liu, A. J. Willner, P. Song, H. Hashemi, H. Yao, D. Macfarlane, R. Henderson, N. Ashrafi, S. Ashrafi, S. Talwar, S. Sajuyigbe, M. Tur, A. F. Molisch, and A. E. Willner, "A dual-channel 60 GHz communications link using patch antenna arrays to generate data-carrying orbital-angular-momentum beams," in *2016 IEEE International Conference on Communications (ICC)* (IEEE, 2016), p. 1.
- ⁵⁸G. Xie, Z. Zhao, Y. Yan, L. Li, Y. Ren, N. Ahmed, Y. Cao, A. J. Willner, C. Bao, Z. Wang, C. Liu, M. Ziyadi, S. Talwar, S. Sajuyigbe, S. Ashrafi, M. Tur, A. F. Molisch, and A. E. Willner, "Demonstration of tunable steering and multiplexing of two 28 GHz data carrying orbital angular momentum beams using antenna array," *Sci. Rep.* **6**, 37078 (2016).
- ⁵⁹M. Lin, Y. Gao, P. Liu, and J. Liu, "Theoretical analyses and design of circular array to generate orbital angular momentum," *IEEE Trans. Antennas Propag.* **65**, 3510 (2017).
- ⁶⁰S. Yu, L. Li, G. Shi, C. Zhu, X. Zhou, and Y. Shi, "Design, fabrication, and measurement of reflective metasurface for orbital angular momentum vortex wave in radio frequency domain," *Appl. Phys. Lett.* **108**, 121903 (2016).
- ⁶¹X. Wei, L. Zhu, Z. Zhang, K. Wang, J. Liu, and J. Wang, "Orbit angular momentum multiplexing in 0.1-THz free-space communication via 3D printed spiral phase plates," in *2014 Conference on Lasers and Electro-Optics (CLEO)-Laser Science to Photonic Applications* (IEEE, 2014), Paper No. STu2F.2.
- ⁶²C. Liu, X. Wei, L. Niu, K. Wang, Z. Yang, and J. Liu, "Discrimination of orbital angular momentum modes of the terahertz vortex beam using a diffractive mode transformer," *Opt. Express* **24**, 12534 (2016).
- ⁶³Q. Wu and R. Zhang, "Intelligent reflecting surface enhanced wireless network via joint active and passive beamforming," *IEEE Trans. Wireless Commun.* **18**, 5394 (2019).
- ⁶⁴X. G. Zhang, W. X. Jiang, H. L. Jiang, Q. Wang, H. W. Tian, L. Bai, Z. J. Luo, S. Sun, Y. Luo, C.-W. Qiu, and T. J. Cui, "An optically driven digital metasurface for programming electromagnetic functions," *Nat. Electron.* **3**, 165 (2020).
- ⁶⁵H. Elgala, R. Mesleh, and H. Haas, "Indoor optical wireless communication: Potential and state-of-the-art," *IEEE Commun. Mag.* **49**, 56 (2011).
- ⁶⁶D.-S. Ly-Gagnon, S. Tsukamoto, K. Katoh, and K. Kikuchi, "Coherent detection of optical quadrature phase-shift keying signals with carrier phase estimation," *J. Light Technol.* **24**, 12 (2006).
- ⁶⁷W. Freude, R. Schmogrow, B. Nebendahl, M. Winter, A. Josten, D. Hillerkuss, S. Koenig, J. Meyer, M. Dreschmann, M. Huebner, C. Koos, J. Becker, and J. Leuthold, "Quality metrics for optical signals: Eye diagram, Q-factor, OSNR, EVM and BER," in *2012 14th International Conference on Transparent Optical Networks (ICTON)* (IEEE, 2012), Paper No. Mo.B1.5.
- ⁶⁸M. W. Beijersbergen, R. P. C. Coerwinkel, M. Kristensen, and J. P. Woerdman, "Helical-wavefront laser beams produced with a spiral phaseplate," *Opt. Commun.* **112**, 321 (1994).
- ⁶⁹W. Harm, S. Bernet, M. Ritsch-Marte, I. Harder, and N. Lindlein, "Adjustable diffractive spiral phase plates," *Opt. Express* **23**, 413 (2015).
- ⁷⁰K. Weber, F. Hütt, S. Thiele, T. Gissibl, A. Herkommmer, and H. Giessen, "Single mode fiber based delivery of OAM light by 3D direct laser writing," *Opt. Express* **25**, 19672 (2017).
- ⁷¹H. Li, D. B. Phillips, X. Wang, Y.-L. D. Ho, L. Chen, X. Zhou, J. Zhu, S. Yu, and X. Cai, "Orbital angular momentum vertical-cavity surface-emitting lasers," *Optica* **2**, 547 (2015).
- ⁷²J. Liu and J. Wang, "Demonstration of polarization-insensitive spatial light modulation using a single polarization-sensitive spatial light modulator," *Sci. Rep.* **5**, 9959 (2015).
- ⁷³N. Heckenberg, R. McDuff, C. Smith, and A. White, "Generation of optical phase singularities by computer-generated holograms," *Opt. Lett.* **17**, 221 (1992).
- ⁷⁴N. Matsumoto, T. Ando, T. Inoue, Y. Ohtake, N. Fukuchi, and T. Hara, "Generation of high-quality higher-order Laguerre-Gaussian beams using liquid-crystal-on-silicon spatial light modulators," *J. Opt. Soc. Am. A* **25**, 1642 (2008).
- ⁷⁵T. Ando, Y. Ohtake, N. Matsumoto, T. Inoue, and N. Fukuchi, "Mode purities of Laguerre-Gaussian beams generated via complex-amplitude modulation using phase-only spatial light modulators," *Opt. Lett.* **34**, 34 (2009).
- ⁷⁶I. Nape, B. Sephton, Y.-W. Huang, A. Vallés, C.-W. Qiu, A. Ambrosio, F. Capasso, and A. Forbes, "Enhancing the modal purity of orbital angular momentum photons," *APL Photonics* **5**, 070802 (2020).
- ⁷⁷E. Karimi, G. Zito, B. Piccirillo, L. Marrucci, and E. Santamato, "Hypergeometric-Gaussian modes," *Opt. Lett.* **32**, 3053 (2007).
- ⁷⁸X. Wang, Z. Nie, Y. Liang, J. Wang, T. Li, and B. Jia, "Recent advances on optical vortex generation," *Nanophotonics* **7**, 1533 (2018).
- ⁷⁹P. Genevet, N. Yu, F. Aieta, J. Lin, M. A. Kats, R. Blanchard, M. O. Scully, Z. Gaburro, and F. Capasso, "Ultra-thin plasmonic optical vortex plate based on phase discontinuities," *Appl. Phys. Lett.* **100**, 013101 (2012).
- ⁸⁰E. Karimi, S. A. Schulz, I. De Leon, H. Qassim, J. Upham, and R. W. Boyd, "Generating optical orbital angular momentum at visible wavelengths using a plasmonic metasurface," *Light: Sci. Appl.* **3**, e167 (2014).
- ⁸¹R. C. Devlin, A. Ambrosio, N. A. Rubin, J. P. B. Mueller, and F. Capasso, "Arbitrary spin-to-orbital angular momentum conversion of light," *Science* **358**, 896 (2017).
- ⁸²H. Sroor, Y.-W. Huang, B. Sephton, D. Naidoo, A. Valles, V. Ginis, C.-W. Qiu, A. Ambrosio, F. Capasso, and A. Forbes, "High-purity orbital angular momentum states from a visible metasurface laser," *Nat. Photonics* **14**, 498 (2020).
- ⁸³Y. Yang, W. Wang, P. Moitra, I. I. Kravchenko, D. P. Briggs, and J. Valentine, "Dielectric meta-reflectarray for broadband linear polarization conversion and optical vortex generation," *Nano Lett.* **14**, 1394 (2014).
- ⁸⁴T. Y. Fan, "Laser beam combining for high-power, high-radiance sources," *IEEE J. Sel. Top. Quantum Electron.* **11**, 567 (2005).
- ⁸⁵V. P. Aksenen, V. V. Dudorov, V. V. Kolosov, and M. E. Levitsky, "Synthesized vortex beams in the turbulent atmosphere," *Front. Phys.* **8**, 143 (2020).
- ⁸⁶Z. S. Eznaveh, J. C. A. Zacarias, J. E. A. Lopez, K. Shi, G. Milione, Y. Jung, B. C. Thomsen, D. J. Richardson, N. Fontaine, S. G. Leon-Saval, and R. A. Correa, "Photonic lantern broadband orbital angular momentum mode multiplexer," *Opt. Express* **26**, 30042 (2018).
- ⁸⁷Y. Han, Y.-G. Liu, Z. Wang, W. Huang, L. Chen, H.-W. Zhang, and K. Yang, "Controllable all-fiber generation/conversion of circularly polarized orbital angular momentum beams using long period fiber gratings," *Nanophotonics* **7**, 287 (2018).
- ⁸⁸J. Leach, J. Courtial, K. Skeldon, S. M. Barnett, S. Franke-Arnold, and M. J. Padgett, "Interferometric methods to measure orbital and spin, or the total angular momentum of a single photon," *Phys. Rev. Lett.* **92**, 013601 (2004).
- ⁸⁹Y. Zhou, M. Mirhosseini, D. Fu, J. Zhao, S. M. H. Rafsanjani, A. E. Willner, and R. W. Boyd, "Sorting photons by radial quantum number," *Phys. Rev. Lett.* **119**, 263602 (2017).
- ⁹⁰T. Lei, M. Zhang, Y. Li, P. Jia, G. N. Liu, X. Xu, Z. Li, C. Min, J. Lin, C. Yu, H. Niu, and X. Yuan, "Massive individual orbital angular momentum channels for multiplexing enabled by Dammann gratings," *Light: Sci. Appl.* **4**, e257 (2015).
- ⁹¹G. C. Berkhout, M. P. J. Lavery, J. Courtial, M. W. Beijersbergen, and M. J. Padgett, "Efficient sorting of orbital angular momentum states of light," *Phys. Rev. Lett.* **105**, 153601 (2010).
- ⁹²N. K. Fontaine, R. Ryf, H. Chen, D. T. Neilson, K. Kim, and J. Carpenter, "Laguerre-Gaussian mode sorter," *Nat. Commun.* **10**, 1865 (2019).
- ⁹³Z. Lin, Y. Wen, Y. Chen, and S. Yu, "Transmissive multi-plane light conversion for demultiplexing orbital angular momentum modes," in *CLEO: Science and Innovations* (OSA, 2020), Paper No. SF1J.5.
- ⁹⁴Y. Awaji, N. Wada, and Y. Toda, "Demonstration of spatial mode division multiplexing using Laguerre-Gaussian mode beam in telecom-wavelength," in *2010 23rd Annual Meeting of the IEEE Photonics Society* (IEEE, 2010), p. 551.
- ⁹⁵J. Wang, J.-Y. Yang, I. M. Fazal, N. Ahmed, Y. Yan, B. Shamee, A. E. Willner, K. Birnbaum, J. Choi, B. Erkmen, S. Dolinar, and M. Tur, "Demonstration of 12.8-bit/s/Hz spectral efficiency using 16-QAM signals over multiple orbital-

- angular-momentum modes," in *2011 37th European Conference and Exhibition on Optical Communication* (IEEE, 2011), Paper No. We.10.P1.76.
- ⁹⁶J. Wang, S. Li, M. Luo, J. Liu, L. Zhu, C. Li, D. Xie, Q. Yang, S. Yu, J. Sun, X. Zhang, W. Shieh, and A. E. Willner, "N-dimensional multiplexing link with 1.036-Pbit/s transmission capacity and 112.6-bit/s/Hz spectral efficiency using OFDM-8QAM signals over 368 WDM pol-muxed 26 OAM modes," in *2014 The European Conference on Optical Communication (ECOC)* (IEEE, 2014), p. Mo.4.5.1.
- ⁹⁷Y. Ren, Z. Wang, P. Liao, L. Li, G. Xie, H. Huang, Z. Zhao, Y. Yan, N. Ahmed, A. J. Willner, M. P. J. Lavery, N. Ashrafi, S. Ashrafi, R. Bock, M. Tur, I. B. Djordjevic, M. A. Neifeld, and A. E. Willner, "Experimental characterization of a 400 Gbit/s orbital angular momentum multiplexed free-space optical link over 120 m," *Opt. Lett.* **41**, 622 (2016).
- ⁹⁸Y. Zhao, J. Liu, J. Du, S. Li, Y. Luo, A. Wang, L. Zhu, and J. Wang, "Experimental demonstration of 260-meter security free-space optical data transmission using 16-QAM carrying orbital angular momentum (OAM) beams multiplexing," in *Optical Fiber Communication Conference* (OSA, 2016), Paper No. Th1H.3.
- ⁹⁹C. Maurer, A. Jesacher, S. Fürhapter, S. Bernet, and M. Ritsch-Marte, "Tailoring of arbitrary optical vector beams," *New J. Phys.* **9**, 78 (2007).
- ¹⁰⁰M. V. Vasnetsov, V. A. Pas'ko, and M. S. Soskin, "Analysis of orbital angular momentum of a misaligned optical beam," *New J. Phys.* **7**, 46 (2005).
- ¹⁰¹A. E. Siegman, "How to (maybe) measure laser beam quality," in *Diode Pumped Solid State Lasers: Applications and Issues* (Optical Society of America, 1998), p. MQ1.
- ¹⁰²C. Schulze, D. Flamm, M. Duparré, and A. Forbes, "Beam-quality measurements using a spatial light modulator," *Opt. Lett.* **37**, 4687–4689 (2012).
- ¹⁰³M. J. Padgett, F. M. Miatto, M. P. J. Lavery, A. Zeilinger, and R. W. Boyd, "Divergence of an orbital-angular-momentum-carrying beam upon propagation," *New J. Phys.* **17**, 023011 (2015).
- ¹⁰⁴K. Pang, H. Song, X. Su, K. Zou, Z. Zhao, H. Song, A. Almaiman, R. Zhang, C. Liu, N. Hu, S. Zach, N. Cohen, B. Lynn, A. F. Molisch, R. W. Boyd, M. Tur, and A. E. Willner, "Simultaneous orthogonalizing and shaping of multiple LG beams to mitigate crosstalk and power loss by transmitting each of four data channels on multiple modes in a 400-Gbit/s free-space link," in *Optical Fiber Communication Conference* (OSA, 2020), Paper No. W1G.2.
- ¹⁰⁵S. Clifford, G. R. Ochs, and R. S. Lawrence, "Saturation of optical scintillation by strong turbulence," *J. Opt. Soc. Am. A* **64**, 148 (1974).
- ¹⁰⁶D. P. Greenwood, "Bandwidth specification for adaptive optics systems," *J. Opt. Soc. Am. A* **67**, 390 (1977).
- ¹⁰⁷M. R. Bhatnagar and Z. Ghassemlooy, "Performance analysis of Gamma-Gamma fading FSO MIMO links with pointing errors," *J. Light Technol.* **34**, 2158 (2016).
- ¹⁰⁸H. Samimi, "Distribution of the sum of K-distributed random variables and applications in free-space optical communications," *IET Optoelectron.* **6**, 1 (2012).
- ¹⁰⁹D. L. Fried, "Optical resolution through a randomly inhomogeneous medium for very long and very short exposures," *J. Opt. Soc. Am. A* **56**, 1372 (1966).
- ¹¹⁰M. A. Cox, N. Mphuthi, I. Nape, N. Mashaba, L. Cheng, and A. Forbes, "Structured light in turbulence," *IEEE J. Sel. Top. Quantum Electron.* **27**, 1 (2020).
- ¹¹¹L. Li, G. Xie, Y. Ren, N. Ahmed, H. Huang, Z. Zhao, P. Liao, M. P. J. Lavery, Y. Yan, C. Bao, Z. Wang, A. J. Willner, N. Ashrafi, S. Ashrafi, M. Tur, and A. E. Willner, "Orbital-angular-momentum-multiplexed free-space optical communication link using transmitter lenses," *Appl. Opt.* **55**, 2098 (2016).
- ¹¹²G. Xie, Y. Ren, H. Huang, N. Ahmed, L. Li, Y. Yan, M. P. J. Lavery, M. J. Padgett, M. Tur, S. J. Dolinar, and A. E. Willner, "Experimental comparison of single and double partial receiver apertures for recovering signals transmitted using orbital-angular-momentum," in *CLEO: Science and Innovations* (OSA, 2014), Paper No. SM3J.2.
- ¹¹³G. Xie, Y. Ren, H. Huang, Y. Yan, C. Bao, N. Ahmed, M. Willner, M. P. J. Lavery, M. J. Padgett, and A. E. Willner, "Analysis of aperture size for partially receiving and de-multiplexing 100-Gbit/s optical orbital angular momentum channels over free-space link," in *2013 IEEE Globecom Workshops (GC Wkshps)* (IEEE, 2013), p. 1116.
- ¹¹⁴S. Zheng, X. Hui, J. Zhu, H. Chi, X. Jin, S. Yu, and X. Zhang, "Orbital angular momentum mode-demultiplexing scheme with partial angular receiving aperture," *Opt. Express* **23**, 12251 (2015).
- ¹¹⁵K. Pang, H. Song, X. Su, K. Zou, Z. Zhao, H. Song, A. Almaiman, R. Zhang, C. Liu, N. Hu, S. Zach, N. Cohen, B. Lynn, A. F. Molisch, R. W. Boyd, M. Tur, and A. E. Willner, "Experimental mitigation of the effects of the limited size aperture or misalignment by singular-value-decomposition-based beam orthogonalization in a free-space optical link using Laguerre-Gaussian modes," *Opt. Lett.* **45**, 6310 (2020).
- ¹¹⁶L. Li, R. Zhang, G. Xie, Y. Ren, Z. Zhao, Z. Wang, C. Liu, H. Song, K. Pang, R. Bock, M. Tur, and A. E. Willner, "Experimental demonstration of beaconless beam displacement tracking for an orbital angular momentum multiplexed free-space optical link," *Opt. Lett.* **43**, 2392 (2018).
- ¹¹⁷G. Xie, L. Li, Y. Ren, Y. Yan, N. Ahmed, Z. Zhao, Z. Wang, N. Ashrafi, S. Ashrafi, R. D. Linquist, et al., "Exploiting the unique intensity gradient of an orbital-angular-momentum beam for accurate receiver alignment monitoring in a free-space communication link," in *2015 European Conference on Optical Communication (ECOC)* (IEEE, 2015), Paper No. Th.2.3.5.
- ¹¹⁸G. Xie, L. Li, Y. Ren, Y. Yan, N. Ahmed, Z. Zhao, C. Bao, Z. Wang, C. Liu, H. Song, R. Zhang, K. Pang, S. Ashrafi, M. Tur, and A. E. Willner, "Localization from the unique intensity gradient of an orbital-angular-momentum beam," *Opt. Lett.* **42**, 395 (2017).
- ¹¹⁹K. Kazaura, K. Omae, T. Suzuki, M. Matsumoto, E. Mutafungwa, T. O. Korhonen, T. Murakami, K. Takahashi, H. Matsumoto, K. Wakamori, and Y. Arimoto, "Enhancing performance of next generation FSO communication systems using soft computing based predictions," *Opt. Express* **14**, 4958 (2006).
- ¹²⁰H. Huang, Y. Cao, G. Xie, Y. Ren, Y. Yan, C. Bao, N. Ahmed, M. A. Neifeld, S. J. Dolinar, and A. E. Willner, "Crosstalk mitigation in a free-space orbital angular momentum multiplexed communication link using 4 × 4 MIMO equalization," *Opt. Lett.* **39**, 4360 (2014).
- ¹²¹E. G. Larsson, O. Edfors, F. Tufvesson, and T. L. Marzetta, "Massive MIMO for next generation wireless systems," *IEEE Commun. Mag.* **52**, 186 (2014).
- ¹²²S. Randel, R. Ryf, A. Sierra, P. J. Winzer, A. H. Gnauck, C. A. Bolle, R.-J. Essiambre, D. W. Peckham, A. McCurdy, and R. Lingle, "6 × 56-Gb/s mode-division multiplexed transmission over 33-km few-mode fiber enabled by 6 × 6 MIMO equalization," *Opt. Express* **19**, 16697 (2011).
- ¹²³P. J. Winzer and G. J. Foschini, "MIMO capacities and outage probabilities in spatially multiplexed optical transport systems," *Opt. Express* **19**, 16680 (2011).
- ¹²⁴Y. Ren, G. Xie, H. Huang, C. Bao, Y. Yan, N. Ahmed, M. P. J. Lavery, B. I. Erkmen, S. Dolinar, M. Tur, M. A. Neifeld, M. J. Padgett, R. W. Boyd, J. H. Shapiro, and A. E. Willner, "Adaptive optics compensation of multiple orbital angular momentum beams propagating through emulated atmospheric turbulence," *Opt. Lett.* **39**, 2845 (2014).
- ¹²⁵Y. Ren, G. Xie, H. Huang, L. Li, N. Ahmed, Y. Yan, M. P. J. Lavery, R. Bock, M. Tur, M. A. Neifeld, R. W. Boyd, J. H. Shapiro, and A. E. Willner, "Turbulence compensation of an orbital angular momentum and polarization-multiplexed link using a data-carrying beacon on a separate wavelength," *Opt. Lett.* **40**, 2249 (2015).
- ¹²⁶Y. Ren, G. Xie, H. Huang, N. Ahmed, Y. Yan, L. Li, C. Bao, M. P. J. Lavery, M. Tur, M. A. Neifeld, R. W. Boyd, J. H. Shapiro, and A. E. Willner, "Adaptive-optics-based simultaneous pre- and post-turbulence compensation of multiple orbital-angular-momentum beams in a bidirectional free-space optical link," *Optica* **1**, 376 (2014).
- ¹²⁷H. Song, H. Song, R. Zhang, K. Manukyan, L. Li, Z. Zhao, K. Pang, C. Liu, A. Almaiman, R. Bock, B. Lynn, M. Tur, and A. E. Willner, "Experimental mitigation of atmospheric turbulence effect using pre-signal combining for uni-and bi-directional free-space optical links with two 100-Gbit/s OAM-multiplexed channels," *J. Light Technol.* **38**, 82 (2020).
- ¹²⁸R. Fickler, M. Ginoya, and R. W. Boyd, "Custom-tailored spatial mode sorting by controlled random scattering," *Phys. Rev. B* **95**, 161108 (2017).
- ¹²⁹R. Zhang, H. Song, Z. Zhao, H. Song, J. Du, C. Liu, K. Pang, L. Li, H. Zhou, A. N. Willner, A. Almaiman, Y. Zhou, R. W. Boyd, B. Lynn, R. Bock, M. Tur, and A. E. Willner, "Simultaneous turbulence mitigation and channel demultiplexing for two 100 Gbit/s orbital-angular-momentum multiplexed beams by adaptive wavefront shaping and diffusing," *Opt. Lett.* **45**, 702 (2020).

- ¹³⁰H. Song, X. Su, H. Song, R. Zhang, Z. Zhao, C. Liu, K. Pang, N. Hu, A. Almaiman, S. Zach, N. Cohen, A. F. Molisch, R. W. Boyd, M. Tur, and A. E. Willner, "Simultaneous turbulence mitigation and mode demultiplexing using one MPLC in a two-mode 200-Gbit/s free-space OAM-multiplexed link," in *Optical Fiber Communication Conference* (OSA, 2020), Paper No. W1G.3.
- ¹³¹Y. Zhou, J. Zhao, B. Braverman, K. Pang, R. Zhang, A. E. Willner, Z. Shi, and R. W. Boyd, "Multiprobe time reversal for high-fidelity vortex-mode-division multiplexing over a turbulent free-space link," *Phys. Rev. Appl.* **15**, 034011 (2021).
- ¹³²W. Roh, J.-Y. Seol, J. Park, B. Lee, J. Lee, Y. Kim, J. Cho, K. Cheun, and F. Aryanfar, "Millimeter-wave beamforming as an enabling technology for 5G cellular communications: Theoretical feasibility and prototype results," *IEEE Commun. Mag.* **52**, 106 (2014).
- ¹³³S. Abado, S. Gordeyev, and E. J. Jumper, "Two-dimensional high-bandwidth Shack-Hartmann wavefront sensor: Design guidelines and evaluation testing," *Opt. Eng.* **49**, 064403 (2010).
- ¹³⁴Z. Shi, M. Mirhosseini, J. Margiewicz, M. Malik, F. Rivera, Z. Zhu, and R. W. Boyd, "Scan-free direct measurement of an extremely high-dimensional photonic state," *Optica* **2**, 388 (2015).
- ¹³⁵A. K. Majumdar, "Free-space optical (FSO) platforms: Unmanned aerial vehicle (UAV) and mobile," in *Advanced Free Space Optics (FSO)* (Springer, 2015), p. 203.
- ¹³⁶J. Cunningham, D. Foulke, T. Goode, D. Baber, B. Gaughan, M. Fletcher, D. W. Young, J. C. Juarez, J. E. Sluz, and J. L. Riggins, "Long range field testing of free space optical communications terminals on mobile platforms," in *MILCOM 2009–2009 IEEE Military Communications Conference* (IEEE, 2009), Paper No. 901469.
- ¹³⁷S. S. Muhammad, T. Plank, E. Leitgeb, A. Friedl, K. Zettl, T. Javornik, and N. Schmitt, "Challenges in establishing free space optical communications between flying vehicles," in *2008 6th International Symposium on Communication Systems, Networks and Digital Signal Processing* (IEEE, 2008), p. 82.
- ¹³⁸R. Fields, C. Lunde, R. Wong, J. Wicker, D. Kozlowski, J. Jordan, B. Hansen, G. Muehl nikel, W. Scheel, U. Sterr, R. Kahle, and R. Meyer, "NFIRE-to-TerraSAR-X laser communication results: Satellite pointing, disturbances, and other attributes consistent with successful performance," *Proc. SPIE* **7330**, 7330Q.
- ¹³⁹F. Heine, G. Mühl nikel, H. Zech, S. Philipp-May, and R. Meyer, "The European data relay system, high speed laser based data links," in *2014 7th Advanced Satellite Multimedia Systems Conference and the 13th Signal Processing for Space Communications Workshop (ASMS/SPSC)* (IEEE, 2014), p. 284.
- ¹⁴⁰L. Li, R. Zhang, Z. Zhao, G. Xie, P. Liao, K. Pang, H. Song, C. Liu, Y. Ren, G. Labroille, P. Jian, D. Starodubov, B. Lynn, R. Bock, M. Tur, and A. E. Willner, "High-capacity free-space optical communications between a ground transmitter and a ground receiver via a UAV using multiplexing of multiple orbital-angular-momentum beams," *Sci. Rep.* **7**, 17427 (2017).
- ¹⁴¹K. E. Zarganis and A. Hatziefremidis, "Performance analysis of coherent optical OFDM applied to UAV mobile FSO systems," *J. Opt. Photonics* **3**, 5 (2015).
- ¹⁴²A. Kaadan, H. Refai, and P. G. LoPresti, "Spherical FSO receivers for UAV communication: Geometric coverage models," *IEEE Trans. Aerosp. Electron. Syst.* **52**, 2157 (2016).
- ¹⁴³A. Kaadan, H. H. Refai, and P. G. LoPresti, "Multielement FSO transceivers alignment for inter-UAV communications," *J. Light Technol.* **32**, 4785 (2014).
- ¹⁴⁴L. Li, R. Zhang, P. Liao, Y. Cao, H. Song, Y. Zhao, J. Du, Z. Zhao, C. Liu, K. Pang, S. Hao, A. Almaiman, D. Starodubov, B. Lynn, R. Bock, M. Tur, A. F. Molisch, and A. E. Willner, "Mitigation for turbulence effects in a 40-Gbit/s orbital-angular-momentum-multiplexed free-space optical link between a ground station and a retro-reflecting UAV using MIMO equalization," *Opt. Lett.* **44**, 5181 (2019).
- ¹⁴⁵A. E. Willner, "Advances in components and integrated devices for OAM-based systems," in *Invited Tutorial in Conference on Lasers and Electro-Optics (CLEO)* (OSA, 2018), Paper No. Stu3B.1.
- ¹⁴⁶N. Friedman, *The Naval Institute Guide to World Naval Weapon Systems* (Naval Institute Press, 2006).
- ¹⁴⁷M. Stojanovic, "Recent advances in high-speed underwater acoustic communications," *IEEE J. Ocean. Eng.* **21**, 125 (1996).
- ¹⁴⁸J. Wang, C. Lu, S. Li, and Z. Xu, "100 m/500 Mbps underwater optical wireless communication using an NRZ-OOK modulated 520 nm laser diode," *Opt. Express* **27**, 12171 (2019).
- ¹⁴⁹Y. Ren, L. Li, Z. Wang, S. M. Kamali, E. Arbabi, A. Arbabi, Z. Zhao, G. Xie, Y. Cao, N. Ahmed, Y. Yan, C. Liu, A. J. Willner, S. Ashrafi, M. Tur, A. Faraon, and A. E. Willner, "Orbital angular momentum-based space division multiplexing for high-capacity underwater optical communications," *Sci. Rep.* **6**, 33306 (2016).
- ¹⁵⁰K. S. Morgan, J. K. Miller, B. M. Cochenour, W. Li, Y. Li, R. J. Watkins, and E. G. Johnson, "Free space propagation of concentric vortices through underwater turbid environments," *J. Opt.* **18**, 104004 (2016).
- ¹⁵¹J. Baghdady, K. Miller, K. Morgan, M. Byrd, S. Osler, R. Ragusa, W. Li, B. M. Cochenour, and E. G. Johnson, "Multi-gigabit/s underwater optical communication link using orbital angular momentum multiplexing," *Opt. Express* **24**, 9794 (2016).
- ¹⁵²R. Sahoo, S. K. Sahu, and P. Shanmugam, "Estimation of the channel characteristics of a vertically downward optical wireless communication link in realistic oceanic waters," *Opt. Laser Technol.* **116**, 144 (2019).
- ¹⁵³R. F. Lutomirski, "An analytic model for optical beam propagation through the marine boundary layer," *Proc. SPIE* **160**, 110 (1978).
- ¹⁵⁴M. A. Cox, L. Cheng, C. Rosales-Guzmán, and A. Forbes, "Modal diversity for robust free-space optical communications," *Phys. Rev. Appl.* **10**, 024020 (2018).
- ¹⁵⁵B. M. Levine, E. A. Martinsen, A. Wirth, A. Jankevics, M. Toledo-Quinones, F. Landers, and T. L. Bruno, "Horizontal line-of-sight turbulence over near-ground paths and implications for adaptive optics corrections in laser communications," *Appl. Opt.* **37**, 4553 (1998).
- ¹⁵⁶H. Kaushal and G. Kaddoum, "Optical communication in space: Challenges and mitigation techniques," *IEEE Commun. Surv. Tutor.* **19**, 57 (2016).
- ¹⁵⁷X. Zhu and J. M. Kahn, "Free-space optical communication through atmospheric turbulence channels," *IEEE Trans. Commun.* **50**, 1293–1300 (2002).
- ¹⁵⁸M. A. Khalighi and M. Uysal, "Survey on free space optical communication: A communication theory perspective," *IEEE Commun. Surv. Tutor.* **16**, 2231 (2014).
- ¹⁵⁹Y. Ren, Z. Wang, G. Xie, L. Li, A. J. Willner, Y. Cao, Z. Zhao, Y. Yan, N. Ahmed, N. Ashrafi, R. Bock, M. Tur, and A. E. Willner, "Atmospheric turbulence mitigation in an OAM-based MIMO free-space optical link using spatial diversity combined with MIMO equalization," *Opt. Lett.* **41**, 2406 (2016).
- ¹⁶⁰S. Huang, G. R. Mehrpoor, and M. Safari, "Spatial-mode diversity and multiplexing for FSO communication with direct detection," *IEEE Trans. Commun.* **66**, 2079 (2018).
- ¹⁶¹H. Song, L. Li, K. Pang, R. Zhang, K. Zou, Z. Zhao, J. Du, H. Song, C. Liu, Y. Cao, A. N. Willner, A. Almaiman, R. Bock, B. Lynn, M. Tur, and A. E. Willner, "Demonstration of using two aperture pairs combined with multiple-mode receivers and MIMO signal processing for enhanced tolerance to turbulence and misalignment in a 10 Gbit/s QPSK FSO link," *Opt. Lett.* **45**, 3042 (2020).
- ¹⁶²L. Li, H. Song, R. Zhang, Z. Zhao, C. Liu, K. Pang, H. Song, J. Du, A. N. Willner, A. Almaiman, B. Lynn, R. Bock, M. Tur, and A. E. Willner, "Increasing system tolerance to turbulence in a 100-Gbit/s QPSK free-space optical link using both mode and space diversity," *Opt. Commun.* **480**, 126488 (2021).
- ¹⁶³S. Berdagüe and P. Facq, "Mode division multiplexing in optical fibers," *Appl. Opt.* **21**, 1950 (1982).
- ¹⁶⁴G. P. Agrawal, "Multimode fibers," in *Nonlinear Fiber Optics*, 6th ed., edited by G. P. Agrawal (Academic Press, 2019), Chap. 14, p. 621.
- ¹⁶⁵A. Ghatak and K. Thyagarajan, *An Introduction to Fiber Optics* (Cambridge University Press, 1998).
- ¹⁶⁶M. Ikeda, M. Tateda, and H. Yoshiakiyo, "Refractive index profile of a graded index fiber: Measurement by a reflection method," *Appl. Opt.* **14**, 814 (1975).
- ¹⁶⁷D. Gloge, "Weakly guiding fibers," *Appl. Opt.* **10**, 2252 (1971).
- ¹⁶⁸S. Ramachandran and P. Kristensen, "Optical vortices in fiber," *Nanophotonics* **2**, 455 (2013).
- ¹⁶⁹L. Feng, Y. Li, S. Wu, W. Li, J. Qiu, H. Guo, X. Hong, Y. Zuo, and J. Wu, "A review of tunable orbital angular momentum modes in fiber: Principle and generation," *Appl. Sci.* **9**, 2408 (2019).
- ¹⁷⁰H. Huang, G. Milione, M. P. Lavery, G. Xie, Y. Ren, Y. Cao, N. Ahmed, T. A. Nguyen, D. A. Nolan, M.-J. Li, M. Tur, A. R. R, and A. E. Willner, "Mode

- division multiplexing using an orbital angular momentum mode sorter and MIMO-DSP over a graded-index few-mode optical fibre," *Sci. Rep.* **5**, 14931 (2015).
- ¹⁷¹S. Mumtaz, R.-J. Essiambre, and G. P. Agrawal, "Nonlinear propagation in multimode and multicore fibers: Generalization of the Manakov equations," *J. Light Technol.* **31**, 398 (2012).
- ¹⁷²J. Carpenter, B. C. Thomsen, and T. D. Wilkinson, "Degenerate mode-group division multiplexing," *J. Light Technol.* **30**, 3946 (2012).
- ¹⁷³S. Ramachandran, J. M. Fini, M. Mermelstein, J. W. Nicholson, S. Ghalmi, and M. F. Yan, "Ultra-large effective-area, higher-order mode fibers: A new strategy for high-power lasers," *Laser Photonics Rev.* **2**, 429 (2008).
- ¹⁷⁴A. Wang, L. Zhu, L. Wang, J. Ai, S. Chen, and J. Wang, "Directly using 8.8-km conventional multi-mode fiber for 6-mode orbital angular momentum multiplexing transmission," *Opt. Express* **26**, 10038 (2018).
- ¹⁷⁵R. Zhang, H. Song, H. Song, Z. Zhao, G. Milione, K. Pang, J. Du, L. Li, K. Zou, H. Zhou, C. Liu, K. Manukyan, N. Hu, A. Almaiman, J. Stone, M.-J. Li, B. Lynn, R. W. Boyd, M. Tur, and A. E. Willner, "Utilizing adaptive optics to mitigate intra-modal-group power coupling of graded-index few-mode fiber in a 200-Gbit/s mode-division-multiplexed link," *Opt. Lett.* **45**, 3577 (2020).
- ¹⁷⁶S. Bae, Y. Jung, B. G. Kim, and Y. C. Chung, "Compensation of mode crosstalk in MDM system using digital optical phase conjugation," *IEEE Photonics Technol. Lett.* **31**, 739 (2019).
- ¹⁷⁷K. Ingerslev, P. Gregg, M. Galili, F. Da Ros, H. Hu, F. Bao, M. A. U. Castaneda, P. Kristensen, A. Rubano, L. Marrucci, K. Rottwitt, T. Morioka, S. Ramachandran, and L. K. Oxenløwe, "12 mode, WDM, MIMO-free orbital angular momentum transmission," *Opt. Express* **26**, 20225 (2018).
- ¹⁷⁸R. M. Nejad, K. Allahverdyan, P. Vaity, S. Amiralizadeh, C. Brunet, Y. Messaddeq, S. LaRochelle, and L. A. Rusch, "Mode division multiplexing using orbital angular momentum modes over 1.4-km ring core fiber," *J. Light Technol.* **34**, 4252 (2016).
- ¹⁷⁹L. Zhu, G. Zhu, A. Wang, L. Wang, J. Ai, S. Chen, C. Du, J. Liu, S. Yu, and J. Wang, "18 km low-crosstalk OAM+ WDM transmission with 224 individual channels enabled by a ring-core fiber with large high-order mode group separation," *Opt. Lett.* **43**, 1890 (2018).
- ¹⁸⁰E. Ip, G. Milione, M.-J. Li, N. Cvjetic, K. Kanonakis, J. Stone, G. Peng, X. Prieto, C. Montero, V. Moreno, and L. Jesús, "SDM transmission of real-time 10GbE traffic using commercial SFP+ transceivers over 0.5 km elliptical-core few-mode fiber," *Opt. Express* **23**, 17120 (2015).
- ¹⁸¹C. Brunet, B. Ung, L. Wang, Y. Messaddeq, S. LaRochelle, and L. A. Rusch, "Design of a family of ring-core fibers for OAM transmission studies," *Opt. Express* **23**, 10553 (2015).
- ¹⁸²C. Brunet, B. Ung, P.-A. Bélanger, Y. Messaddeq, S. LaRochelle, and L. A. Rusch, "Vector mode analysis of ring-core fibers: Design tools for spatial division multiplexing," *J. Light Technol.* **32**, 4046 (2014).
- ¹⁸³P. Gregg, P. Kristensen, and S. Ramachandran, "Conservation of orbital angular momentum in air-core optical fibers," *Optica* **2**, 267 (2015).
- ¹⁸⁴Y. Jung, Q. Kang, R. Sidharthan, D. Ho, S. Yoo, P. Gregg, S. Ramachandran, S.-U. Alam, and D. J. Richardson, "Optical orbital angular momentum amplifier based on an air-hole erbium-doped fiber," *J. Light Technol.* **35**, 430 (2017).
- ¹⁸⁵L. Zhu, J. Li, G. Zhu, L. Wang, C. Cai, A. Wang, S. Li, M. Tang, Z. He, S. Yu, C. Du, W. Luo, J. Liu, J. Du, and J. Wang, "First demonstration of orbital angular momentum (OAM) distributed Raman amplifier over 18-km OAM fiber with data-carrying OAM multiplexing and wavelength-division multiplexing," in *Optical Fiber Communication Conference* (Optical Society of America, 2018), Paper No. W4C.4.
- ¹⁸⁶J. Liu, S. Chen, H. Wang, S. Zheng, L. Zhu, A. Wang, L. Wang, C. Du, and J. Wang, "Amplifying orbital angular momentum modes in ring-core erbium-doped fiber," *Research* **2020**, 7623751.
- ¹⁸⁷N. Gisin, G. Ribordy, W. Tittel, and H. Zbinden, "Quantum cryptography," *Rev. Mod. Phys.* **74**, 145 (2002).
- ¹⁸⁸H. Takenaka, A. Carrasco-Casado, M. Fujiwara, M. Kitamura, M. Sasaki, and M. Toyoshima, "Satellite-to-ground quantum-limited communication using a 50-kg-class microsatellite," *Nat. Photonics* **11**, 502 (2017).
- ¹⁸⁹N. Namekata, H. Takesue, T. Honjo, Y. Tokura, and S. Inoue, "High-rate quantum key distribution over 100 km using ultra-low-noise, 2-GHz sinusoidally gated InGaAs/InP avalanche photodiodes," *Opt. Express* **19**, 10632 (2011).
- ¹⁹⁰H. Bechmann-Pasquinucci and W. Tittel, "Quantum cryptography using larger alphabets," *Phys. Rev. A* **61**, 062308 (2000).
- ¹⁹¹N. J. Cerf, M. Bourennane, A. Karlsson, and N. Gisin, "Security of quantum key distribution using d-level systems," *Phys. Rev. Lett.* **88**, 127902 (2002).
- ¹⁹²D. V. Sych, B. A. Grishanin, and V. N. Zadkov, "Critical error rate of quantum-key-distribution protocols versus the size and dimensionality of the quantum alphabet," *Phys. Rev. A* **70**, 052331 (2004).
- ¹⁹³S. P. Walborn, D. S. Lemelle, M. P. Almeida, and P. H. S. Ribeiro, "Quantum key distribution with higher-order alphabets using spatially encoded qudits," *Phys. Rev. Lett.* **96**, 090501 (2006).
- ¹⁹⁴A. R. Dixon, Z. L. Yuan, J. F. Dynes, A. W. Sharpe, and A. J. Shields, "Gigahertz decoy quantum key distribution with 1 Mbit/s secure key rate," *Opt. Express* **19**, 18790 (2008).
- ¹⁹⁵M. Erhard, R. Fickler, M. Krenn, and A. Zeilinger, "Twisted photons: New quantum perspectives in high dimensions," *Light: Sci. Appl.* **7**, 17146 (2018).
- ¹⁹⁶Y. Ren, C. Liu, K. Pang, J. Zhao, Y. Cao, G. Xie, L. Li, P. Liao, Z. Zhao, M. Tur, and A. E. Willner, "Spatially multiplexed orbital-angular-momentum-encoded single photon and classical channels in a free-space optical communication link," *Opt. Lett.* **42**, 4881 (2017).
- ¹⁹⁷H. Hübel, M. R. Vanner, T. Lederer, B. Blauensteiner, T. Lorünser, A. Poppe, and A. Zeilinger, "High-fidelity transmission of polarization encoded qubits from an entangled source over 100 km of fiber," *Opt. Express* **15**, 7853 (2007).
- ¹⁹⁸C.-Z. Peng, J. Zhang, D. Yang, W.-B. Gao, H.-X. Ma, H. Yin, H.-P. Zeng, T. Yang, X.-B. Wang, and J.-W. Pan, "Experimental long-distance decoy-state quantum key distribution based on polarization encoding," *Phys. Rev. Lett.* **98**, 010505 (2007).
- ¹⁹⁹S.-K. Liao, W.-Q. Cai, W.-Y. Liu, L. Zhang, Y. Li, J.-G. Ren, J. Yin, Q. Shen, Y. Cao, Z.-P. Li, F.-Z. Li, X.-W. Chen, L.-H. Sun, J.-J. Jia, J.-C. Wu, X.-J. Jiang, J.-F. Wang, Y.-M. Huang, Q. Wang, Y.-L. Zhou, L. Deng, T. Xi, L. Ma, T. Hu, Q. Zhang, Y.-A. Chen, N.-L. Liu, X.-B. Wang, Z.-C. Zhu, C.-Y. Lu, R. Shu, C.-Z. Peng, J.-Y. Wang, and J.-W. Pan, "Satellite-to-ground quantum key distribution," *Nat. Photonics* **549**, 43 (2017).
- ²⁰⁰C. H. Brassard and G. Brassard, "Quantum cryptography: Public key distribution and coin tossing," in *Proceedings of International Conference on Computers, Systems and Signal Processing* (IEEE, 1984), p. 175.
- ²⁰¹A. Sit, F. Bouchard, R. Fickler, J. Gagnon-Bischoff, H. Larocque, K. Heshami, D. Elser, C. Peuntinger, K. Günthner, B. Heim, C. Marquardt, G. Leuchs, R. W. Boyd, and E. Karimi, "High-dimensional intracity quantum cryptography with structured photons," *Optica* **4**, 1006 (2017).
- ²⁰²G. Vallone, V. D'Ambrosio, A. Sponselli, S. Slussarenko, L. Marrucci, F. Sciarrino, and P. Villoresi, "Free-space quantum key distribution by rotation-invariant twisted photons," *Phys. Rev. Lett.* **113**, 060503 (2014).
- ²⁰³M. Mafu, A. Dudley, S. Goyal, D. Giovannini, M. McLaren, M. J. Padgett, T. Konrad, F. Petruccione, N. Lütkenhaus, and A. Forbes, "Higher-dimensional orbital-angular-momentum-based quantum key distribution with mutually unbiased bases," *Phys. Rev. A* **88**, 032305 (2013).
- ²⁰⁴C. Liu, K. Pang, Z. Zhao, P. Liao, R. Zhang, H. Song, Y. Cao, J. Du, L. Li, H. Song, Y. Ren, G. Xie, Y. Zhao, J. Zhao, S. M. Rafsanjani, A. N. Willner, J. H. Shapiro, R. W. Boyd, M. Tur, and A. E. Willner, "Single-end adaptive optics compensation for emulated turbulence in a bi-directional 10-Mbit/s per channel free-space quantum communication link using orbital-angular-momentum encoding," *Research* **2019**, 8326701.
- ²⁰⁵F. Bouchard, A. Sit, F. Hufnagel, A. Abbas, Y. Zhang, K. Heshami, R. Fickler, C. Marquardt, G. Leuchs, R. W. Boyd, and E. Karimi, "Quantum cryptography with twisted photons through an outdoor underwater channel," *Opt. Express* **26**, 22563 (2018).
- ²⁰⁶J. Zhao, Y. Zhou, B. Braverman, C. Liu, K. Pang, N. K. Steinhoff, G. A. Tyler, A. E. Willner, and R. W. Boyd, "Performance of real-time adaptive optics compensation in a turbulent channel with high-dimensional spatial-mode encoding," *Opt. Express* **28**, 15376 (2020).
- ²⁰⁷A. E. Willner, Z. Zhao, Y. Ren, L. Li, G. Xie, H. Song, C. Liu, R. Zhang, C. Bao, and K. Pang, "Underwater optical communications using orbital angular momentum-based spatial division multiplexing," *Opt. Commun.* **408**, 21 (2018).
- ²⁰⁸S. Zhao, W. Li, Y. Shen, Y. Yu, X. Han, H. Zeng, M. Cai, T. Qian, S. Wang, Z. Wang, Y. Xiao, and Y. Gu, "Experimental investigation of quantum key distribution over a water channel," *Appl. Opt.* **58**, 3902 (2019).

- ²⁰⁹C.-Q. Hu, Z.-Q. Yan, J. Gao, Z.-Q. Jiao, Z.-M. Li, W.-G. Shen, Y. Chen, R.-J. Ren, L.-F. Qiao, A.-L. Yang, H. Tang, and X.-M. Jin, "Transmission of photonic polarization states through 55-m water: Towards air-to-sea quantum communication," *Photonics Res.* **7**, A40 (2019).
- ²¹⁰F. Hufnagel, A. Sit, F. Bouchard, Y. Zhang, D. England, K. Heshami, B. J. Sussman, and E. Karimi, "Investigation of underwater quantum channels in a 30 meter flume tank using structured photons," *New J. Phys.* **22**, 093074 (2020).
- ²¹¹D. Cozzolino, D. Bacco, B. Da Lio, K. Ingerslev, Y. Ding, K. Dalgaard, P. Kristensen, M. Galili, K. Rottwitt, S. Ramachandran, and L. K. Oxenløwe, "Orbital angular momentum states enabling fiber-based high-dimensional quantum communication," *Phys. Rev. Appl.* **11**, 064058 (2019).
- ²¹²J. Pinnell, I. Nape, M. de Oliveira, N. Tabebordbar, and A. Forbes, "Experimental demonstration of 11-dimensional 10-party quantum secret sharing," *Laser Photonics Rev.* **14**, 2000012 (2020).
- ²¹³M. Hillery, V. Bužek, and A. Berthiaume, "Quantum secret sharing," *Phys. Rev. A* **59**, 1829 (1999).
- ²¹⁴F.-G. Deng, H.-Y. Zhou, and G. L. Long, "Bidirectional quantum secret sharing and secret splitting with polarized single photons," *Phys. Lett. A* **337**, 329 (2005).
- ²¹⁵M. D. Oliveira, I. Nape, J. Pinnell, N. Tabebordbar, and A. Forbes, "Experimental high-dimensional quantum secret sharing with spin-orbit-structured photons," *Phys. Rev. A* **101**, 042303 (2020).
- ²¹⁶Z. Zhao, Y. Ren, G. Xie, Y. Yan, L. Li, H. Huang, C. Bao, N. Ahmed, M. P. Laverty, C. Zhang, N. Ashrafi, S. Ashrafi, S. Talwar, S. Sajuyigbe, M. Tur, A. F. Molisch, and A. E. Willner, "Experimental demonstration of 16-Gbit/s millimeter-wave communications link using thin metasurface plates to generate data-carrying orbital-angular-momentum beams," in *2015 IEEE International Conference on Communications (ICC)* (IEEE, 2015), p. 1392.
- ²¹⁷W. Cheng, W. Zhang, H. Jing, S. Gao, and H. Zhang, "Orbital angular momentum for wireless communications," *IEEE Wireless Commun.* **26**, 100 (2018).
- ²¹⁸Y. Yan, L. Li, Z. Zhao, G. Xie, Z. Wang, Y. Ren, N. Ahmed, S. Sajuyigbe, S. Talwar, M. Tur, N. Ashrafi, S. Ashrafi, A. F. Molisch, and A. E. Willner, "32-Gbit/s 60-GHz millimeter-wave wireless communication using orbital angular momentum and polarization multiplexing," in *2016 IEEE International Conference on Communications (ICC)* (IEEE, 2016), p. 1.
- ²¹⁹H. Sasaki, Y. Yagi, T. Yamada, T. Semoto, and D. Lee, "An experimental demonstration of over 100 Gbit/s OAM multiplexing transmission at a distance of 100 m on 40 GHz band," in *2020 IEEE International Conference on Communications Workshops (ICC Workshops)* (IEEE, 2020), p. 1.
- ²²⁰H. Zhou, X. Su, A. Minoofar, R. Zhang, H. Song, K. Pang, K. Zou, H. Song, N. Hu, Z. Zhao, Z. Zhao, A. Alaiman, S. Zach, M. Tur, A. Molisch, H. Sasaki, D. Lee, and A. Willner, "Experimental demonstration of 8-Gbit/s QPSK communications using two multiplexed orbital-angular-momentum beams in the 0.27–0.32 THz range," in *CLEO: Science and Innovations* (OSA, 2021), Paper No. STh2F.7.
- ²²¹S. Koenig, D. Lopez-Diaz, J. Antes, F. Boes, R. Henneberger, A. Leuther, A. Tessmann, R. Schmogrow, D. Hillerkuss, R. Palmer, T. Zwick, C. Koos, W. Freude, O. Ambacher, J. Leuthold, and I. Kallfass, "Wireless sub-THz communication system with high data rate," *Nat. Photonics* **7**, 977 (2013).
- ²²²T. Nagatsuma, S. Horiguchi, Y. Minamikata, Y. Yoshimizu, S. Hisatake, S. Kuwano, N. Yoshimoto, J. Terada, and H. Takahashi, "Terahertz wireless communications based on photonics technologies," *Opt. Express* **21**, 23736 (2013).
- ²²³X. Shams, M. J. Fice, L. Gonzalez-Guerrero, C. C. Renaud, F. van Dijk, and A. J. Seeds, "Sub-THz wireless over fiber for frequency band 220–280 GHz," *J. Light Technol.* **34**, 4786 (2016).
- ²²⁴X. Li, J. Yu, J. Zhang, Z. Dong, F. Li, and N. Chi, "A 400G optical wireless integration delivery system," *Opt. Express* **21**, 18812 (2013).
- ²²⁵X. Su, H. Zhou, K. Zou, A. Minoofar, H. Song, R. Zhang, K. Pang, H. Song, N. Hu, Z. Zhao *et al.*, "Demonstration of 8-channel 32-gbit/s qpsk wireless communications at 0.28–0.33 thz using 2 frequency, 2 polarization, and 2 mode multiplexing," in *2021 Optical Fiber Communications Conference and Exhibition (OFC)* (IEEE, 2021), pp. 1–3.
- ²²⁶Z. Zhao, R. Zhang, H. Song, K. Pang, A. Alaiman, H. Zhou, H. Song, C. Liu, N. Hu, X. Su, A. Minoofar, H. Sasaki, D. Lee, M. Tur, A. F. Molisch, and A. E. Willner, "Modal coupling and crosstalk due to turbulence and divergence on free space THz links using multiple orbital angular momentum beams," *Sci. Rep.* **11**, 2110 (2021).
- ²²⁷Y. Yan, L. Li, G. Xie, C. Bao, P. Liao, H. Huang, Y. Ren, N. Ahmed, Z. Zhao, Z. Wang, N. Ashrafi, S. Ashrafi, S. Talwar, S. Sajuyigbe, M. Tur, A. F. Molisch, and A. E. Willner, "Multipath effects in millimetre-wave wireless communication using orbital angular momentum multiplexing," *Sci. Rep.* **6**, 33482 (2016).
- ²²⁸A. F. Molisch, *Wireless Communications*, Vol. 34 (John Wiley & Sons, 2012).
- ²²⁹X. Su, R. Zhang, Z. Zhao, H. Song, A. Minoofar, N. Hu, H. Zhou, K. Zou, K. Pang, H. Song, B. Lynn, S. Zach, N. Cohen, M. Tur, A. F. Molisch, H. Sasaki, D. Lee, and A. E. Willner, "Multipath and receiver aperture effects in a THz wireless communications link using OAM multiplexing," in *2020 IEEE Globecom Workshops (GC Wkshps)* (IEEE, 2020), p. 1.
- ²³⁰A. Trichili, M. A. Cox, B. S. Ooi, and M.-S. Alouini, "Roadmap to free space optics," *J. Opt. Soc. Am. B* **37**, A184 (2020).
- ²³¹H. Khalid, S. S. Muhammad, H. E. Nistazakis, and G. S. Tombras, "Performance analysis of hard-switching based hybrid FSO/RF system over turbulence channels," *Computation* **7**, 28 (2019).
- ²³²F. Ahdi and S. Subramaniam, "Optimal placement of FSO links in hybrid wireless optical networks," in *2011 IEEE Global Telecommunications Conference—GLOBECOM 2011* (IEEE, 2011), p. 1.
- ²³³X. Cai, J. Wang, M. J. Strain, B. Johnson-Morris, J. Zhu, M. Sorel, J. L. O'Brien, M. G. Thompson, and S. Yu, "Integrated compact optical vortex beam emitters," *Science* **338**, 363 (2012).
- ²³⁴T. Su, R. P. Scott, S. S. Djordjevic, N. K. Fontaine, D. J. Geisler, X. Cai, and S. J. B. Yoo, "Demonstration of free space coherent optical communication using integrated silicon photonic orbital angular momentum devices," *Opt. Express* **20**, 9396 (2012).
- ²³⁵Z. Xie, T. Lei, F. Li, H. Qiu, Z. Zhang, H. Wang, C. Min, L. Du, Z. Li, and X. Yuan, "Ultra-broadband on-chip twisted light emitter for optical communications," *Light: Sci. Appl.* **7**, 18001 (2018).
- ²³⁶P. Genevet, J. Lin, M. A. Kats, and F. Capasso, "Holographic detection of the orbital angular momentum of light with plasmonic photodiodes," *Nat. Commun.* **3**, 1278 (2012).
- ²³⁷Z. Ji, W. Liu, S. Krlyuk, X. Fan, Z. Zhang, A. Pan, L. Feng, A. Davydov, and R. Agarwal, "Photocurrent detection of the orbital angular momentum of light," *Science* **368**, 763 (2020).
- ²³⁸J. Zhu, X. Cai, Y. Chen, and S. Yu, "Theoretical model for angular grating-based integrated optical vortex beam emitters," *Opt. Lett.* **38**, 1343 (2013).
- ²³⁹M. J. Strain, X. Cai, J. Wang, J. Zhu, D. B. Phillips, L. Chen, M. Lopez-Garcia, J. L. O'Brien, M. G. Thompson, M. Sorel, and S. Yu, "Fast electrical switching of orbital angular momentum modes using ultra-compact integrated vortex emitters," *Nat. Commun.* **5**, 4856 (2014).
- ²⁴⁰J. Liu, S.-M. Li, L. Zhu, A.-D. Wang, S. Chen, C. Klitis, C. Du, Q. Mo, M. Sorel, S.-Y. Yu, X.-L. Cai, and J. Wang, "Direct fiber vector eigenmode multiplexing transmission seeded by integrated optical vortex emitters," *Light: Sci. Appl.* **7**, 17148 (2018).
- ²⁴¹S. Li, Z. Nong, X. Wu, W. Yu, M. He, C. Klitis, Y. Zhu, S. Gao, J. Liu, Z. Li, L. Liu, M. Sorel, S. Yu, and X. Cai, "Orbital angular momentum vector modes (de) multiplexer based on multimode micro-ring," *Opt. Express* **26**, 29895 (2018).
- ²⁴²N. Zhang, M. Scaffardi, C. Klitis, M. N. Malik, V. Toccafondo, F. Fresi, J. Zhu, X. Cai, S. Yu, A. Bogoni, and M. Sorel, "Large-scale integrated reconfigurable orbital angular momentum mode multiplexer," preprint [arXiv:2008.00680](https://arxiv.org/abs/2008.00680) (2020).
- ²⁴³J. Sun, M. Moresco, G. Leake, D. Coolbaugh, and M. R. Watts, "Generating and identifying optical orbital angular momentum with silicon photonic circuits," *Opt. Lett.* **39**, 5977 (2014).
- ²⁴⁴J. Sun, A. Yaacobi, M. Moresco, D. Coolbaugh, and M. R. Watts, "Integrated continuously tunable optical orbital angular momentum generator," in *CLEO: Science and Innovations* (OSA, 2015), Paper No. JTh5A.5.
- ²⁴⁵B. Guan, R. P. Scott, C. Qin, N. K. Fontaine, T. Su, C. Ferrari, M. Cappuzzo, F. Klemens, B. Keller, M. Earnshaw, and S. J. B. Yoo, "Free-space coherent optical communication with orbital angular momentum multiplexing/demultiplexing using a hybrid 3D photonic integrated circuit," *Opt. Express* **22**, 145 (2014).

- ²⁴⁶Y. Chen, Z. Lin, S. B-d Villers, L. A. Rusch, and W. Shi, "WDM-compatible polarization-diverse OAM generator and multiplexer in silicon photonics," *IEEE J. Sel. Top. Quantum Electron.* **26**, 6100107 (2019).
- ²⁴⁷N. Zhou, S. Zheng, X. Cao, Y. Zhao, S. Gao, Y. Zhu, M. He, X. Cai, and J. Wang, "Ultra-compact broadband polarization diversity orbital angular momentum generator with $3.6 \times 3.6 \mu\text{m}^2$ footprint," *Sci. Adv.* **5**, eaau9593 (2019).
- ²⁴⁸H. Song, Z. Zhao, R. Zhang, H. Song, H. Zhou, K. Pang, J. Du, L. Li, C. Liu, X. Su, A. Almainian, R. Bock, M. Tur, and A. E. Willner, "Utilizing phase delays of an integrated pixel-array structure to generate orbital-angular-momentum beams with tunable orders and a broad bandwidth," *Opt. Lett.* **45**, 4144 (2020d).
- ²⁴⁹A. Liu, M. Wu, R. Zhuang, J. Hong, Q. Wang, and X. Ren, "On-chip generation of the reconfigurable orbital angular momentum with high order," *Opt. Express* **28**, 17957 (2020).
- ²⁵⁰P. Miao, Z. Zhang, J. Sun, W. Walasik, S. Longhi, N. M. Litchinitser, and L. Feng, "Orbital angular momentum microlaser," *Science* **353**, 464 (2016).
- ²⁵¹Z. Zhang, X. Qiao, B. Midya, K. Liu, J. Sun, T. Wu, W. Liu, R. Agarwal, J. M. Jornet, S. Longhi, N. M. Litchinister, and L. Feng, "Tunable topological charge vortex microlaser," *Science* **368**, 760 (2020e).
- ²⁵²A. B. Matsko, A. A. Savchenkov, D. Strekalov, and L. Maleki, "Whispering gallery resonators for studying orbital angular momentum of a photon," *Phys. Rev. Lett.* **95**, 143904 (2005).
- ²⁵³K. Cicek, Z. Hu, J. Zhu, L. Meriggi, S. Li, Z. Nong, S. Gao, N. Zhang, X. Wang, X. Cai, M. Sorel, and S. Yu, "Integrated optical vortex beam receivers," *Opt. Express* **24**, 28529 (2016).
- ²⁵⁴N. Zhang, M. Scaffardi, M. N. Malik, V. Toccafondo, C. Klitis, M. P. J. Lavery, G. Meloni, F. Fresi, E. Lazzeri, D. Marini, J. Zhu, X. Cai, S. Yu, L. Poti, G. Preve, A. Bogoni, and M. Sorel, "4 OAM x 4 WDM optical switching based on an innovative integrated tunable OAM multiplexer," in *Optical Fiber Communication Conference* (OSA, 2018), Paper No. Th3H.1.
- ²⁵⁵Y. Liu, L. S. Rishøj, Y. Ding, Q. Saudan, L. K. Oxenløwe, and T. Morioka, "Orbital angular momentum mode multiplexing and data transmission using a silicon photonic integrated mux," in *Optical Fiber Communication Conference* (Optical Society of America, 2021), pp. F4A–F45.
- ²⁵⁶H. Song, H. Zhou, K. Zou, R. Zhang, K. Pang, H. Song, X. Su, A. Minoofar, N. Hu, C. Liu *et al.*, "Demonstration of a tunable, broadband pixel-array-based photonic-integrated-circuit receiver for recovering two 100-gbit/s qpsk orbital-angular-momentum multiplexed channels," in *2021 Optical Fiber Communications Conference and Exhibition (OFC)* (IEEE, 2021), pp. 1–3.
- ²⁵⁷S. Li and J. Wang, "Adaptive free-space optical communications through turbulence using self-healing Bessel beams," *Sci. Rep.* **7**, 43233 (2017).
- ²⁵⁸N. Mphuthi, L. Gaile, I. Litvin, A. Dudley, R. Botha, and A. Forbes, "Free-space optical communication link with shape-invariant orbital angular momentum Bessel beams," *Appl. Opt.* **58**, 4258–4264 (2019).
- ²⁵⁹N. Ahmed, Z. Zhao, L. Li, H. Huang, M. P. J. Lavery, P. Liao, Y. Yan, Z. Wang, G. Xie, Y. Ren, A. Almainian, A. J. Willner, S. Ashrafi, A. F. Molisch, M. Tur, and A. E. Willner, "Mode-division-multiplexing of multiple Bessel-Gaussian beams carrying orbital-angular-momentum for obstruction-tolerant free-space optical and millimetre-wave communication links," *Sci. Rep.* **6**, 22082 (2016).
- ²⁶⁰R. Vasilyeu, A. Dudley, N. Khilo, and A. Forbes, "Generating superpositions of higher-order Bessel beams," *Opt. Express* **17**, 23389 (2009).
- ²⁶¹D. S. Simon, *A Guided Tour of Light Beams* (Morgan & Claypool Publishers, 2016).
- ²⁶²G. Zhu, Y. Wen, X. Wu, Y. Chen, J. Liu, and S. Yu, "Obstacle evasion in free-space optical communications utilizing Airy beams," *Opt. Lett.* **43**, 1203 (2018).
- ²⁶³L. Zhu, Z. Yang, S. Fu, Z. Cao, Y. Wang, Y. Qin, and A. M. J. Koonen, "Airy beam for free-space photonic interconnection: Generation strategy and trajectory manipulation," *J. Light Technol.* **38**, 6474 (2020).
- ²⁶⁴L. Zhu, A. Wang, and J. Wang, "Free-space data-carrying bendable light communications," *Sci. Rep.* **9**, 14969 (2019).
- ²⁶⁵H. T. Dai, Y. J. Liu, D. Luo, and X. W. Sun, "Propagation properties of an optical vortex carried by an Airy beam: Experimental implementation," *Opt. Lett.* **36**, 1617 (2011).
- ²⁶⁶J. A. Davis, D. M. Cottrell, and D. Sand, "Abruptly autofocusing vortex beams," *Opt. Express* **20**, 13302 (2012).
- ²⁶⁷D. Bongiovanni, D. Li, M. Goutsoulas, Y. Hu, D. Song, R. Morandotti, N. K. Efremidis, and Z. Chen, "Demonstration of vortex optical pin beams," in *Nonlinear Photonics* (Optical Society of America, 2020), Paper No. NpW2D.5.
- ²⁶⁸Z. Lin, X. Guo, J. Tu, Q. Ma, J. Wu, and D. Zhang, "Acoustic non-diffracting Airy beam," *J. Appl. Phys.* **117**, 104503 (2015).
- ²⁶⁹P. Zhang, T. Li, J. Zhu, X. Zhu, S. Yang, Y. Wang, X. Yin, and X. Zhang, "Generation of acoustic self-bending and bottle beams by phase engineering," *Nat. Commun.* **5**, 4316 (2014).
- ²⁷⁰S. Liu, A. Noor, L. L. Du, L. Zhang, Q. Xu, K. Luan, T. Q. Wang, Z. Tian, W. X. Tang, J. G. Han, W. L. Zhang, X. Y. Zhou, Q. Cheng, and T. J. Cui, "Anomalous refraction and nondiffractive Bessel-beam generation of terahertz waves through transmission-type coding metasurfaces," *ACS Photonics* **3**, 1968 (2016).
- ²⁷¹C. Liu, L. Niu, K. Wang, and J. Liu, "3D-printed diffractive elements induced accelerating terahertz Airy beam," *Opt. Express* **24**, 29342 (2016).